Application of Fly Ash from Solid Fuel Combustion in Concrete

Pedersen, Kim Hougaard

Publication date:
2008

Document Version
Early version, also known as pre-print

Application of Fly Ash from Solid Fuel Combustion in Concrete

Kim Hougaard Pedersen

2008

Application of Fly Ash from Solid Fuel Combustion in Concrete

Ph.D. Thesis

Kim Hougaard Pedersen

June 30, 2008

Supervisors:
Anker Degn Jensen
Kim Dam-Johansen

CHEC Research Centre
Department of Chemical and Biochemical Engineering
Technical University of Denmark

Preface

The present dissertation is written to meet the requirements of obtaining a Ph.D. degree at the Technical University of Denmark, Lyngby. The work has been conducted at the Combustion and Harmful Emission Control (CHEC) research center, the Department of Chemical and Biochemical Engineering between September 2004 and June 2008. The experimental work was funded by the Technical University of Denmark, Nordic Energy Research and the Danish Research Council for Technology and Production Sciences (FTP). The supervisors were Professor Anker Degn Jensen and Professor Kim Dam-Johansen.

At CHEC, I would like to express my sincere gratitude to my supervisors for their inspiration and constructive criticism during my project and for raising the funding for the experimental work. I am grateful to the M.Sc. students Faisal Al-Nakeeb and Mercé Casanovas Meliá for their contribution to the experimental work. I would also like to thank the technical staff and other colleagues in the CHEC group for their support and contribution to a pleasant working environment.

I would like to express my thanks to Bo Sander from DONG Energy A/S who initiated this study and who has provided valuable input to the work. My sincere thanks goes to Mogens Berg and Leif Høgh Olsen from Vattenfall A/S for making the experiments at Nordjyllandsværket possible. The technical staff at Nordjyllandsværket is also acknowledged. I am very grateful to Simon Iver Andersen for his guidance during the method development and Martin Skov-Skjøth Rasmussen, for his valuable input in the startup of this project and in the CFD work.

Finally, and most important I would like to thank my family for supporting me during this study and for reminding me about the world outside the world of fly ash.

Kim Hougaard Pedersen
June 2008

Abstract

Industrial utilization of fly ash from pulverized coal combustion plays an important role in environmentally clean and cost effective power generation. Today, the primary market for fly ash utilization is as pozzolanic additive in the production of concrete. However, the residual carbon in fly ash can adsorb the air entraining admixtures (AEAs) added to enhance air entrainment in concrete in order to increase its workability and resistance toward freezing and thawing conditions. The problem has increased with implementation of low-NO_x combustion technologies. The present thesis concerns three areas of importance within this field: 1) testing of fly ash adsorption behavior; 2) the influence of fuel type and combustion conditions on the ash adsorption behavior including full-scale experiments at the power plant Nordjyllandsværket, unit 3; 3) post treatment of fly ash to lower its AEA adsorptivity.

The foam index test is the method usually employed to determine the degree of fly ash interference with AEAs in concrete. The test involves the use of commercial AEAs and visual observation of foam stability. These facts reduce the reproducibility of the test, because commercially available AEAs vary in strength, and the criteria for foam stability are operator dependent. The objectives were to develop a new method based on dynamic surface tension measurements, using the bubble pressure method, on filtrate from a fly ash and cement suspension. A pure surfactant was added to the suspension as a substitute for a commercial AEA. The new method and the foam index test have been compared on fly ashes acquired from power plants in Denmark and the U.S. The results revealed a good relationship between the two methods. However, the new method has a low sensitivity toward small variations in AEA adsorption between different fly ashes and it requires further work before a finished procedure is accomplished. Finally, it was shown that changes in temperature affect both test methods.

Pulverized fuel has been combusted in an entrained flow reactor to test the impact of changes in operating conditions and fuel type on the AEA adsorption of ash and NO_x formation. Increased oxidizing conditions, obtained by improved fuel-air mixing or higher excess air, decreased the AEA

requirements of the produced ash by up to a factor of 25. This was due to a lower carbon content in the ash and a lower specific AEA adsorptivity of the carbon. The latter was suggested to be caused by changes in the adsorption properties of the unburned char and a decreased formation of soot, which was found to have a large AEA adsorption capacity based on measurements on a carbon black. The reactor was modeled with CFD and a relationship between oxygen concentration in the early stage of combustion and the AEA adsorption properties of the ash was observed. The NO_x formation increased by up to three times with more oxidizing conditions and thus, there was a trade-off between the AEA requirements of the ash and NO_x formation. The type of fuel had high impact on the AEA adsorption behavior of the ash. Ashes produced from a Columbian and a Polish coal showed similar AEA requirements, but the specific AEA adsorptivity of the carbon in the Columbian coal ash was up to six times higher. The AEA requirements of a South African coal ash was unaffected by the applied operating conditions and showed up to 12 times higher AEA adsorption compared to the two other coal ashes. This may be caused by larger particles formed by agglomeration of the primary coal particles in the feeding phase or during the combustion process, which gave rise to increased formation of soot.

A low-NO_x tangential fired 875 MW_{th} power plant burning bituminous coal have been operated under extreme conditions in order to test the impact of the operating conditions on fly ash adsorption behavior and NO_x formation. It was found that the AEA adsorption of the fly ash was reduced up to five times compared to reference operation, when the plant was operated with minimum furnace air staging, three levels of burners instead of four and without recycled flue gas. The lower AEA requirements of the fly ash at these conditions were primarily caused by a reduction in total carbon content, while the AEA adsorptivity of the residual carbon was lowered to about 60 % of reference value. The tested operation mode, however, increased the NO_x level in the flue gas before the $DeNO_x$ plant by 60 % compared to reference operation.

The AEA requirements of a fly ash can be suppressed by exposing it to oxidizing species, which oxidizes the carbon surface and thus prevents the AEA to be adsorbed. In the present work, two fly ashes have been ozonated in a fixed bed reactor and the results showed that ozonation is a potential post treatment method that can lower the AEA requirements of a fly ash up to six times. The kinetics of the carbon oxidation by ozone was found to be fast. A kinetic model has been formulated describing the passivation of carbon and it includes the stoichiometry of the ozone consumption (0.8 mol O_3/kg C) and an ineffective ozone loss caused by catalytic decomposition. The simulated results correlated well with the experimental data.

Dansk Resumé

Anvendelse af flyveaske fra suspensionsfyret forbrænding af kul ved produktion af el og varme, er af stor betydning ud fra både et miljømæssigt og et økonomisk synspunkt. I dag anvendes størstedelen af flyveasken som puzzolant additiv ved produktion af beton. Flyveaske kan imidlertid i visse tilfælde have en negativ indflydelse på luftindblandingen i beton, hvormed betonens bearbejdelighed og styrke over for frostsprængning reduceres. Den primære årsag til dette er at små mængder restkoks i flyveasken kan adsorbere luftindblandingsmidler (LIM), der tilsættes for at øge luftindblandingen. Moderne højeffektive og miljøvenlige kraftværker med lav-NO_x forbrændingsteknologier kan utilsigtet føre til at problemet forværres. Denne afhandling omhandler tre vigtige områder indenfor det nævnte felt: 1) test af flyveaskens evne til at adsorbere LIM; 2) undersøgelse af hvordan brændselstype og forbrændingsbetingelser påvirker LIM adsorptionen af flyveaske. I forbindelse med dette er der udført fuldskalaforsøg på Nordjyllandsværket, blok 3; 3) efterbehandling af flyveaske med henblik på at reducere dens adsorption af LIM.

Flyveaskekvaliteten, mht. påvirkning af luftindblanding i beton, bestemmes oftest ved den såkaldte skumindekstest. I testen anvendes et kommercielt LIM og skumstabiliteten vurderes visuelt. Dette forringer reproducerbarheden af testen, da kemisk sammensætning af kommercielt LIM varierer og vurdering af skumstabilitet er subjektivt. Formålet med arbejdet var at udvikle en ny metode baseret på måling af den dynamiske overfladespænding af filtrat fra en suspension af flyveaske og cement vha. "bubble pressure" testen. Ydermere blev det kommercielle LIM erstattet af et veldefineret overfladeaktivt stof. Den nye metode og skumindekstesten blev sammenlignet på flyveasker opsamlet fra danske og amerikanske kraftværker. Resultaterne påviste en god sammenhæng mellem de to metoder. Den nye metode har dog en lav følsomhed og der kræves derfor yderligere arbejde før metoden er færdigudviklet. Det blev desuden påvist at temperaturen påvirker begge testmetoder.

Askeprøver blev produceret under forbrændingsforsøg i en fastbrændselsreaktor for at teste, hvorledes driftsbetingelser og brændselstype påvirker NO_x dannelsen og askens optag af LIM. Ved at forøge det totale luftover-

skud eller opblandingen i mellem kul og luft, og derved øge de oxiderende forhold under forbrændingsprocessen, blev askens optag af LIM reduceret op til 25 gange. Askens mindre optag af LIM var forårsaget af et reduceret indhold af restkoks, der samtidig udviste en lavere adsorptionskapacitet. Reaktoren blev modeleret med CFD og der blev påvist en sammenhæng mellem iltkoncentrationen i det tidlige stadie af forbrændingsprocessen og askens evne til at adsorbere LIM. NO_x dannelsen steg op til tre gange under de øgede oxiderende betingelser. Udover driftsbetingelserne havde brændslet også indflydelse på asken egenskaber. Askeprøver produceret fra et columbiansk og et polsk kul udviste samme optag af LIM, men den columbianske aske indeholdt restkoks med op til seks gange højere LIM adsorptionskapacitet. Restkoksen i aske produceret fra et sydafrikansk kul havde en væsentligt højere LIM adsorptionskapacitet. Askens totale optag af LIM var upåvirket af de anvendte driftsbetingelser og var op til 12 gange højere end asker produ-ceret fra de to andre kul. Dette kan muligvis tilskrives denne kultypes øgede tendens til at agglomerere, hvilket forårsagede en øget dannelse af sod under forbrænding. I forbindelse med dette viste forsøg at sod kan have en stor adsorptionskapacitet af LIM.

Nordjyllandsværket, blok 3, er et lav-NO_x tangentielt fyret kraftværk, der brænder bituminøse kul. I forbindelse med dette projekt blev der udført fuldskalaforsøg hvor værket blev kørt i en ekstrem driftstilstand for at undersøge hvorledes askens optag af LIM og NO_x dannelsen blev påvirket. Forsøgene viste at det var muligt at reducere askens optag af LIM op til fem gange sammenlignet med et reference forsøg ved at anvende minimal trinvis lufttilsætning i kedlen, benytte 3 brændersektioner i stedet for 4 samt at undlade at recirkulere røggassen. Det lavere optag af LIM var primært forårsaget at et reduceret restkoksindhold i asken, mens restkoksens adsorption af LIM samtidig blev reduceret til 60 % af værdien for reference asken. NO_x koncentrationen i røggassen steg med 60 % under de anvendte driftsbetingelser.

Flyveaskes adsorption af LIM kan mindskes ved at behandle den med oxiderende kemikalier. I dette arbejde blev to flyveasker fra Nordjyllandsværket, blok 3, ozonbehandlet og resultaterne viste at dette er en potentiel efterbehandlingsmetode, der kan nedsætte LIM optaget af flyveaske op til seks gange. Kinetikken for ozons oxidering af restkoksen blev fundet til at være hurtig. En model, der beskriver passiveringen af restkoksen, blev konstrueret og den inkluderede støkiometrien af ozonforbruget (0.8 mol O_3/kg C) samt et ineffektivt ozontab forårsaget af katalytisk dekomponering. De simulerede resultater vist god overensstemmelse med de eksperimentelle data.

Introduction to this Thesis

The primary energy use of the world is projected to grow with 56 % in 2030 compared to today's consumption (2004) [1]. Approximately one fourth of the energy production in 2005 is generated from the combustion of coal [2] and because coal is cheap and abundant, its use is believed to increase in order to meet the future energy requirements [3] (projected increase of 74 % in 2030 [1]). However, burning coal has an adverse environmental impact due to the release of air pollutants like SO_2, NO_x and solid materials and major progress has been made in reducing these emissions. In recent years, the control of mercury and CO_2 emissions, the latter being a greenhouse gas, has attracted attention as well. This study focus on the particulate matter characterized as fly ash, which is removed from the flue gas by filters or electrostatic precipitators. The collected fly ash is a useful additive in the production of concrete, but it can interfere with the air entrainment in the concrete by adsorbing the added air-entraining admixtures (AEAs). Such a scenario has been observed when utilizing fly ash from the Danish coal fired power plant, Nordjyllandsværket, Unit 3. The plant started operation in 1998 and since first day of operation, the fly ash has been reported to negatively affect the air entrainment in concrete to unacceptable levels. This observation has initiated the present study.

During the literature study, the areas of importance within this field have been identified and the present thesis covers three of them: 1) the test method that determines the AEA adsorption of a fly ash suffers from having a low reproducibility. The test should be improved or replaced by an alternative method; 2) the implementation of combustion technologies that lowers the NO_x emissions can increase the AEA adsorption of fly ash. A better understanding of this relationship is of interest for an environmentally clean and cost effective power generation; 3) as an alternative to control the AEA adsorptivity of fly ash by changing the operating conditions or fuel type, a post treatment method can be applied. The treatment process can use ozone as a reacting agent.

This thesis is written as manuscripts to scientific journals. A general

introduction to the field is given in chapter 1. Chapter 2 presents the effort towards the development of an alternative method for determination the AEA adsorption of fly ash. Chapter 3 deals with combustion experiments performed on an entrained flow reactor with the aim of testing the influence of operating conditions and fuel type on the AEA adsorptivity of the ash. The work has given rise to full-scale tests at Nordjyllandsværket, which is presented in chapter 4. Chapter 5 concerns the work of exposing fly ash to ozone that lowers its negative effect on air entrainment in concrete. Each chapter can be read separately, but it is recommended to start with chapter 1 in order for the reader to acquire a general introduction to the field.

Chapter 1 has been published in *Progress in Energy and Combustion Science*: K.H. Pedersen, A.D. Jensen, M.S. Skjøth-Rasmussen and K. Dam-Johansen, A review of the interference of carbon containing fly ash with air entrainment in concrete, vol. 34 (2008) 135-154.

Chapter 2 has been published in *Cement and Concrete Research*: K.H. Pedersen, S.I. Andersen, A.D. Jensen and K. Dam-Johansen, Replacement of the foam index test with surface tension measurements, vol. 37 (2007), 996-1004.

Chapter 3 has been submitted to *Combustion and Flame*: K.H. Pedersen, A.D. Jensen and K. Dam-Johansen, The effect of combustion conditions and fuel type on fly ash adsorption behavior in concrete.

Chapter 4 is in press in *Fuel Processing Technology*: K.H. Pedersen, A.D. Jensen, M. Berg, L.H. Olsen and K. Dam-Johansen, The effect of combustion conditions in a full-scale low-NO_x coal fired unit to fly ash properties for its application in concrete mixtures.

Chapter 5 is in press in *Energy and Fuels*: K.H. Pedersen, M.C. Melià, A.D. Jensen and K. Dam-Johansen, Post treatment of fly ash by ozone in a fixed bed reactor.

References

[1] International Energy Annual 2007, World Coal Consumption 1980–2005, Energy Information Administration (EIA), U.S. Department of Energy.

[2] International energy outlook 2007, DOE/EIA-0484(2007), The U.S Department of Energy (DOE), Energy Information Administration (EIA).

[3] The future of coal, An Interdisciplinary MIT Study, Massachussetts Institute of Technology (2007).

Contents

Chapter 1

Literature Study

Abstract. Industrial utilization of fly ash from pulverized coal combustion plays an important role in environmentally clean and cost effective power generation. Today, the primary market for fly ash utilization is as pozzolanic additive in the production of concrete. However, the residual carbon in fly ash may interfere with air entraining admixtures (AEAs) added to enhance air entrainment in concrete in order to increase its workability and resistance toward freezing and thawing conditions. The problem has increased with implementation of low–NO_x combustion technologies.

This review presents the past work carried out to identify the mechanisms causing the interactions between AEAs and fly ash in concrete mixtures, emphasizing the residual carbon. It has been shown that not only the amount, but also the properties of carbon, such as particle size and surface chemistry, has an impact on the adsorption capacity of AEAs. The type of fuel used in the combustion process influences the amount and properties of the residual carbon. Fly ash derived from bituminous coal has generally higher carbon content compared with fly ash produced from subbituminous coal or lignite, but shows a lower AEA adsorption capacity per mass of carbon. Cases reporting increased residual carbon content due to low–NO_x combustion are described, together with observations from a pilot scale experiment, where increased AEA adsorption capacity of carbon appeared to relate with firing at low–NO_x conditions. Post-treatment methods applied to improve fly ash quality are described in the review. Ozonation, thermal treatment and physical cleaning of carbon have been found to improve the fly ash performance for concrete utilization. Ultimately, recommendations for further work are outlined in the discussion.

1.1 Introduction

Approximately one fourth of the electricity produced worldwide (2002) is generated in coal fired power plants [1], which are primarily based on pulverized fuel combustion technologies [2]. Due to the content of sulphur, nitrogen and minerals in coal, considerable quantities of pollutants like SO_2, NO_x and solid materials are produced. The demand for environmentally clean and cost effective power generation has led to new technologies which have highly decreased the emission of these pollutants. Today, SO_2 is removed in desulphurization plants, while the emission of NO_x is minimized by improved combustion technologies and installation of downstream NO_x–reduction methods [3]. The solid materials are either collected as bottom ash or fly ash, where the latter is removed in filters or electrostatic precipitators. In pulverized coal combustion, the fly ash contributes about 75-90 wt% of the total ash produced [4–6] and the efficiency in fly ash removal is usually above 99.5 wt% [7].

Industrial utilization of fly ash from coal combustion is an important environmental and economic issue. Disposal of fly ash, e.g. in a landfill, enhances the risk of contaminating the ground water by leaching of heavy metals contained in the fly ash [4, 8]. In addition, the widespread introduction of taxes on landfill has increased the motivation for power producers to reuse fly ash [9]. In the U.S. approximately 40 % of the fly ash produced in the year 2004 (71 million tons) was used of which 59 % was utilized in the cement and concrete industry [10]. In the EU, 47 % of the 44 million tons of fly ash generated in 2003 was used and 71 % of this was used in the manufacture of cement and concrete [11].

1.2 Pulverized Fuel Combustion Technologies

This section provides the reader with a brief summary of pulverized fuel combustion technologies. More detailed descriptions are found elsewhere [2, 12].

The coal is ground to a fine powder, e.g. it may be to a fineness where 20-30 wt% is retained on a sieve with 74 μm apertures [2]. The milled coal particles are introduced into the furnace together with a part of the combustion air (primary air). The remaining air may be added as secondary-, tertiary-, over burner-, and over fire air through the burners or in ports further downstream to ensure complete burnout. The coal particles are transported in suspension through the furnace, where they devolatilize, ignite and burn thereby producing ash [2]. The residence time of the coal particles is

approximately 1-2 seconds before reaching the super heaters.

The swirl burner and the jet burner are the two major types of pulverized coal burner technologies applied in the process [2]. The former type introduces the coal, primary air and secondary air into the furnace with a strong swirling motion. Due to the swirl, a low pressure region is formed close to the burner leading to recirculation of hot combustion gases back to the burner. This promotes ignition and flame stability. The swirling effect is not obtained with the jet burner, where the coal, primary air and secondary air enter the furnace as jets. The burners are placed at the walls or in the corners of the furnace. In the latter position, the burners are configured to fire fuel and air tangentially to an imaginary vertical cylinder at the center of the furnace. This generates rotation of the combustion gases in the center of the furnace and establishes a vortex core where the combustion takes place as sketched in Fig. 1.1a.

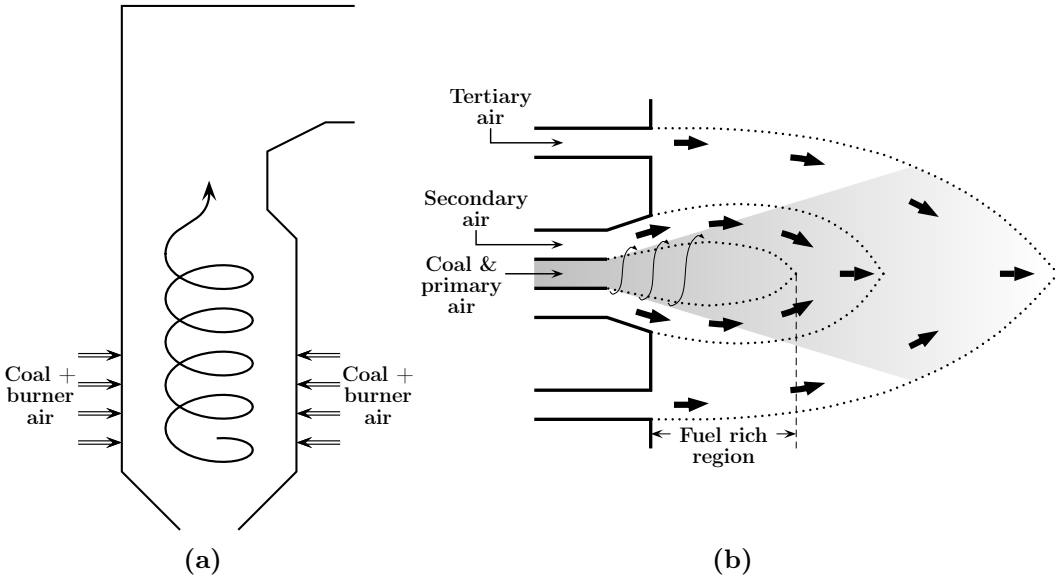

Figure 1.1: (a) Tangential burner configuration in a furnace. Adapted from Smoot [2]. (b) Concept of low–NO_x burner. Adapted from Tomeczek [12].

Improved burner technologies have been implemented in order to reduce NO_x formation. The burners have been modified to lower oxygen concentrations and reduce temperatures in the regions of fuel–NO_x and thermal–NO_x formation, respectively. An example of a low–NO_x burner is presented in Fig. 1.1b, where coal particles and primary air are gradually mixed with secondary and tertiary air [12]. The air staging leads to formation of fuel-rich zones, which reduces NO_x formation.

1.3 Concrete

The major structural building material today is concrete [13] being a composite material made from cement, aggregates, admixtures and water [14]. The aggregates are sand and stone.

Cement is manufactured from burning ground limestone and clay into clinker (1300-1450 °C) followed by mixing with gypsum [14]. The major composition of cement is calcium silicates ($3CaO{\cdot}SiO_2$ and $2CaO{\cdot}SiO_2$) with a CaO/SiO mass ratio above 2 [13]. The remaining components in cement are Al_2O_3, Fe_2O_3, MgO and other oxides [13]. Upon hydration of cement, an amorphous calcium silicate hydrate phase is formed together with calcium hydroxide. The former product controls to a great extent the setting and hardening of the concrete paste [13].

Admixtures for concrete are materials other than cement, water and aggregates [15]. The admixtures can be chemicals and the most important are added in order to accelerate or retard the setting and hardening process, reduce the amount of water required to obtain a given workability, and to enhance air entrainment in concrete [15]. Pozzolans, which are siliceous or siliceous and aluminous materials that together with water and calcium hydroxide form cementitous products at ambient temperatures [16], are also admixtures. Fly ash from pulverized coal combustion is categorized as such a pozzolan.

1.3.1 Fly Ash in Concrete

The pozzolanic properties of pulverized coal fly ash makes it useful in the concrete industry, where several benefits arise from this such as improved workability of the freshly mixed concrete and lower heat evolution during hydration. The hardened fly ash concrete shows increased strength together with a lower permeability, where the latter leads to a higher resistance toward aggressive agents [15–18]. In addition, partial replacement of cement with fly ash reduces the production costs of concrete due to the lower price of fly ash compared to cement [18]. In general, the amount of fly ash for typical durable concrete ranges from 15 wt% to 35 wt% of total mass of fly ash and cement, but the amount can be up to 70 wt% for concrete in constructions like pavement, walls and parking lots [18] and 80 wt% in autoclaved aerated concrete [19].

Fly ash can be divided into two types depending on the coal's origin. Burning high rank coal such as anthracite or bituminous coal produces ashes with a high content of silica and alumina and a low concentration of lime. Burning subbituminous coal or lignite (lower in rank), results in ashes with a

higher content of lime. The latter do not only show pozzolanic properties, but do possess cementitous properties as well due to their high content of lime [16] and utilization of these ashes in concrete may not lower the heat of hydration [18]. According to the American Society for Testing Materials (ASTM C618) [20], the ashes containing more than 70 wt% SiO_2+Al_2O_3+Fe_2O_3 and being low in lime are defined as class F, while those with a SiO_2+Al_2O_3+Fe_2O_3 content between 50 wt% and 70 wt% and high in lime are defined as class C.

Fly ash particles from pulverized coal combustion have gone through a molten stage at high temperatures and, subsequently, these are generally spherical in shape with diameters ranging from below 1 μm to above 150 μm [13]. The particle size distribution of fly ash can be measured in various ways, but is usually measured by sieve analysis [16], a method suitable for particles greater than approximately 45 μm [21]. Examples of size distributions obtained by dry sieving are illustrated in Fig. 1.2 [22]. The results

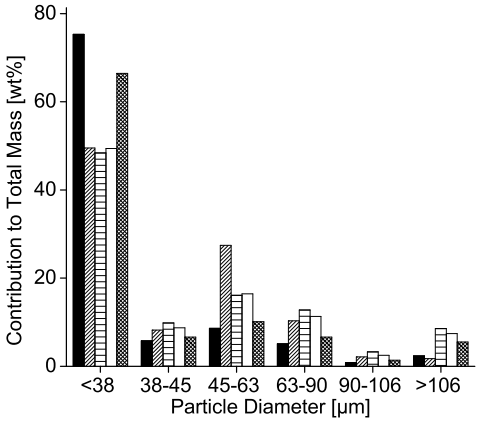

Figure 1.2: Particle size distribution (dry sieving) of fly ashes generated from the combustion of bituminous coal [22].

show how the highest contribution to the total mass comes from the fly ash particles below 38 μm in size, which is broadly consistent with several studies described by Helmuth [23]. It may be noted, that the size distribution is affected by combustion conditions and fineness of the pulverized coal [16]. In addition, different methods deviate in measured distributions [21], where certain methods, such as sieving, are affected by daily variations in moisture and electrostatic charging [24] .

1.3.2 Air Entrainment in Concrete

Several properties of concrete are improved when air is entrained. The inclusion of air as small, sub-millimeter air bubbles (less than 250 μm) makes the concrete more resistant toward damage from freezing and thawing and improves its workability and cohesion [25–27], without or only to a small degree affecting the production costs [28, 29]. On the other hand, too high air content reduces the strength of the concrete [26, 30]. Air entrainment occurs during agitation of the concrete paste, and the amount, which is approximately 5-6 vol%, is controlled by air-entraining admixtures (AEAs). These are typically aqueous mixtures of ionic or nonionic surfactants derived from either natural sources (wood resins, tall oil) or based on synthetic chemicals [13, 31]. Today, modern AEAs are mostly anionic in character [29]. Vinsol resin extracted from pinewood is one of the most effective AEAs among the natural surfactants. The active compound is the sodium salt of abietic acid (AAS) shown in Fig. 1.3.a. Other well–known examples of synthetic anionic AEAs are illustrated in Figs. 1.3.b–d [13].

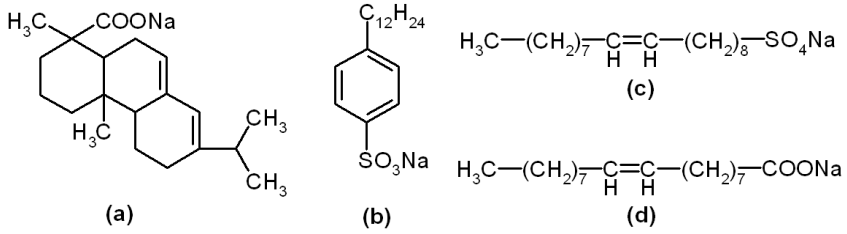

Figure 1.3: Molecular structure of well known natural and synthetic AEAs taken from [13]. (a) Sodium abietate (AAS), Mw = 302.46 g/mol. (b) Sodium dodecyl benzene sulfonate (SDBS), Mw = 348.48 g/mol. (c) Sodium oleyl sulfate, Mw = 370.53 g/mol. (d) Sodium oleate, Mw = 304.45 g/mol.

The surfactants adsorb strongly to the air–water/cement interface, having their non–polar end toward the interior of the air bubble and their polar end in the aqueous phase or adsorbed on the surface of the cement particle [13, 26]. This effect stabilizes the air bubbles, which in the case of missing AEAs would coalescence into larger bubbles leaving the concrete mixture [14].

The required amount of air to prevent concrete from freeze–thaw damages has been discussed by Nasvik *et al.* [30], who argues that modern surfactants create smaller bubbles with less spacing between each other in the concrete paste. With this combination, less entrained air is needed to obtain a freeze–

thaw resistance.

1.3.3 Interactions Between Fly Ash and Air–Entraining Admixtures

The utilization of fly ash in concrete has been reported to affect the required dosage of AEAs to entrain the proper amount of air in the concrete mixture [16, 32–39]. Instead of stabilizing the air–water/cement interface, the AEAs are strongly adsorbed by some fractions of the fly ash, leading to a reduced amount of AEAs stabilizing the entrained air [40, 41]. An increased dosage of AEAs may compensate for the adsorption loss, but normal variations in ash properties give rise to large and unacceptable variations in entrained air [40, 42]. Helmuth [23] has summarized how variations in several properties of fly ash have been found, even in ashes acquired from the same power plant. These variations can emerge from fluctuating load conditions [39]. In addition, air entrained fly ash concrete has been reported to loose its air over time [35, 37, 38]. For instance during transport and handling due to a continuous loss of "active" AEAs in the paste [43]. The air loss tends to be higher for fly ashes with increased AEA requirements [37]. However, laboratory data have shown that air loss may be due to the type of AEA used [35] and loss of air over time in cement samples without fly ash added has been reported as well [29, 36].

The unburned carbon, and not the inorganic fraction (mineral matter) of the fly ash, appears to be responsible for the adsorption of AEAs [31, 37, 39–42]. A large part of the carbon surface is non–polar compared with the polar surface of the inorganic particles. This provide active adsorption sites for the hydrophobic part of the surfactants, thus the carbon competes with the air/water interface as illustrated in Fig. 1.4. The interactions between carbon and AEAs are discussed in more detail below.

Baltrus *et al.* [44] investigated the impact on air entrainment from alkaline ions such as Ca^{++} and Mg^{++}, which are able to form insoluble products with surfactants. A significant decrease in surfactant adsorption of a fly ash was observed, after it had been washed with deionized water to remove soluble ions. Furthermore, the filtrate containing these ions was added to an AEA solution and it immediately turned cloudy indicating that the surfactants precipitated. Similar behavior was observed when a calcium containing fly ash was added to an AEA solution. However, in this case, the surfactants were simultaneously adsorbed by the fly ash and the initially formed precipitate did slowly dissolve again. The same effect is seen in concrete pastes where the surfactants are adsorbed on the surface of cement particles and

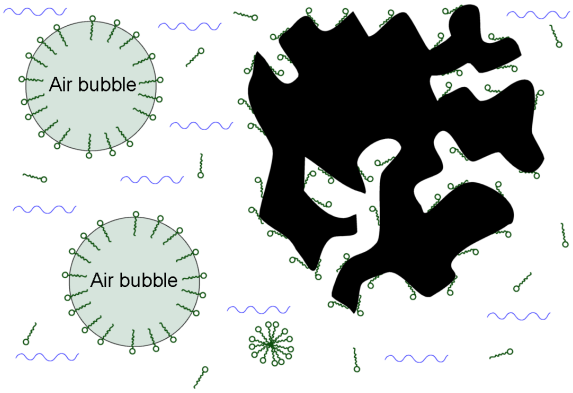

Figure 1.4: Adsorption sites for AEAs at air/water interface and at carbon surface inspired by Hachmann *et al.* [40]. The small circles of the AEAs correspond to the polar end and the tail correspond to the hydrophobic end. The components are not properly scaled, i.e. surfactant molecules and carbon micropores are estimated to be in the order of 10^7 times smaller than the carbon particles [40].

therefore, hardly any precipitation of surfactants occur. The polar ends of the surfactants are oriented toward the particle making them still able to contribute to air entrainment [26, 44].

Other compounds of fly ash, which may influence the air entrainment in concrete, have been reported by Gebler and Klieger [37]. Laboratory data indicated that increased SO_3 or total alkalis (as Na_2O) content in fly ash lead to reduced air loss or decreased AEA requirements in freshly mixed concrete, respectively. The latter observation is noted to be in agreement with work by others [43, 45] showing that less AEAs were required in Portland–cement mortars with increased alkalis. Finally, higher fineness of fly ash has been argued to lead to increased required dosage of AEAs [29, 33], but has been stated by others to be of minor importance [36, 39].

1.4 The Foam Index Test

To what extent a given fly ash interferes with air entrainment in concrete is commonly determined by the foam index test [24]. The test is a simple laboratory titration method and a proposed procedure is outlined by Dodson [29]. A diluted commercial AEA is added in small aliquots to a suspension of cement and water. The bottle containing the suspension is capped and

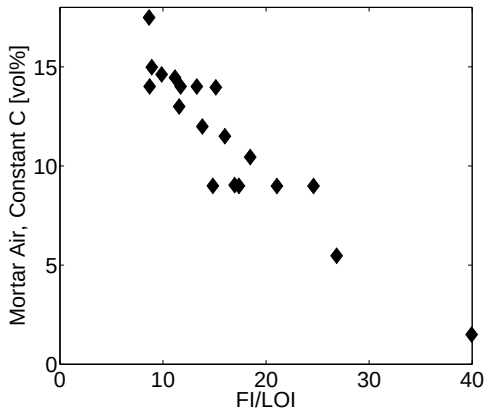

Figure 1.5: Amount of air in fly ash mortar with a constant carbon mass of 6 gram as a function of foam index/LOI [46].

shaken for 15 seconds after each addition. The surfactant behavior of the AEA results in foam formation, which is visually observed for stability. Further addition of AEA increases the foam stability, and the test is continued until no bursting of bubbles is observed in a period of 15 seconds. The amount of AEA added to produce the stable foam corresponds to the foam index value of the cement. Several modified variants of the test procedure, where the cement is partially replaced with fly ash, have been described in the literature [37, 40–44]. The cement/fly ash ratio is typically four on weight basis and the resulting suspension corresponds to a concrete mixture with a thin consistency. Usually, the foam index value of a pure cement sample is used as blank and subtracted from the value of the cement/fly ash sample in order to eliminate any variations in the foam index value caused by the cement.

The foam index value is equivalent to the surfactant adsorption capacity of the tested fly ash. When the active adsorption sites of the fly ash becomes saturated, the AEA starts showing surfactant behavior in the water phase and a stable foam is formed on its surface [43]. In other words, a poor–quality fly ash tends to adsorb more AEA than a high–quality fly ash and, hence, further addition of AEAs is required before a stable foam is formed. This behavior was confirmed in a study by Hill *et al.* [46], illustrated in Fig. 1.5. The amount of air in mortar prepared from sand, cement, fly ash and with a constant dosage of AEAs (ash content varied to keep a constant quantity of 6 grams of carbon) was found to correlate well with the foam index normalized by the LOI of the fly ash. Increasing foam index/LOI, i.e. higher AEA adsorptivity of the unburned carbon, results in a decline in

the amount of mortar air due to less AEAs are available to stabilize the air. Others have reported a good correlation between air entrainment in concrete [29] or AEA requirements in mortar/concrete [37, 47] and foam index values as well. The latter study [47] is repeated in [23].

The foam index test is not a standardized method and, as explained, is carried out in various modified ways by different research groups. Factors which make the test difficult to standardize have been discussed by Külaots *et al.* [43]. Commercial AEAs show different chemical nature, since they are derived from various natural and synthetic sources and are often purchased in different aqueous concentrations [43]. The age of the AEA [43] and the individual user criterion of stable foam endpoint influence the foam index results as well [44]. The types of AEAs are further discussed in section 1.7. Testing time was discovered by Freeman *et al.* [42] to affect the result. Further addition of AEAs was required to obtain stable foam when testing time was prolonged. Experiments have shown that adsorption of surfactants (detected by UV–Vis measurements, stirred under atmospheric air) still occurs up to 20 minutes [44] and more than 60 minutes [48] after being added, which is longer than the total test time on 10 minutes often used in the foam index test. However, this may be due to the presence of CO_2 in the atmosphere which react with the surfactants to form insoluble acids [43, 44]. An effect prevented by conducting the mixing in closed system [41] or under N_2 [44], where a level off in adsorption was detected after approximately 10 minutes [41] and no change in measured absorbance could be detected between 10 and 20 minutes of mixing [44], respectively. Thus, the influence of the discussed parameters makes it difficult to compare results between different laboratories and research groups.

1.5 Carbon in Fly Ash

The effect of residual carbon in fly ash concrete, besides poor air entrainment behavior, is increased water requirement to obtain normal consistency in the concrete paste [16], mixture segregation [42], and discoloration [15, 42]. The latter is aesthetically unacceptable in certain applications. Carbon in fly ash is found in porous spherical or irregular shapes [15] and it can be distinguished by two morphologies, which is consistent with a mixture of soot and char [49]. The fraction of soot increases with decreasing particle size fraction of fly ash [31, 50].

Recent work concerning fly ash interference with air entrainment in concrete by Hurt and co–workers [24, 31, 40, 42, 48, 51], argue that the following properties of unburned carbon contribute to the AEA adsorption: (1) the

amount; (2) the specific surface area; (3) the accessibility of the surface area; (4) the chemical nature of the surface.

1.5.1 Carbon Content

The unburned carbon content is routinely determined by weight loss after burning the fly ash in the loss–on–ignition test (LOI). The reported procedures follow the ASTM C311 [52] standard to a large extent [16, 22, 43, 53–55]. The weight loss takes place due to decomposition of carbonates, removal of water combined in clay minerals and combustion of carbon, with the latter being the major contributing component [16]. Oxidation of S and Fe may on the other hand lead to a gain in weight [16]. It is stated that carbon account for at least 99 % of the total weight loss [29], but others have reported higher errors between carbon content and LOI [54–57].

The relationship between unburned carbon in fly ash and adsorption of AEAs was demonstrated in a study by Külaots *et al.* [43]. No AEA adsorption was detected after the residual carbon in two fly ashes was removed by oxidation in a laboratory oven for 2 hours at 740 °C in atmospheric air according to the LOI test, as shown by others too [39, 40, 42].

The problem with decreased air entrainment in fly ash concrete due to unburned carbon has lead to regulations worldwide that limit the amount of carbon in fly ash for concrete utilization. The allowable carbon content depends on local practice but according to the ASTM C618 [20], it is not permitted to exceed 6 wt%. The European Standard EN 450–1 [58] limits the carbon content to 5 wt% for a category A fly ash, which corresponds to a class F ash in the U.S. classification. However, problems with air entrainment have been reported even at unburned carbon levels below 3 wt% [42] and 3.7 wt% [32].

Studies have revealed that the LOI test is not always sufficient to determine the fly ash capacity for AEA adsorption [24, 31, 37, 41, 42, 46, 51, 59]. Results from some of these studies are shown in Fig. 1.6a, where the foam index test is compared with the LOI. All the experiments were carried out on 2 grams of fly ash and 8 grams of cement using Darex® II as AEA except for the study by Freeman *et al.* [42], where Daravier® 1000 was used. Even though the experiments were carried out within the same research group, the reader should be careful in comparing the results between the different studies due to the reasons described in section 1.4. All studies report the foam index values in milliliters AEA per 2 gram of fly ash. Only the results published by Yu *et al.* [48] show a strong correlation between LOI and foam index test, while the results in the other studies correlate to a lesser degree between foam index and LOI. The poor correlation is especially pronounced

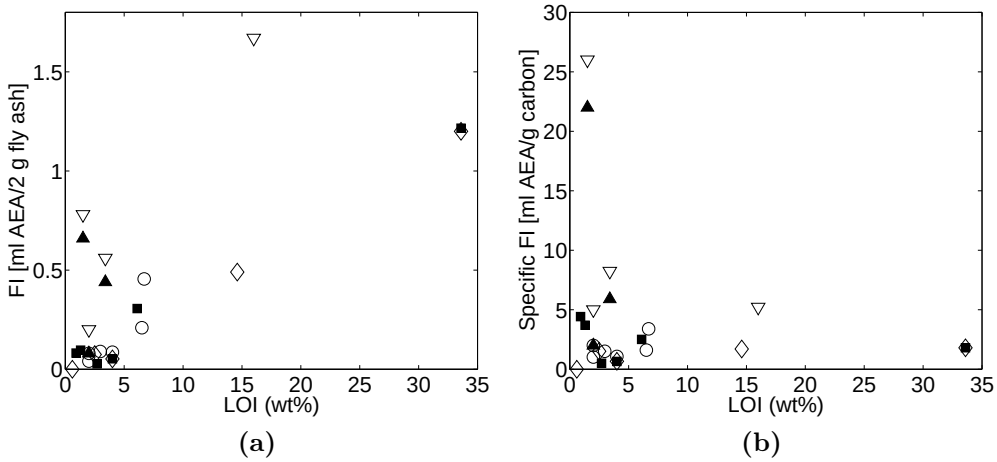

Figure 1.6: (a) Foam index and (b) specific foam index versus carbon content in five different studies. (▽) Freeman *et al.* [42] (◇) Yu *et al.* [48] (▲) Gao *et al.* [31] (■) Külaots *et al.* [24] (○) Gao *et al.* [51].

in the studies by Gao *et al.* [31] and Freeman *et al.* [42]. Gao *et al.* [31] refers to a publication by Clendenning *et al.* [39], who reported a good relationship between AEA requirement and carbon content in ashes coming from the same plant, but not necessarily between ashes collected from different plants. The results from Freeman *et al.* [42] may support this observation. Three of the ashes are taken from a single source and shows a linear behavior between carbon content and foam index. One ash (LOI = 1.5 wt%) shows considerably higher AEA requirements, taken its low carbon content into account, and this may be explained by it being acquired under uncontrolled combustion conditions. As a note to the foam index results, Gebler and Klieger [37] reported a better correlation between foam index values and organic matter in fly ash than LOI. The method to determine organic matter was apparently used to evaluate soil and uses sodium dichromate and sulfuric acid.

The foam index values shown in Fig. 1.6b are normalized into per gram of carbon in the fly ashes, also called the specific foam index. This presentation of data eliminates the influence of the varying carbon content of the samples, i.e. the adsorption of AEA per gram of carbon is revealed. The results in Fig. 1.6b clearly show how the residual fly ash carbons differ in adsorption capacities of AEAs. The largest variations in the specific foam indexes are observed at low values of LOI. A reason for this could be, that for low carbon ashes, there is a risk for overshooting the exact amount needed for stable foam formation since AEAs are added in small aliquots [60]. The results at low values of LOI may, therefore, be associated with greater uncertainties.

1.5.2 Specific Surface Area

The active surfactant adsorption sites are found at the surface of carbon, which makes surface area essential in its adsorption capacity of surfactants. Experimental data collected from three different authors are shown in Fig. 1.7. The data are presented as specific foam index values toward carbon

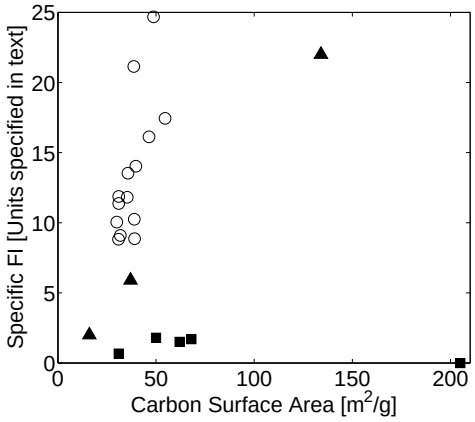

Figure 1.7: Specific foam index versus N_2-BET carbon area. (■) Yu *et al.* [48] (▲) Gao *et al.* [31] (○) Hill *et al.* [46]. The two former are given as ml AEA/g C, while the latter is given in drops of AEA/LOI.

surface areas measured by the Brunauer–Emmett–Teller method (BET) applying N_2 gas adsorption isotherms [61]. The reported adsorption capacities of the residual carbon is found to correlate well with its surface area in the study by Gao *et al.* [31], who found similar positive correlation on pilot scale produced ashes [51] (results not included in Fig. 1.7). Increasing AEA adsorption with the carbon surface area was observed in the study by Hill *et al.* [46] as well, however with less clear trend, e.g. ashes with similar carbon surface area, showed different specific foam index values even though the fly ashes were collected from a single source. Yu *et al.* [48] found a linear relationship between foam index values and carbon content as discussed in section 1.5.1 (Fig. 1.6a). The same ashes are observed to correlate poorly with the carbon surface area, especially the ash having a carbon surface area of 205 m^2/g C but shows no adsorption capacity. However, the result may be influenced with greater uncertainties due to its low LOI (0.6 wt%).

Determination of fly ash surface areas were included in a study from Külaots *et al.* [24]. The surface area of the mineral matter was found to be approximately 0.7–0.8 m^2/g ash, whereas the surface area of carbon ranged

from 45 to 400 m^2/g C. The surface area of the inorganic fraction was determined after removal of carbon, by burning the ash sample. The study found a poor correlation between the AEA adsorption and surface area of carbon. However, the AEA requirements tended to increase with the carbon surface area as observed in the study from Gao *et al.* [31] and Hill *et al.* [46] shown in Fig. 1.7. Similar inorganic surface areas were ascertained by Freeman *et al.* [42], while the surface area of carbon was measured to be between 16–134 m^2 per gram carbon.

Hachmann *et al.* [40] investigated the surface area of a bituminous coal and a lignite combusted to various levels. An initial increase of surface area per gram combustible matter followed by a subsequent decrease during coal conversion was observed, but it could not be related to the adsorption capacity of carbon. The initial increase in surface area was explained to be caused by pore opening due to devolatilization and early char combustion, while further conversion decreases the surface area of carbon at high temperatures. The latter is opposite to low temperature combustion, which is stated to activate or increase the surface area [51]. Similar trends in surface area developments, as found by Hachmann *et al.* [40], have been observed in laboratory burnout experiments on fly ashes acquired from utility boilers [62].

1.5.3 Accessibility of the Surface Area

The relationship between fly ash particle size and the adsorption capacity of carbon in six different ashes have been investigated by Külaots *et al.* [24]. The samples were distributed into size fractions by dry sieving and the results are shown in Fig. 1.8a together with results published by Yu *et al.* [48]. In this case, the different size fractions were obtained by grinding a fly ash between 150–212 μm in size into smaller fractions. Both studies found that the weight percent of carbon tends to become higher with increasing particle size fraction and this has been observed by others as well [22, 56, 63, 64]. Nevertheless, as Fig. 1.8a reveals, the AEA adsorption capacity of carbon decreases with increasing particle size. The same trend was observed for carbon blacks and activated carbons investigated by Gao *et al.* [31] and Yu *et al.* [48], respectively.

Another important issue in the adsorption capacity of carbon in fly ash is the pore size distribution. According to the IUPAC classification, the carbon pores can be divided into micropores (<2 nm), mesopores (2–50 nm), and macropores (>50 nm). The carbon in the fly ashes represented by (▲) and (■) in Fig. 1.8a have the largest AEA adsorptivities for almost all particle sizes. However, the carbon surface area of these ashes was by Külaots *et al.*

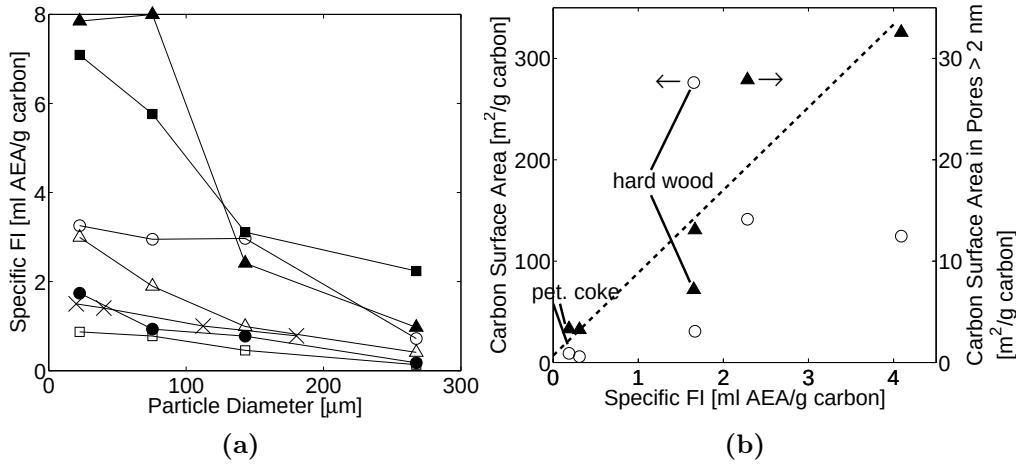

Figure 1.8: (a) Specific foam index versus particle size of fly ash. (×) Yu *et al.* [48], others from Külaots *et al.* [24]. The particle diameter corresponds to the average value of each fraction. (b) Specific foam index versus carbon surface area [51], total (○) and in pores > 2 nm (▲).

[24] found to be even higher than the other ashes and furthermore increasing with the particle size. Külaots *et al.* [24] and others [17, 31, 42, 48] have concluded that even though larger carbon particles contribute with a high surface area (often measured using the small N_2 molecule), their fine micropores are ineffective in the AEA adsorption. A large char particle may possess a high surface area, but a large contribution comes from the microporosity lying deep within the particle and therefore inaccessible for the large AEA molecule within testing time. Therefore, the AEA adsorption capacity of carbon appears to depend on transport limitations, making the accessibility of the active adsorption sites on carbon greater for small particles. Moreover, it has been suggested, that the size of micropores are comparable with the size of the AEA molecules [17, 42].

The low contribution to the AEA adsorption from the surface area in the micropores was to some extent supported by Gao *et al.* [51]. In chars generated from coal, wood and petroleum coke in laboratory and pilot scale experiments, a better correlation between adsorption of AEAs and non microporous char surface area, than with the total surface area was established (Fig. 1.8b). The non microporous area was determined by applying the Barrett Joyner Hallender (BJH) theory to N_2 adsorption isotherm data.

Gao *et al.* [51] investigated the AEA adsorption capacity of soot and char. A high carbon fly ash (app. 26 wt%) was separated by liquid–suspension gravity separation into a fine and a coarse particle size fraction suggested to

be soot and char, respectively. The method is described by Veranth *et al.* [50]. A 40 % higher specific adsorptivity by the fine fraction compared with coarse fraction was observed. Gao *et al.* [51] relates this behavior with BJH data. Out of a total BET–N_2 area of 38.3 m^2/g, the non microporous area of the fine fraction contributed with 34.5 m^2/g. This corresponds well with soot, where the area is located on the surface of nanosized particles. Thus, soot, which can be identified by transmission electron microscopy (TEM) in fly ashes acquired from pulverized coal fired boilers [31], is considered to be easy accessible for the AEAs [51] and estimated to have 2–5 times higher adsorption capacity compared with char–derived carbon [31]. Larger amounts of soot in fly ash may therefore cause lower quality for concrete utilization, but for typical fly ashes soot is believed to be present in low amounts [31].

1.5.4 Surface Polarity

Several studies have shown that the surface chemistry of carbon affects the surfactant adsorption [31, 40, 51, 65–67]. Fig. 1.9a provides the results from the work by Gao *et al.* [66], where two class F fly ashes (low in lime) were treated with ozone in a fixed bed reactor. The results demonstrate a significant decline in surfactant adsorptivity after ozone treatment, which

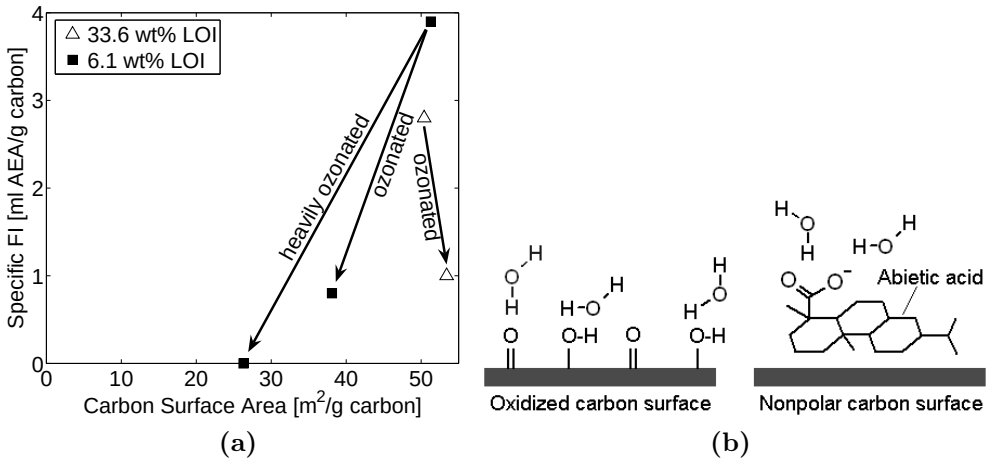

Figure 1.9: (a) Influence of ozonation on AEA adsorption [66].
(b) Nonpolar (right) and polar (left) surface of carbon inspired by Gao *et al.* [51].

was confirmed in a later study by the same author [51]. The surface area of carbon is observed to be only slightly affected by ozonation indicating that

the reduced AEA adsorption is caused by a change in surface chemistry. A reduced carbon surface area is measured in the low carbon ash (■), but it only partly accounts for the loss in adsorptivity. The amount of carbon in the ash was found not to be influenced by the ozone treatment and in addition, Gao *et al.* [51] were able to restore most of the initial surfactant adsorptivity of the low carbon ash (3.0 ml AEA/g C) by heat treating it in He at 1000 °C. In an earlier study published by Hachmann *et al.* [40], it was even possible to achieve higher adsorption capacity of a fly ash, which had gone trough heat treatment in inert gas. Here the adsorption capacity changed from approximately 2.6 ml AEA/g C to 3.6 ml AEA/g C after being treated for 2 hours at 900 °C in argon. Studies on carbon blacks show same tendency [65]. It has been discussed whether the loss in adsorptivity was caused by oxides blocking the fine pores of carbon, but based on experimental work on carbon blacks it was suggested that the non microporous area, which is accessible for the AEAs, was not easily blocked by surface oxides [51, 65]. Other studies have proved that BET surface areas of carbon are not significantly affected by surface oxidation [67].

The key role of surface chemistry was discussed in the publication by Gao *et al.* [51] and supported by Chen *et al.* [65]. It states [51], that surface oxides introduced from combustion or post–treatment, either by air oxidation or ozone treatment, creates carbon with less adsorptivity and thus, improves the fly ash quality as sketched in Fig. 1.9b. The hydrophobic part of a surfactant molecule (in this case abietic acid, Fig. 1.3a.) interacts by dispersion forces (van der Waals), with the non–polar carbon surface (right). On the other hand, at the polar carbon surface (left), water molecules interact with the surface oxides by hydrogen bonding. The dispersion forces from the surfactant are not strong enough to displace water and hence, the surfactant is not adsorbed by the carbon. The role of carbon surface polarity was also discussed by Hill *et al.* [41]. In this work, chemical analysis of carbon in low quality fly ashes revealed higher oxygen content compared to ashes being high in quality. Based on these results, it was concluded that a polar surface provides sites for AEA adsorption, which is opposite to the conclusions in the other studies described in this section.

X–ray photoelectron spectroscopy (XPS) measurements carried out by Gao *et al.* [51] on oxidized carbon blacks revealed, that surface oxide functional groups, such as O–C, C=O and O–C=O, were introduced by oxidation. Two other studies support this observation [65, 67]. Chen *et al.* [65] measured pH in carbon black slurries and discovered a decline in pH of the oxidized carbon blacks compared to an untreated carbon black. Furthermore, IR–spectra showed carboxylic functionalities, and from these observations, Chen *et al.* [65] concluded that primarily acidic oxygen complexes are introduced on the

surface by oxidation of carbon blacks.

1.6 Influence of Fuel and Combustion Conditions on Fly Ash Quality

1.6.1 Type of Fuel

1.6.1.1 Coal

Fly ashes produced from various types of coal have been included in the studies described above. As discussed in section 1.3.1, fly ash is in the U.S. divided into class F and class C depending on the origin of coal. Both fly ash classes were included in a study carried out by Külaots *et al.* [24] described in section 1.5.3. Burnout were found to be significantly higher of the class C ashes (LOI 0.7–1.3 wt%) compared with class F ashes (LOI 2.7–33.6 wt%), and all ashes showed increasing carbon content with the particle size. The fraction of carbon in small particle sizes of class F ashes were substantially larger compared with class C ashes, where only particle size fractions larger than 180 μm contained more than 10 wt% carbon. The unburned carbon in the small size fractions may partly be present as soot [31, 50]. The carbon contribution in each particle size fraction to the total carbon content of the ashes was calculated and the results are shown in Fig. 1.10a. A significant

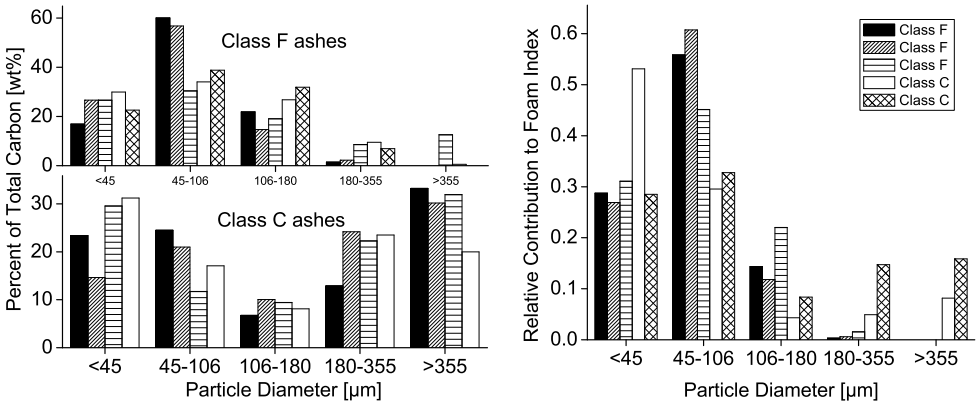

(a) **(b)**

Figure 1.10: (a) Carbon distribution of particle size fractions of both class C and class F ashes [24]. (b) Relative contribution to the foam index of class C and class F ashes [24].

contribution of the carbon in class F ashes lies in particles less than 106 μm

whereas for class C ashes, the carbon has a bimodal distribution, with a high contribution from large carbon particles. However, others have reported at bimodal carbon distribution of class F ashes as well [50, 68] and in one study more than 50 wt% of total carbon was found in class F ashes >106 μm in diameter [22].

Külaots *et al.* [24] attribute the observed behavior to the rank of coal. Coals resulting in class C ashes are typically low in rank, i.e. more reactive with a greater burnout. Then again, coals resulting in class F ashes are high in rank and, therefore, less reactive. This may give higher content of unburned carbon and greater survival of small carbon particles. The extent that each particle size fraction contributes to the total foam index for three class F ashes and two class C ashes is shown in Fig. 1.10b. Even though a significant quantity of the total carbon mass is present in larger size particle fractions of class C ashes, the highest contribution to the total foam index comes from the smaller fractions. Again a key role for the adsorption capacity of fly ash is the particle size as discussed in section 1.5.3. Moreover, the AEA adsorptivity of carbon in the two types of ashes were already revealed in Fig. 1.8a. Fly ash (▲) and (■) are class C ashes and the unburned carbon in these ashes show a significantly higher adsorption capacity of AEAs compared with the carbon in class F ashes. Based on these results, Külaots *et al.* [24] concluded that large carbon particles, particularly present in class C ashes, only makes a minor contribution to the AEA adsorption. However, the higher adsorption capacity of carbon in class C ashes makes the consequence of increasing carbon content worse in these ashes compared with class F ashes. Gebler and Klieger [37] showed that less AEA are generally required to obtain proper air entrainment with class C ashes compared with class F ashes. Part of the good performance of class C ashes was most likely caused by their lower carbon content ranging from 0.28 to 0.74 wt% LOI compared with the class F ashes, which had LOI values between 0.93 to 4.86 wt%. The carbon surface areas of class C ashes were found to be significantly higher compared with class F ashes [24]. The carbon surface areas of class C ashes ranged from 309 to 394 m^2/g C while for class F ashes, they were estimated to be between 32 to 63 m^2/g C. These observations have been reported by others as well [48, 51]. Apparently, the high surface area of carbon in class C ashes does not lead to high AEA adsorptivity.

Petrographic analysis of the carbon in fly ashes divides the carbon into three distinct classes, i.e. inertinite particles, isotropic or disordered carbon and anisotropic or ordered carbon [69]. The former appears to be non–fused particles, the second and latter appears to be reacted particles, which have passed through a molten stage. Commercial carbons used as adsorbents are generally isotropic, whereas carbons with low adsorptivity generally are

Feed[a] wt%	LOI [wt%]	FI[b] [ml]	Surface Area $\left[\frac{m^2}{g\ ash}\right]$	$\left[\frac{m^2}{g\ C}\right]$
5	2.4	0	1.2	18
10-15	17.5	0	1.3	4

Table 1.1: Proberties of coal/coke ashes taken from Yu *et al.* [48]. [a]Petroleum coke in feed. [b]Foam index per 2 gram of fly ash and per gram of carbon.

anisotropic [41]. Work from Hower *et al.* [68] found that anisotropic carbon was more frequently found in fly ash produced from the combustion of higher rank coal. The isotropic/anisotropic carbon ratio of class F ashes were investigated by Hill *et al.* [41] and a relationship between decreasing mortar air and increasing ratios of isotropic/anisotropic carbon was discovered. This was even though higher oxygen content was found in isotropic carbon compared to anisotropic carbon. However, a similar relationship could not be found in a later study by Hill *et al.* [46]. The discrepancy was suggested to be caused by the ashes in the later study containing too few carbon particles to reveal any correlation. It is noted that the role of isotropic and anisotropic carbon is reported to be opposite in the adsorption of mercury [70], where the highest amount of Hg appears to be adsorbed by anisotropic coke. The order of surface areas of the three types of carbon are inertinite < istrotropic carbon < anisotropic carbon [17]. The same work confirmed higher oxygen content in isotropic carbon as well.

1.6.1.2 Coal and Petroleum Coke

Petroleum coke is a solid by–product from the oil–refining industry. It is typically low in volatiles and ash content [48] and can with economical benefits be co–fired with coal or other solid fuels e.g. biomass and waste [4]. Two ashes from full scale bituminous–coal/pet–coke co–firing were included in the study by Yu *et al.* [48] discussed in section 1.5.1 and 1.5.2. The properties of the coal fly ashes are shown in Figs. 1.6a, 1.6b, and 1.7 and the properties of the coal/coke ashes are provided in Table 1.1. The results are not conclusive since a reference experiment was not included, but the obtained results are still interesting. The fly ashes produced from petroleum coke/coal co–firing showed no AEA adsorption capacity, even for the ash with 17.4 wt% LOI. The low surfactant adsorptivity of the unburned carbon was argued to be caused by the low surface area of the coke residues, which were estimated by

optical point count to represent approximately 95 wt% of the total carbon in the high carbon ash [48]. The dense and highly ordered molecular structure of petroleum coke leads to combustion residues with low microporosity and internal surface area. The high carbon content of the second coal/pet–coke ash is due to the poor burnout properties of petroleum coke, observed by others as well [71].

1.6.1.3 Coal and Biomass

The increasing demands of using renewable energy sources in order to reduce the consumption of fossil fuels, includes co–combustion of biomass (straw, wood, etc.) with coal in the production of heat and power. In many countries today, up to a certain limit of biomass is allowed in fly ash used as concrete additive, e.g. according to the European Standard EN 450–1 [58], up to 20 wt% biomass on fuel basis is permitted, and it may contribute to no more than 10 wt% of the total fly ash produced.

Wang *et al.* [72] studied how several concrete properties, including AEA requirements, were influenced by adding wood fly ash and fly ash from coal/switch grass co–firing to concrete mixtures. The concrete mixtures were prepared with an air content between 4–6 vol% and 25 wt% of the cement was replaced with fly ash. The results, summarized in Table 1.2, show that

Sample	LOI [wt%]	Air Admixture [oz/100 lbs cement]	Air [vol%]
Cement	–	0.45	4.5
Class C fly ash	1.58	0.79	4
Class F fly ash	0.52	1.76	5.5
20 % switchgrass	2.66	2.5	5.5
10 % switchgrass	2.60	1.67	5.3
Wood	5.44	0.81-1.56	4.5-6

Table 1.2: LOI and AEA requirements in concrete (75 % cement and 25 % fly ash) of fly ashes produced from coal/biomass co-firing [72].

co–firing with 20 % switch grass resulted in a fly ash which required higher amounts of admixture compared with the two coal fly ashes. However, the results do not truly indicate whether the properties of carbon changed, i.e. the increased requirements may only be caused by the higher carbon content in the biomass ash. The carbon in wood ashes show lower admixture requirements and this observation was suggested to be caused by the particles

having a larger average diameter.

Lamers *et al.* [73] investigated the fly ash quality from co–combustion of different secondary fuels with coal, including biomass pellets (5 wt% co–combustion), in large scale experiments. Increased LOI of the fly ash samples was found leading to higher AEA requirements, but a significant difference could not be shown between co–combustion and reference fly ashes. The other types of fuel included petroleum cokes, paper sludge, and dried sewage sludge. The fly ash from biomass pellets contained largest amounts of carbon compared with the other ashes.

1.6.2 Combustion Conditions

1.6.2.1 Observations from Full Scale Combustion

Installation of improved combustion technologies, such as low–NO_x burners and air–staging, significantly reduces NO_x emissions [74–76], e.g. the U.S. Department of Energy reported reduced NO_x emissions ranging from 37 % to 69 % in a demonstration project carried out on four different boiler types [77]. Such modifications of existing plants lead to fly ash with higher carbon content [4, 22, 41, 75, 76] and thus, lower fly ash quality for concrete utilization [51, 78]. Moreover, power plant performance in terms of boiler efficiency and electrostatic separator operation is affected [79, 80].

Three studies describing the conversion of existing power plants to low–NO_x combustion have been published by Hower *et al.* [68, 71, 81]. In the former paper [68], one wall–fired and two tangentially–fired units were investigated before and after conversion to low–NO_x combustion. The reported values of the fly ash carbon content are summarized in Table 1.3 and they reveal an increase in fly ash carbon after conversion to low–NO_x combustion. Nevertheless, the fly ash acquired from the two tangentially–fired units did

Type	LOI [wt%]	
	pre	post
Wall (hot[a])	2.45	3.72
Wall (cool)	2.42	5.31
Tangential	0.38	1.08
Tangential	0.32	1.41

Table 1.3: Change of carbon content in fly ashes produced from wall-fired and tangentially-fired boilers before and after conversion to low–NO_x combustion. [a] Hot and cool refers to the first and second row in the electrostatic precipitator [68].

not exceed the local standard for concrete utilization of 3 wt% LOI. The carbon distribution in the size fractions of the fly ash changed significantly in one of the tangentially–fired boilers. From having about 35 wt% of the total carbon in particles in the –500 mesh fraction (<25 μm) and about 12 wt% in the +100 mesh fraction (>150 μm) before conversion, the carbon distribution changed to more than 50 wt% in the +100 mesh fraction and about 14 wt% in the –500 mesh fraction after conversion to low–NO_x combustion. Finer coal feed before modification compared to the post coal feed was discussed as a cause of this change in carbon distribution. The two other studies published by Hower *et al.* [71, 81] did also found an increase in carbon content after revamping to low–NO_x combustion. However, the latter publication [81] refers to one example where a reduction in carbon content was observed. It was suggested that improved grinding of the coal and additional change in combustion conditions accounted for this observation. Hower *et al.* [81] reports as well, that thin walled and coarser carbon prevailed post modification carbons and proposed that low–NO_x combustion, which involves lower temperatures, makes the carbons able to survive. These carbons were easily combusted at higher combustion temperatures, which were present in the furnace before conversion.

The relationship between excess air, NO_x emissions, and carbon burnout was investigated by Jun *et al.* [74]. The experiments took place in three tangentially–fired full scale boilers equipped with jet burners, burning anthracite and bituminous coal. Higher excess air was observed to reduce the unburned carbon content in fly ash and increase NO_x emissions in most cases (Fig. 1.11a). Introducing more air into the furnace may increase the combustion intensity, i.e. high flame and furnace temperature. Thus, enhanced thermal–NO_x formation, higher conversion of coal nitrogen to NO_x, and higher burnout of carbon are obtained. The differences in boiler performance are explained from the furnace design. The furnace in unit a. (▲) and b. (■) operates with staged combustion, i.e. over–fire air (OFA) is introduced above the burner zone. This, together with an assumed well–distributed combustion, prevents high peak temperatures and reduces thermal–NO_x formation. However, as the results from unit b. (■) in Fig. 1.11a show, a further increase in excess air decreases the NO_x formation and the observation was suggested to be caused by lower furnace temperatures. Other contributions to variations in carbon burnout between the units are discussed to be residence time, type, and particle size of the coal.

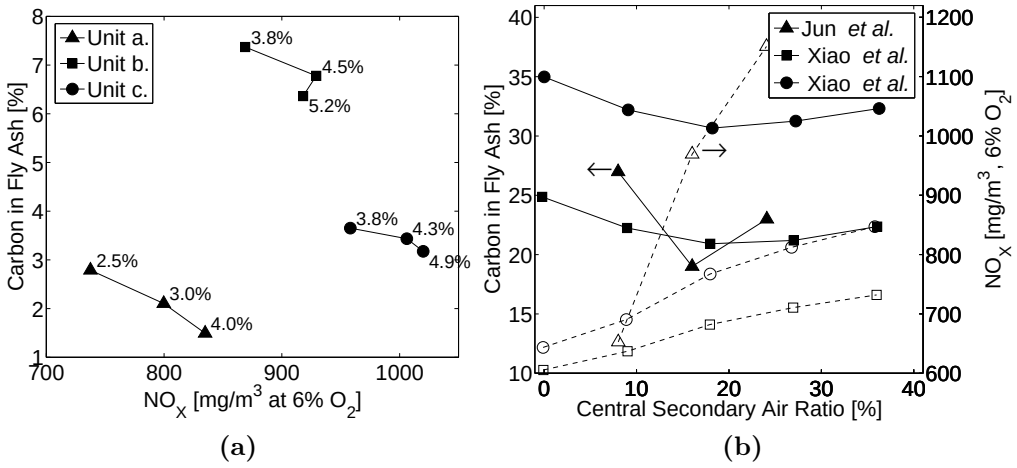

Figure 1.11: (a) Relationship between O_2 in flue gas (data labels), NO_x emission and carbon in fly ash acquired from three different utilites [74]. (b) The influence of air ratio on carbon content (filled markers) and NO_x emission (unfilled markers) [74, 82].

1.6.2.2 Observations from Pilot Scale Combustion

Jun *et al.* [74] also investigated the effect of air staging on NO_x emissions and carbon burnout in a single burner furnace. In the burner, pulverized coal was introduced together with primary air, and secondary air was introduced in a port below the primary port and in two ports above, central and upper port, respectively. The primary air and lower secondary air were kept in a constant ratio to the total combustion air, while only the ratio between central and upper secondary air was changed. Fig. 1.11b shows the experimental data including results from Xiao *et al.* [82]. The carbon content in the generated fly ash is, in both cases, found to gradually decrease followed by a slight increase with higher central secondary air ratio, while the NO_x emission increases with the ratio. The latter is caused by a smaller fuel rich zone at higher ratios leading to increased oxygen concentrations in the early stage of combustion [74]. Regarding the carbon content, Xiao *et al.* [82] suggest that higher ratio initially improves the mixing between coal and air, but a further rise in the central air ratio reduces the concentration of particles in the air flow, which results in a delayed ignition. The temperature profile in the furnace revealed that the peak temperature moved further downstream with increasing central air ratio. Others have reported a gradual increase in carbon content with declining NO_x emissions in pilot scale experiments [49, 75, 83].

The influence of coal particle size on burnout was included in the described studies [74, 82]. Both studies observed a higher burnout with decreasing particle size of coal, which have been supported by others [75, 84]. Smaller particles increase the release rate of volatile matter and show higher reactive surface area. Hence, a fast ignition together with higher flame temperature is obtained [75, 82].

Gao *et al.* [51] studied how AEA adsorptivity of carbon was influenced by high– and low–NO_x firing of two bituminous coals in a 29 kW down fired U–shaped furnace (results are presented in Fig. 1.12a). The adsorptivity

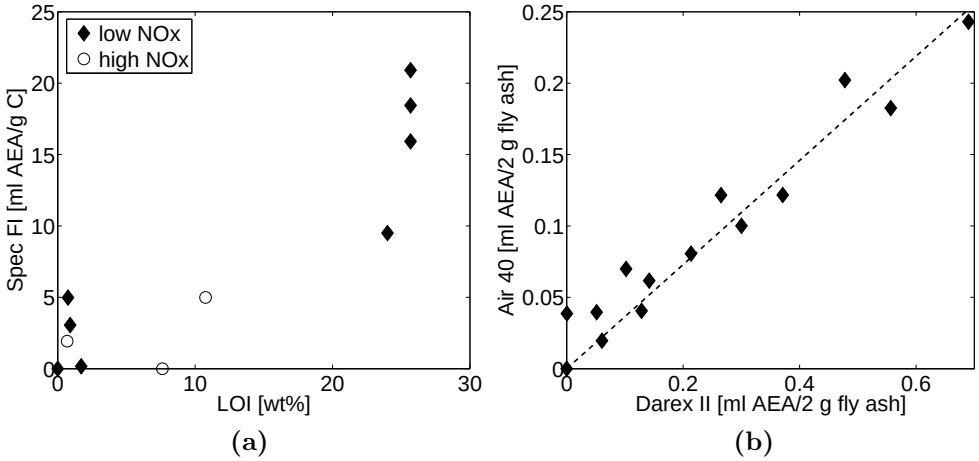

Figure 1.12: (a) AEA adsorption capacity of fly ash carbon produced at high– and low–NO_x combustion conditions [51]. (b) Foam index values using 10 vol% Darex II and 10 vol% Air 40. [43].

of carbon in fly ashes produced at low–NO_x conditions was mostly found to be high compared with carbon in high–NO_x produced ashes and those with a poor burnout appeared to have the highest adsorption capacity of AEAs. Similar tendency was seen with the carbon surface area, which, to a greater extent, could be related to the AEA adsorption compared than LOI. Attempts to correlate NO_x emissions with AEA requirements did not succeed.

Based on their own results and results from Lizzio *et al.* [85], who investigated the effect of oxygen chemisorption on char gasification, Gao *et al.* [51] discussed how combustion conditions affect residual carbon in fly ash. A stable film of oxides, which prevent adsorption of AEAs, is formed on the surface of carbon during conversion in a low–temperature and oxidizing environment. Opposite to this, fuel–rich and high–temperature combustion conditions will drive off surface oxides, leading to a less polar carbon surface.

These fuel–rich zones are usually found near the burner in low–NO_x environments, where they reduce the formation of thermal–NO_x but lead to lower burnout. In case of poor downstream mixing with remaining combustion air, carbon having a high surface area and a less polar surface will be mixed with the fly ash, giving rise to poor fly ash quality. On the other hand, the influence of fuel–rich zones on poor fly ash quality can be reduced with a good down stream mixing, where oxides are reintroduced to the carbon surface giving rise to further conversion, destruction of surface area and enhanced polarity of the carbon surface [51].

1.7 Influence of Type of AEA on Air Entrainment

Külaots *et al.* [43] compared two different commercial AEAs and three pure surfactants using the foam index procedure (2 grams of fly ash and 8 grams of cement). The AEAs were Darex® II from W.R. Grace & Co.–Conn., which is described as "a complex mixture of organic salts" [86] and Eucon Air 40® from The Euclid Chemical Company reported as "a stabilized modified resin surfactant" [87]. The experimental data, illustrated in Fig. 1.12b, show a good correlation between the two AEAs with Air 40 having approximately three times stronger effect on foam stability than Darex II. The non volatile content of Air 40 was determined to be about 20 % higher compared with Darex II, but further investigation to characterize their chemical nature and concentrations, was not carried out.

The three tested pure surfactants were prepared as aqueous solutions and compared with Darex II. The surfactants were AAS (Fig. 1.3.a), SDBS (Fig. 1.3.b), and sodium dodecyl sulfate (SDS), all described as suitable in the formulation of air–entraining admixtures [27]. All three surfactants were found to correlate well with Darex II foam index values, but the molar uptake of AAS appeared to be five times higher at the endpoint of the test compared with SDBS and SDS. Based on mass, SDS was found to be a more powerful surfactant than Darex II. Külaots *et al.* [43] discussed how the results support that different commercial materials will show similar air entraining behavior, and concluded that possibilities exist in replacing a commercial AEA with a pure surfactant in the foam index test.

The performance of different AEAs was demonstrated in an earlier study [35], and significant variations in strength of the AEAs were found as well. Air entrainment with long–chain hydrocarbons (fatty acid, sulphonated hydrocarbons) required higher doses compared with vinsol resin–based AEAs

in agreement with other published results [36]. Moreover, the long–chain hydrocarbon surfactants appeared to be less sensitive to the varying properties of the fly ashes. This may be consistent with results published by Külaots *et al.* [43], who found that the sulphonated hydrocarbon, SDBS, appeared to be less sensitive to soluble compounds provided by the ash compared with commercial AEAs, and as Corr *et al.* [88] showed that calcium ions and suspended particles, provided by cement, lowered the foam volume in the foam index test more when the fatty acid salt, sodium olyate, was used as AEA than SDBS. However, sodium olyate resulted in a more stable foam. Finally, Zhang *et al.* [35] included investigation of how air loss in concrete was influenced by fly ash and the type of AEA. The air content in eight fly ash concretes were determined after 60 minutes and compared with the 15–minutes content. During the intervening time, the mixtures had gone trough mixing cycles to simulate handling and agitation of concrete. The lowest percentage of air retained was with a protenation surfactant (41 ± 9 vol%) and two vinsol resin based AEAs (53 ± 13 vol% and 71 ± 14 vol%), while even higher air content was retained with three long chain hydrocarbon based AEAs (approximately 120 vol%). A large increase in air content was obtained with an epoxy sulphate AEA (144 ± 39 vol%) [35].

1.8 Improvement of Fly Ash Quality

1.8.1 Oxidation

The capability of the residual carbon to adsorb AEAs can be reduced by exposing fly ash to an oxidizing environment, which increases the oxygen population on the surface. Gao *et al.* [66] discuss how both wet and dry methods can be applied to improve fly ash quality, but they argue that wet methods give rise to problems such as high drying costs and loss of pozzolanic activity of the treated ashes.

Low temperature oxidation of fly ash was carried out in a study by Hachmann *et al.* [40]. A high carbon ash (LOI = 66 wt%) was oxidized in air for two hours in a bench–top furnace at temperatures from 20 to 900 °C followed by foam index measurements. The laboratory data, presented in Fig. 1.13a, show how the AEA requirements and carbon content of the fly ash decreases with increasing oxidizing temperatures, as expected. The interesting part is the observed decline in adsorptivity to about half its initial value at 450 °C before any conversion of carbon takes place. Hachmann *et al.* [40] discuss, with reference to other studies [89, 90], how the initial step in carbon oxidation is oxygen chemisorption leading to stable oxygen complexes

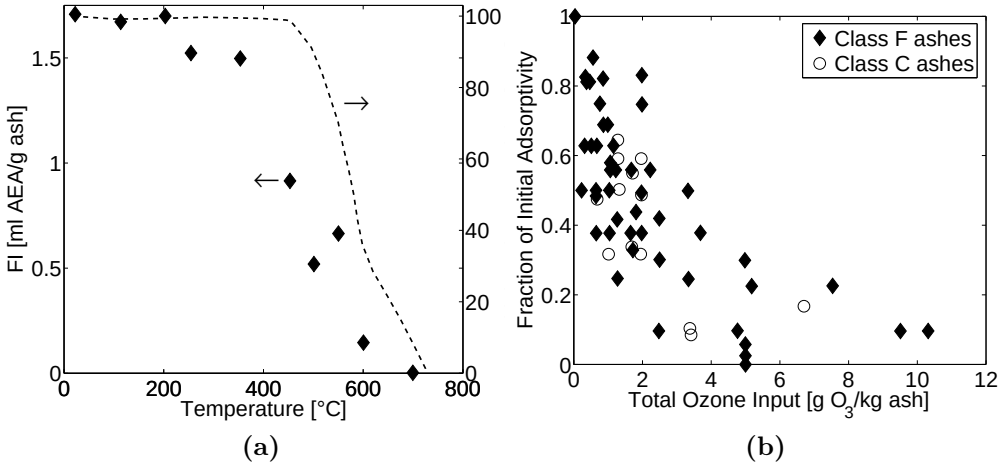

Figure 1.13: (a) Foam index and carbon content of a single fly ash sample during low temperature oxidation [40]. (b) Changes in AEA adsorption capacity of commercial ashes by ozone treatment [66].

during early stage of low temperature oxidation [85, 91]. The polarity of the carbon surface is believed to increase and thus, its AEA adsorption capacity is reduced. The initial oxygen chemisorption is assumed to take place from 300–450 °C. The outcome of the discussion is supported in a later study by Gao *et al.* [51] (see section 1.6.2.2).

Gao *et al.*'s [66] studies of oxidation with ozone (section 1.5.4) included an extensive number of ozonation experiments on both class C and class F ashes. 50 to 200 grams of fly ash were placed in a fixed bed reactor and ozone in concentrations ranging from 500 ppm to 2 vol% in air was allowed to flow upward through the ash for 1 minute to 20 hours at ambient temperature and pressure, while the exit ozone concentration was continuously measured. Fig. 1.13b shows the fraction in initial adsorptivity measured by the foam index test of the treated ash samples as a function of cumulative ozone input (integrated values) and the highest reduction in AEA requirements is found to occur in the range of 0 to 3 g O_3/kg ash. Initially, only traces of ozone were reported in the exit of the reactor in most cases, which was followed by fast ascent in concentration corresponding to a breakthrough of ozone through the bed. Based on the observations, Gao *et al.* [66] discuss how the reaction kinetics appear to be fast, making the ozone consumption limited by the supply. By expressing the total ozone input/carbon mass, the unburned carbon in class C ashes were discovered to require more ozone than class F ashes to achieve similar reduction in AEA adsorption. Carbon surface area of the investigated ashes were determined as well, and by calculating the

ozone consumption to an equivalent number of oxides present on the carbon surface, Gao *et al.* [66] proposed that the largest reduction in adsorptivity was achieved during the formation of an oxide monolayer. Chen *et al.* [65] suggested, that oxides present on the surface could initiate nucleation of water molecule clusters, which due to steric hindrance, suppressed the adsorption of AEAs even at oxygen coverage much lower than 100 %.

From the evaluation of laboratory data and economic calculations based on ozone requirements, price of ozone, fly ash sales price, and disposal costs, Gao *et al.* [66] estimated that development of a commercial post–treatment process based on ozone appears to be profitable. The process can take place at ambient temperature, while thermal treatment in air requires more than 300 °C, which is considered to be impractical by the authors [66]. Nevertheless, thermal post–treatment of fly ash has successfully been implemented in at least one case [92], where fly ash with an average LOI on 12.5 wt% was treated in a fluidized bed combustor. The process was operated without additional fuel. The LOI of the product was approximately 2.5 wt% and it performed well in concrete. It is noted, that patents have been drawn by Hurt *et al.* [93, 94], which describes a method for improvement of fly ash quality by ozone treatment.

1.8.2 Physical Cleaning

Separation processes can recover carbon from fly ashes, making the mineral–rich fraction suitable as concrete additive. Several studies have been published describing how carbon in fly ash can be reduced by physical cleaning [22, 41, 63, 95–103] and many patents have been drawn. However, none of the studies compared the AEA adsorptivity of the ashes before or after the cleaning process. The recovered carbon product is often disposed in landfills [104].

Dry triboelectrostatic separation of carbon from fly ash were applied in several of the studies [41, 63, 96–98]. The principle in the method is to charge a stream of fly ash and let it pass through two parallel and charged Cu–plates. The particles deflect in the charged field, with the carbon–enriched fraction attracted to the negative electrode and the mineral–enriched fraction to the positive electrode. The particles may be collected on the plates [63] or directed toward two cyclones [96, 97]. Ban *et al.* [63] noted, that 60–80 wt% of ash with a carbon content less than 5 wt% could be recovered. The carbon–rich fraction contained more than 50 wt% carbon and up to 50 wt% of the total carbon was recovered. The carbon content in the feed was found to affect the collection efficiency and, moreover, recycling of fly ash increased the ash recovery. Gray *et al.* [96] showed a carbon recovery of 50 wt% with

LOI = 27.5 wt% in the carbon–rich fraction obtained from a fly ash with 17.7 wt% LOI. The carbon content in the mineral–rich fraction was not reported. The experimental data showed room for improvement in cleaning efficiency and implementation of multistage cleaning circuits were suggested. However, Baltrus *et al.* [102] noted that a high purity of the products is often achieved by the cost of a lower yield. Baltrus *et al.* [102] showed that the triboelectrostatic method was very sensitive to moisture and it was actually possible to reverse the charge of the particles when exposing them to deionized water before separation. Others have demonstrated that the method could benefit from initial sieving of the ashes [97], where products with carbon contents less than 3 wt% from ashes ranging between 12–14 wt% in carbon were achieved.

At least two cases have been described where triboelectrostatic separation has been implemented in large scale [99, 105]. Two separators, each with capacities of 18 T/h, have been installed at coal burning utilities. The separators consist of two charged plates, where two opposite moving belts transport the fly ash in between. The belts are constructed as open meshes allowing the fly ash particles to pass trough. The electric field charges the fly ash particles and they move toward one of the plates depending on their charge. The ash particles are subsequently transported away by the moving belts in mineral–rich and carbon–rich fractions. One of the installed separators demonstrated a mineral–rich fraction less than 3 wt% in LOI from feed ashes with LOI values ranging from 6 to 25 wt%. The power consumption during operation was found to be less than 1 kWh/T fly ash.

Other methods, which have been applied to separate carbon from fly ash, are fluidization [22], different kinds of flotation methods [96, 101, 103], and ultrasonic column agglomeration [95, 96]. Some of these methods have a higher efficiency than the tribolectrostatic method described above. The two latter methods suffer from being wet processes, which lead to drying costs and possible loss of pozzolanic activity [66], as discussed in section 1.8.1. Required long retention times and high reagent costs may lower their suitability as well [103]. Furthermore, dry methods are preferred in the U.S., where more than 90 % of the fly ash is handled in dry state [63].

Separation of carbon from fly ash has been discussed by Gao *et al.* [51]. In case the carbon in the ash shows a high adsorptivity toward AEAs, the ash may not fulfill the requirements for concrete utilization even though a large fraction of carbon is removed from the ash. The authors refer to an industrial case where this has been observed.

1.9 Development of Test Methods to Determine Fly Ash quality

Based on the successful experiments to replace commercial AEAs with pure surfactants in the foam index test, described in section 1.7, Külaots *et al.* [43] recommended to proceed with SDBS in further work. Problems like varying strength and aging of commercial AEAs would thereby be avoided. Moreover, Manz *et al.* [18] have recommended to develop spectroscopic assays to determine AEA adsorption, and application of pure surfactants will be beneficial for such methods [43]. Külaots *et al.* [43] showed the importance of solid particles and pH in the foam index test. Alkaline solutions containing monovalant cations such as NaOH, Na_2CO_4, and K_2CO_4 resulted in foam formation; whereas, Na_2SO_4, NaCl, $CaCl_2$ (acidic), or $Ca(OH)_2$ (alkaline) solutions did not. The latter was suggested to be caused by formation of insoluble products of the AEA with the calcium ion. On the other hand, introducing AEA to $CaCO_3$ particles suspended in water resulted in good foaming behavior, which increased with decreasing particle size. $CaCO_3$ was stated to have a low solubility and thus, being present as particles, they were proposed to support good foaming behavior. It was discussed how cement particles in the foam index provides similar behavior and it was recommended to utilize cement in the foam index test. The cement also imparts a constant pH above 12 to the solution [65], which may avoid pH–related surfactant precipitation [43].

In at least two studies, attempts were made at developing analysis methods, different from the foam index test, to determine how fly ash interacts with AEAs in concrete [44, 46]. Adsorption measurements using a UV–visual method have been tested by Baltrus and LaCount [44]. Fly ash was allowed to mix with Darex II AEA followed by removal of solid particles and UV–visual measurements (195–300 nm) of the liquid phase. The results were compared with foam index values and carbon concentrations of pure fly ash samples (cement not included), but no correlation could be established between foam index or carbon concentration and AEA adsorption. The poor correlation between carbon concentration and AEA adsorption was suggested to be caused by low adsorption capacities of carbon, compared with the interference from soluble ions (see section 1.3.3) provided in various amounts by the fly ashes. Hill *et al.* [46] attempted to relate the specific foam index with differential thermal analysis (DTA) curves of fly ashes. The curves appeared to be comprised of three individual overlapping peaks, which could be quantified by a curve fitting program. The low peak temperature areas of the ashes were suggested to represent highly adsorptive, isotropic carbon, but

they could not be related with the specific foam index of the ashes. Further investigation showed that apparently, the low temperature peak was catalytic induced and not related to the AEA adsorptivity.

1.10 Discussion

Fly ash produced from pulverized coal combustion is used in concrete as pozzolanic additive, but has in some cases been reported to interact with air–entraining admixtures (AEAs), which are important to enhance air entrainment in concrete. The interaction between AEAs and fly ash appears to be related to the residual carbon present in fly ash due to its capability to adsorb the AEAs in the concrete mixture. Regulations for approval of fly ash as concrete additive are typically based on the carbon content determined by the loss–on–ignition test (LOI). However, the wide installation of improved combustion technologies in order to reduce NO_x emissions has lead to generation of fly ashes containing residual carbon having a higher adsorption capacity of AEAs (per unit mass of carbon). Therefore, fly ashes can show poor performance in concrete utilization even at LOI values within the established regulations. There are still some unresolved issues within this field, and we recommend the following potential subjects to be included in further work.

- Steps should be taken toward a better understanding of the relationship between combustion conditions and fly ash quality. This could be beneficial in future design of combustion technologies, where both low NO_x emissions and high fly ash quality may be achieved. Experimental work should be performed to reveal if small changes in the combustion process at certain conditions (e.g. temperatures or excess air) have impact on the fly ash quality without influencing the NO_x emission significantly.

- The relative contribution of soot and char to poor fly ash quality is still an unresolved issue which need further investigation. Methods to distinguish and separate soot from char need to be further developed in order to verify if soot contributes to the poor performance of some fly ashes in concrete. Moreover, work should include optimization of combustion conditions in order to avoid soot formation and destroy or passivate formed soot in the furnace.

- An alternative approach to improve fly ash quality, other than changing combustion conditions, is implementation of post–treatment methods.

Published data have shown that it is possible to reduce AEA requirements of fly ash by thermal or ozone treatment without removal or only partial removal of carbon. Reintroduction of fly ash into the furnace or separation of the high carbon fraction may solve the problem as well. However, the latter has been reported to not always improve the fly ash performance in concrete [51]. Both model and further experimental work will be useful in predicting optimal conditions, which can be implemented in simple and economical feasible utilities.

- The demand of renewable energy sources has increased the use of biomass in the production of heat and electricity. Approval of fly ash from biomass combustion as concrete additive may give rise to new problems with air entrainment in concrete, especially in power plants where highly reducing combustion conditions are implemented. Only few studies have focused on this field and additional experiments and case studies are necessary to uncover whether there is a problem. Combustion of other alternative fuels may also affect the fly ash quality, e.g. fly ash from coal/petroleum coke co-firing has shown a low AEA adsorption capacity.

- The commonly used foam index test to determine how fly ash interacts with AEAs appears to have a low reproducibility. The influence of several testing parameters causes a low reproducibility of the test, making it difficult to standardize. Further work needs to be done in order to be able to more exactly compare ashes and distinguish good ashes from poor ashes. Development of a standardized method should eventually lead to establishment of criteria for acceptable limits of fly ash interference with air entrainment in concrete. The method may be based on pure surfactants instead of commercial AEAs and it ought to avoid any influence from the operator, e.g. no visual observation of foam stability.

- It has been shown that both the particle size and the surface chemistry of carbon have impact on AEA adsorption. Detailed characterization of available adsorption sites, controlled by carbon properties such as porosity and surface complexes, can help in development of diffusion models for the AEAs into carbon in the concrete mixtures. A model can be used as a tool to quantitatively predict AEA requirements, both initial and over time, to obtain the needed air entrainment in fly ash concrete mixtures. It may include other interfering parameters such as formation of insoluble compounds, particles, ionic strength, mixing procedure and handling.

- The announced regulation of mercury emission from U.S. power plants [106] may include injection of powdered activated carbon (PAC) into the flue gas before particle separators [107]. The PAC's have an impact on the commercial utilization of fly ash in the production of concrete, due to their capability of adsorbing AEA's, as published foam index results have shown [108, 109]. Zhou *et al.* [109] suggest a range of measures to avoid the problem: 1) injection of mercury sorbent after the particulate collector, 2) deactivation or separation of the carbon in generated fly ash and 3) use a sorbent material, which does not or only to a small extent adsorb the AEAs. The study presented a mercury sorbent that appeared to fulfill the latter requirement. Regulation of mercury emissions is an important growth area and numerous papers have been published. The reader can find more information about this field in published reviews [106, 107, 110–112].

1.11 Acknowledgments

The research activities of CHEC are co-funded by the Technical University of Denmark, DONG Energy A/S, Vattenfall A/S, Energinet.dk, the Danish Council for Production and Technology Sciences, the Danish Energy Research Programme, Nordic Energy Research, EU, and many industrial partners.

1.12 References

[1] International Energy Annual 2002, World Coal Consumption 1980–2002, Energy Information Administration (EIA), U.S. Department of Energy.
URL `http://www.eia.doe.gov/pub/international/iealf/table29.xls`

[2] L. D. Smoot, Fundamentals of coal combustion for clean an efficient use, Elsevier, Amsterdam, 1993, Ch. 1.

[3] S. R. Turns, An introduction to combustion: concepts and applications, 2nd Edition, McGraw-Hill International Editions, Singapore, 2000.

[4] M. L. Hall, W. R. Livingston, Fly ash quality, past, present and future, and the effect of ash on the development of novel products, Journal of Chemical Technology and Biotechnology 77 (3) (2002) 234–239.

[5] M. M. Maroto-Valer, D. N. Taulbee, J. C. Hower, Novel separation of the differing forms of unburned carbon present in fly ash using density gradient centrifugation, Energy and Fuels 13 (4) (1999) 947–953.

[6] B. Sander, Elsam Engineering A/S, Denmark, Personal communication (June 2006).

[7] N. de Nevers, Air pollution control engineering, 2nd Edition, McGraw-Hill International Editions, Singapore, 2000, pp. 266–280.

[8] R. Gieré, L. E. Carleton, G. R. Lumpkin, Micro- and nanochemistry of fly ash from a coal-fired power plant, American Mineralogist 88 (2003) 1853–1865.

[9] Europes's environment: the third assessment, Environmental assessment report no. 10, European Environment Agency (EEA), Copenhagen, Denmark (2003).

[10] 2004 coal combustion product (CCP) - production and use survey, Tech. rep., American Coal Ash Association, Aurora (2005).
URL `http://www.acaa-usa.org/PDF/2004_CCP_Survey(9-9-05).pdf`

[11] Production and Utilisation of CCPs in 2003 in Europe, European Coal Combustion Products Association, ECOBA.
URL `http://www.ecoba.org/index.html`

[12] J. Tomeczek, Coal combustion, Krieger Publishing Company, Malabar, Florida, 1994, Ch. 3.

[13] P. C. Hewlett (Ed.), Lea's chemistry of cement and concrete, 4th Edition, Elsevier Butterworth-Heinemann, Oxford, 1998, pp. 32, 243, 480–485, 843–849, 908.

[14] V. S. Ramachandran (Ed.), Concrete admixtures handbook. Properties, science, and technology, 1st Edition, Noyes Publications, New Jersey, 1984, pp. 1–2, 276.

[15] H. F. W. Taylor, Cement chemistry, 2nd Edition, Thomas Telford, London, 1997, pp. 261–262, 272–280.

[16] K. Wesche (Ed.), Fly ash in concrete: properties and performance, 1st Edition, E & FN Spoon, London, 1991, pp. 3–24, 42–62, 117–143.

[17] M. Maroto-Valer, D. Taulbee, J. Hower, Characterization of differing forms of unburned carbon present in fly ash separated by density gradient centrifugation, Fuel 80 (6) (2001) 795–800.

[18] O. E. Manz, Coal fly ash: a retrospective and future look, Fuel 78 (2) (1999) 133–136.

[19] R. M. Dilmore, R. D. Neufeld, Autoclaved aerated concrete produced with low-NO_x burner/selective catalytic reduction fly ash, Journal of Energy Engineering 127 (2) (2001) 37–50.

[20] ASTM Standard specification for coal fly ash and raw or calcined natural pozzolan for use in concrete (C618-05), Vol. 04.02 of Annual Book of ASTM standards, Concrete and Aggregates, American Society for Testing Materials, 2005.

[21] M. Rhodes, Introduction to particle technology, 1st Edition, John Wiley & Sons, Chichester, 1998, pp. 55–69.

[22] R. H. Hurt, J. R. Gibbins, Residual carbon from pulverized coal fired boilers: 1. size distribution and combustion reactivity, Fuel 74 (4) (1995) 471–480.

[23] R. Helmuth, Fly ash in cement and concrete, 1st Edition, Portland Cement Association, Illinois, 1987, pp. 58–64, 80–82.

[24] I. Külaots, R. H. Hurt, E. M. Suuberg, Size distribution of unburned carbon in coal fly ash and its implications, Fuel 83 (2) (2004) 223–230.

[25] A. M. Paillére, Application of admixtures in concrete, 1st Edition, E & FN Spoon, London, 1995, pp. 17–22.

[26] G. M. Bruere, Air-entraining actions of anionic surfactants in Portland cement pastes, Journal of Applied Chemistry and Biotechnology 21 (1971) 61–64.

[27] M. R. Rixom, N. P. Mailvaganam, Chemical admixtures for concrete, 2nd Edition, E & FN Spoon, London, 1986, pp. 95–100.

[28] R. Rixom, The economic aspects of admixture use, Cement and Concrete Composites 20 (1998) 141–147.

[29] V. H. Dodson, Concrete admixtures, 1st Edition, Van Nostrand Reinhold, New York, 1990, pp. 129–164.

[30] J. Nasvik, M. Pistilli, Are we placing too much air in our concrete?, Concrete Construction - World of Concrete 49 (2) (2004) 51–55.

[31] Y.-M. Gao, H.-S. Shim, R. H. Hurt, E. M. Suuberg, N. Y. C. Yang, Effects of carbon on air entrainment in fly ash concrete: The role of soot and carbon black, Energy and Fuels 11 (2) (1997) 457–462.

[32] M. T. Hasholt, Afklaring af problemer med NJV-flyveaske. Trin 1: Gennemgang af recepter, Tech. Rep. 1, Danish Technological Institute, Taastrup, Denmark (2002).

[33] N. Bouzoubaa, M. H. Zhang, V. M. Malhotra, Laboratory-produced high-volume fly ash blended cements: Compressive strength and resistance to the chloride-ion penetration of concrete, Cement and Concrete Research 30 (7) (2000) 1037–1046.

[34] A. Samarin, R. L. Munn, J. B. Ashby, The use of fly ash in concrete – Australian experience, in: Proceedings of the Canmet/ACI. First International Conference on the Use of Fly Ash, Silica Fume, Slag and Other Mineral By-Products in Concrete, Vol. 1, 1983, pp. 143–172.

[35] D. S. Zhang, Air entrainment in fresh concrete with pfa, Cement and Concrete Composites 18 (6) (1996) 409–416.

[36] R. K. Dhir, M. J. McCarthy, M. C. Limbachiya, H. I. El Sayad, D. S. Zhang, Pulverized fuel ash concrete: Air entrainment and freeze/thaw durability, Magazine of Concrete Research 51 (1) (1999) 53–64.

[37] S. Gebler, P. Klieger, Effects of fly ash on the air-void stability of concrete, in: Proceedings of the Canmet/ACI. First International Conference on the Use of Fly Ash, Silica Fume, Slag and Other Mineral By-Products in Concrete, Vol. 1, 1983, pp. 103–142.

[38] D. S. Lane, Testing fly ash in mortars for air-entrainment characteristics, Cement, Concrete and Aggregates 13 (1) (1991) 25–31.

[39] T. G. Clendenning, N. D. Durie, Properties and use of fly ash from a steam plant operating under variable load, in: Proceeding of the American Society for Testing Materials, Vol. 62, 1963, pp. 1019–1040.

[40] L. Hachmann, A. Burnett, Y.-M. Gao, R. H. Hurt, E. M. Suuberg, Surfactant adsorptivity of solid products from pulverized-coal combustion under controlled conditions, in: Proceedings of the Combustion Institute, Vol. 27, 1998, pp. 2965–2971.

[41] R. L. Hill, S. L. Sarkar, R. F. Rathbone, J. C. Hower, An examination of fly ash carbon and its interactions with air entraining agent, Cement and Concrete Research 27 (2) (1997) 193–204.

[42] E. Freeman, Y.-M. Gao, R. Hurt, E. Suuberg, Interactions of carbon-containing fly ash with commercial air-entraining admixtures for concrete, Fuel 76 (8) (1997) 761–765.

[43] I. Külaots, A. Hsu, R. H. Hurt, E. M. Suuberg, Adsorption of surfactants on unburned carbon in fly ash and development of a standardized foam index test, Cement and Concrete Research 33 (12) (2003) 2091–2099.

[44] J. P. Baltrus, R. B. LaCount, Measurement of adsorption of air-entraining admixture on fly ash in concrete and cement, Cement and Concrete Research 31 (5) (2001) 819–824.

[45] N. R. Greening, Some causes for variation in required amount of air-entraining agent in portland cement mortars, Portland Cement Association – Research and Development Laboratories – Journal 9 (2) (1967) 22–36.

[46] R. Hill, R. Rathbone, J. C. Hower, Investigation of fly ash carbon by thermal analysis and optical microscopy, Cement and Concrete Research 28 (10) (1998) 1479–1488.

[47] R. C. Meininger, Use of fly ash in air-entrained concrete, Report of Recent NSGA-NRMCA Research Laboratory Studies, National Sand and Gravel Association (1981).

[48] J. Yu, I. Külaots, N. Sabanegh, Y. Gao, R. Hurt, E. Suuberg, *et al.*, Adsorptive and optical properties of fly ash from coal and petroleum coke co-firing, Energy and Fuels 14 (3) (2000) 591–596.

[49] J. M. Veranth, D. W. Pershing, A. F. Sarofim, J. E. Shield, Sources of unburned carbon in the fly ash produced from low-NO_x pulverized coal combustion, in: Proceedings of the Combustion Institute, Vol. 27, 1998, pp. 1737–1744.

[50] J. M. Veranth, T. H. Fletcher, D. W. Pershing, A. F. Sarofim, Measurement of soot and char in pulverized coal fly ash, Fuel 79 (9) (2000) 1067–1075.

[51] Y. Gao, I. Külaots, X. Chen, E. M. Suuberg, R. H. Hurt, J. M. Veranth, The effect of solid fuel type and combustion conditions on residual carbon properties and fly ash quality, in: Proceedings of the Combustion Institute, Vol. 29, 2002, pp. 475–483.

[52] ASTM Standard test methods for sampling and testing fly ash or natural pozzolans for use in Portland-cement concrete (C311-04), Vol. 04.02 of Annual Book of ASTM standards, Concrete and Aggregates, American Society for Testing Materials, 2004, p. 206.

[53] Y. Zhang, Z. Lu, M. M. Maroto-Valer, J. M. Andrésen, H. H. Schobert, Comparison of high-unburned-carbon fly ashes from different combustor types and their steam activated products, Energy and Fuels 17 (2) (2003) 369–377.

[54] M. Fan, R. C. Brown, Comparison of the loss-on-ignition and thermogravimetric analysis techniques in measuring unburned carbon in coal fly ash, Energy and Fuels 15 (6) (2001) 1414–1417.

[55] R. C. Brown, J. Dykstra, Systematic errors in the use of loss-on-ignition to measure unburned carbon in fly ash, Fuel 74 (4) (1995) 570–574.

[56] O. Özdemir, M. S. Çelik, Characterization and recovery of lignitic fly ash byproducts from the Tuncbilek power station, Canadian Metallurgical Quarterly 41 (2) (2002) 143–150.

[57] S. C. Burris, D. Li, J. T. Riley, Comparison of heating losses and macro thermogravimetric analysis procedures for estimating unburned carbon in combustion residues, Energy and Fuels 19 (4) (2005) 1493–1502.

[58] European Committee for Standardization, Brussels, Fly ash for concrete - Part 1: Definition, specifications and conformity criteria (EN 450–1) (2005).

[59] M. T. Hasholt, Afklaring af problemer med NJV-flyveaske. Trin 2: Undersøgelse af asken vha. foam index-metoden, Tech. Rep. 2, Danish Technological Institute, Taastrup, Denmark (2003).

[60] I. Külaots, Ph.D. thesis, Division of Engineering, Brown University (2001).

[61] S. Brunauer, P. H. Emmett, E. Teller, Adsorption of gases in multimolecular layers, Journal of the American Chemical Society 60 (1938) 309–319.

[62] I. Külaots, I. Aarna, M. Calleto, R. H. Hurt, E. M. Suuberg, Development of porosity during coal char combustion, in: Proceedings of the Combustion Institute, Vol. 29, 2002, pp. 495–501.

[63] H. Ban, T. X. Li, J. C. Hower, J. L. Schaefer, J. M. Stencel, Dry triboelectrostatic beneficiation of fly ash, Fuel 76 (8) (1997) 801–805.

[64] J. Payá, J. Monzó, M. Borrachero, E. Perris, F. Amahjour, Thermogravimetric methods for determining carbon content in fly ashes, Cement and Concrete Research 28 (5) (1998) 675–686.

[65] X. Chen, M. Farber, Y. Gao, I. Kulaots, E. M. Suuberg, R. H. Hurt, Mechanisms of surfactant adsorption on non-polar, air-oxidized and ozone-treated carbon surfaces, Carbon 41 (8) (2003) 1489–1500.

[66] Y. Gao, I. Külaots, X. Chen, R. Aggarwal, A. Mehta, E. M. Suuberg, *et al.*, Ozonation for the chemical modification of carbon surfaces in fly ash, Fuel 80 (5) (2001) 765–768.

[67] N. V. Beck, S. E. Meech, P. R. Norman, L. A. Pears, Characterisation of surface oxides on carbon and their influence on dynamic adsorption, Carbon 40 (4) (2002) 531–540.

[68] J. C. Hower, R. F. Rathbone, T. L. Robl, G. A. Thomas, B. O. Haeberlin, A. S. Trimble, Case study of the conversion of tangential- and wall-fired units to low-NO_x combustion: Impact on fly ash quality, Waste Management 17 (4) (1997) 219–229.

[69] J. C. Hower, R. F. Rathbone, U. M. Graham, J. G. Groppo, S. M. Brooks, T. L. Robl, *et al.*, Approaches to the petrographic characterization of fly ash, in: Proceedings of the 11th International Coal Testing Conference, 1995, pp. 49–54.

[70] J. C. Hower, M. M. Maroto-Valer, D. N. Taulbee, T. Sakulpitakphon, Mercury capture by distinct fly ash carbon forms, Energy and Fuels 14 (1) (2000) 224–226.

[71] J. C. Hower, T. L. Robl, G. A. Thomas, Changes in the quality of coal combustion by-products produced by Kentucky power plants, 1978 to 1997: consequences of clean air act directives, Fuel 78 (6) (1999) 701–712.

[72] S. Wang, E. Liamozas, A. B. Miller, L. L. Baxter, The effects of adding biomass fly ash to concrete, in: Proceedings of the 15th international

coal ash association symposium on manegement & use of coal combustion products, 2003, pp. 93,1–15.

[73] F. J. M. Lamers, J. L. J. Vissers, J. W. van der Berg, Effects of co-combustion of secondary fuels on fly ash quality, in: Seventh CANMET/ACI international conference on fly ash, silica fume, slag and natural pozzolans in concrete, Vol. 1, American concrete institute, 2001, pp. 433–457.

[74] X. Jun, X. Sun, S. Hu, D. Yu, An experimental research on boiler combustion performance, Fuel Processing Technology 68 (2) (2000) 139–151.

[75] H. Maier, H. Spliethoff, A. Kicherer, A. Fingerle, K. R. G. Hein, Effect of coal blending and particle size on NO_x emission and burnout, Fuel 73 (9) (1994) 1447–1452.

[76] R. F. Storm, Optimizing combustion in boilers with low-NO_x burners, Power 137 (10) (1993) 53–4, 56, 58, 60, 62.

[77] Clean coal technology: Reducing emissions of nitrogen oxides via low-NO_x burner technologies, Topical report number 5, The U.S Department of Energy (DOE) (1996).
URL `http://www.netl.doe.gov/cctc/topicalreports/documents/topical5.pdf`

[78] C. Giovando, Markets grow for coal-combustion byproducts., Power 145 (1) (2001) 33–39.

[79] R. H. Hurt, K. A. Davis, N. Y. C. Yang, T. J. Headley, G. D. Mitchell, Residual carbon from pulverized-coal-fired boilers : 2. morphology and physicochemical properties, Fuel 74 (9) (1995) 1297–1306.

[80] K. A. Davis, R. H. Hurt, N. Y. C. Yang, T. J. Headley, Evolution of char chemistry, crystallinity, and ultrafine structure during pulverized-coal combustion, Combustion and Flame 100 (1995) 31–40.

[81] J. C. Hower, G. A. Thomas, J. Palmer, Impact of the conversion to low-NO_x combustion on ash characteristics in a utility boiler burning western US coal, Fuel Processing Technology 61 (3) (1999) 175–195.

[82] L. S. Xiao, J. F. Cheng, H. C. Zeng, Effects of bluff-body burner and coal particle size on NO_x emissions and burnout, Journal of the Institute of Energy 72 (493) (1999) 112–116.

[83] R. P. van der Lans, P. Glarborg, K. Dam-Johansen, P. Knudsen, G. Hesselmann, P. Hepburn, Influence of coal quality on combustion performance, Fuel 77 (12) (1998) 1317–1328.

[84] M. Kurihara, K. Ikeda, Y. Izawa, Y. Deguchi, H. Tarui, Optimal boiler control through real-time monitoring of unburned carbon in fly ash by laser-induced breakdown spectroscopy, Applied Optics 42 (30) (2003) 6159–6165.

[85] A. A. Lizzio, A. Piotrowski, L. R. Radovic, Effect of oxygen chemisorption on char gasification reactivity profiles obtained by thermogravimetric analysis, Fuel 67 (12) (1988) 1691–1695.

[86] W.R. Grace & Co.-Conn., Cambridge, Darex II AEA data sheet. URL http://www.na.graceconstruction.com/concrete/download/AIR-3G_1.pdf

[87] The Euclid Chemical Company, Eucon air-series, Technical data. URL http://www.euclidchemical.com/fileshare/ProductFiles/techdata/EuconAirSeries(1).pdf

[88] D. J. Corr, J. Lebourgeois, P. J. M. Monteiro, S. J. Bastacky, E. M. Gartner, Air void morphology in fresh cement pastes, Cement and Concrete Research 32 (7) (2002) 1025–1031.

[89] N. R. Laine, F. J. Vastola, P. L. Walker, Jr., Importance of active surface area in carbon-oxygen reaction, Journal of Physical Chemistry 67 (10) (1963) 2030–2034.

[90] A. A. Lizzio, H. Jiang, L. R. Radovic, On the kinetics of carbon (char) gasification: Reconciling models with experiments, Carbon 28 (1) (1990) 7–19.

[91] J. K. Floess, J. P. Longwell, A. F. Sarofim, Intrinsic reaction kinetics of microporous carbons. 2. catalyzed chars, Energy and Fuels 2 (6) (1988) 756–764.

[92] J. G. Keppeler, Full scale carbon burn-out and ammonia removal experience, in: 2000 Conference on Unburned Carbon on Utility Fly Ash, U.S Department of Energy, National Energy Technology Laboratory, 2000, pp. 1–4.

[93] R. Hurt, E. Suuberg, Y.-M. Gao, A. Burnett, Apparatus and method for deactivating carbon in fly ash, U.S. patent no. 6,136,089, Brown University Research Foundation (Providence, RI) (October 2000).

[94] X. Chen, Y. Gao, R. H. Hurt, E. M. Suuberg, A. K. Mehta, Ozone treatment of fly ash, U.S. patent no. 6,890,507, Brown University Research Foundation (Providence, RI) (May 2005).

[95] M. L. Gray, K. J. Champagne, Y. Soong, D. H. Finseth, Parametric study of the column oil agglomeration of fly ash, Fuel 80 (6) (2001) 867–871.

[96] M. L. Gray, K. J. Champagne, Y. Soong, R. P. Killmeyer, M. M. Maroto-Valer, J. M. Andrésen, *et al.*, Physical cleaning of high carbon fly ash, Fuel Processing Technology 76 (1) (2002) 11–21.

[97] Y. Soong, M. R. Schoffstall, M. L. Gray, J. P. Knoer, K. J. Champagne, R. J. Jones, *et al.*, Dry beneficiation of high loss-on-ignition fly ash, Separation and Purification Technology 26 (2002) 177–184.

[98] I. I. Inculet, M. A. Bergougnou, J. D. Brown, Electrostatic separation of particles below 40 μm in a dilute phase continuous loop, IEEE Transactions on Industry Applications IA-13 (4) (1977) 370–373.

[99] E. Tondu, W. G. Thompson, D. R. Whitlock, J. D. Bittner, A. Vasiliauskas, Commercial separation of unburned carbon from fly ash, Mining Engineering (Littleton, Colorado) 48 (6) (1996) 47–50.

[100] L. A. Zekel, N. V. Krasnobaeva, M. Y. Shpirt, Electroseparation of fly ash of coal combustion for power generation, Solid Fuel Chemistry 38 (3) (2004) 72–81.

[101] M. Niewiadomski, J. Hupka, R. Bokotko, J. D. Miller, Recovery of coke fines from fly ash by air sparged hydrocyclone flotation, Fuel 78 (2) (1999) 161–168.

[102] J. P. Baltrus, J. R. Diehl, Y. Soong, W. Sands, Triboelectrostatic separation of fly ash and charge reversal, Fuel 81 (6) (2002) 757–762.

[103] J. G. Groppo, T. L. Robl, U. M. Graham, C. J. McCormick, Selective beneficiation for high loss-of-ignition fly ash, Mining Engineering (Littleton, Colorado) 48 (6) (1996) 51–53.

[104] J. P. Baltrus, A. W. Wells, D. J. Fauth, J. R. Diehl, C. M. White, Characterization of carbon concentrates from coal-combustion fly ash, Energy and Fuels 15 (2) (2001) 455–462.

[105] J. Makansi, Diverse techniques help create markets for flyash, Power 138 (8) (1994) 37–41.

[106] J. H. Pavlish, E. A. Sondreal, M. D. Mann, E. S. Olson, K. C. Galbreath, D. L. Laudal, *et al.*, Status review of mercury control options for coal-fired power plants, Fuel Processing Technology 82 (2003) 89–165.

[107] T. D. Brown, D. N. Smith, R. A. Hargis Jr., W. J. O'Dowd, Mercury measurement and its control: what we know, have learned, and need to further investigate, Air and Waste Management Association (1999) 1–97.

[108] C. Senior, C. J. Bustard, M. Durham, K. Baldrey, D. Michaud, Characterization of fly ash from full-scale demonstration of sorbent injection for mercury control on coal-fired power plants, Fuel Processing Technology 85 (6-7) (2004) 601–612.

[109] Q. Zhou, Y. Zhang, S. Nelson Jr., R. Minkara, Evaluations of concretes containing mercury sorbents, Combined Power Plant Air Pollutant Control Mega Symposium (2004) 917–929.

[110] A. A. Presto, E. J. Granite, Survey of catalysts for oxidation of mercury in flue gas., Environmental Science and Technology 40 (18) (2006) 5601–5609.

[111] C. L. Senior, S. A. Johnson, Impact of carbon–in–ash on mercury removal across particulate control devices in coal–fired power plants, Energy and Fuels 19 (3) (2005) 859–863.

[112] C. L. Senior, J. J. Helble, A. F. Sarofim, Emissions of mercury, trace elements, and fine particles from stationary combustion sources, Fuel Processing Technology 65-66 (2000) 263–288.

Chapter 2

Replacement of the Foam Index Test with Surface Tension Measurements

Abstract. The foam index test is the method usually employed to determine the degree of fly ash interference with air entrainment in concrete. The test involves the use of commercial air-entraining admixtures (AEAs) and visual observation of foam stability. These facts reduce the reproducibility of the test, because commercially available AEAs vary in strength, and the criteria for foam stability are operator dependent. Therefore, it is of interest to develop a reproducible method, which is able to determine the fly ash quality with respect to air entrainment in concrete. This paper presents efforts toward the development of a new method based on dynamic surface tension measurements, using the bubble pressure method, on filtrate from a fly ash and cement suspension. A pure surfactant is added to the suspension as a substitute for a commercial AEA. The new method and the foam index test have been compared on fly ashes acquired from power plants in Denmark and the U.S. The results reveal a good relationship between the two methods, but the new method requires further work before a finished procedure is accomplished. Finally, it has been shown that changes in temperature affect both test methods.

2.1 Introduction

Fly ash quality, with respect to interference with air entrainment in concrete, is commonly determined by a simple titration method known as the foam index (FI) test [1]. However, the test is diffucult to standardize due

to problems like variations in strength of commercial air-entraining admixtures (AEAs) [2] and the individual operator criteria of foam stability. In the present work, steps are taken toward the development of a test method based on surface tension measurements instead and which uses the anionic surfactants, sodium dodecyl benzene sulfonate (SDBS) as a substitute for the commercial AEA. SDBS further benefits from that its chemical nature makes it suitable for quantitative analysis using UV–absorbance; the absorbance maximum of alkylbenzensulfonates is about 223 nm [3]. Basing the test on surface tension measurements is argued from that the foaming behavior and foam film stability is influenced by the liquid phase composition such as ionic strength [2, 4], insoluble compounds [2], pH [2, 5] and concentration of surface active compounds [4, 6]. Again, many of these parameters affect the surface tension of the liquid phase [7] and a relationship between foam stability and surface tension has been shown [8].

In summary, the final goal is to develop a reproducible method which is able to detect even small differences in fly ash adsorption capacity of surfactants.

2.2 Experimental

2.2.1 Materials

The method developed was evaluated on nine fly ash samples, activated carbon and pure cement. Furthermore, a carbon free fly ash sample was included in the test. The carbon was removed by heating the ash for two hours at 740 °C in atmospheric air. The fly ashes were produced from combustion of bituminous coal or anthracites and are acquired from Danish and U.S. power plants. Their carbon contents range from 2.2 to 30.6 wt% and was determined using an ELTRA model CS-800 apparatus. The activated carbon powder (Norit GSX 100 mesh size) came from Lancaster Synthesis GmbH. A commercial Portland cement (Rapid) with a fineness of 444 m^2/kg and 2.4 wt% loss-of-ignition was included in the test. The cement was provided by Aalborg Portland A/S. Particle size measurements were carried out in dry state using a Malvern Mastersizer. SDBS purchased from Sigma-Aldrich Chemie GmbH was used in the surface tension measurements. The critical micelle concentration (CMC) of SDBS was determined by isothermal titration calorimetry on a MicroCal ITC-2000 calorimeter [9]. The AEA used in the FI test was Conplast 316 AEA. According to the manufacturer (Fosroc), it is a "chloride free air-entraining admixture on a synergistic blend of naturally occurring surfactants".

2.2.2 Foam Index Test

The procedure for the FI test is similar to that which others have proposed [2, 10, 11]. 2 grams of fly ash, 8 grams of Portland cement, and 25 ml of deionized water were poured into a cylindrical glass vessel being 6 cm in diameter, which was capped and shaken on a vortex shaker for 1 minute. A 5 vol% aqueous solution of AEA was added in small aliquot amounts (20 μl) from a diluter and the vessel was shaken for another 15 seconds. The foam was observed for stability, i.e. defined as no bursting of bubbles within 30 seconds. In case the foam was unstable, more AEA was added, and the procedure was repeated until the foam remained stable. The FI test was carried out at least two times on each ash sample, and the reported value is the average. The actual FI value is obtained by subtracting from the measured value the value of a blank performed on a pure cement, and it is given in milliliters per 2 gram of fly ash or normalized to the carbon content in the ash, also known as the spec. FI.

2.2.3 Surface Tension Measurements

The sample preparation differs only slightly from the FI test. The test involved placing 2 grams of fly ash and 8 grams of cement in a plastic beaker. 25 ml of an aqueous SDBS solution (0.5–1.0 g/l) was introduced into the beaker, and it was shaken for 5–30 minutes during the optimizing process of the test and 10 minutes in the final experiments. The suspension was centrifuged for 1 minute followed by filtration of the supernatant (0.45 μm cellulose acetate filter). Surface tension measurements based on the maximum bubble pressure method were carried out on the filtrate using a SITA tensiometer model science line t60. The samples were prepared two times unless otherwise stated, and the reported surface tension is an average of at least five subsequent measurements. In case the difference between the double determinations was higher than 1 mN/m, the sample was prepared a third time and an average of all three samples are reported. The minimum of five subsequent surface tension measurements was chosen as compromise between reducing the standard error and keeping the testing time low. Cement was included in the sample preparation, in order to achieve mixture conditions corresponding to the FI test and to reduce interference from soluble ions provided by the fly ash as suggested by others [12].

The maximum bubble pressure method is a fast and reliable way to determine the dynamic surface tension [13]. Compared with static methods, the surface age in dynamic methods is too short to obtain equilibrium tension where no further surfactants diffuse to the surface [7]. A capillary is

introduced into the solution and bubbles are grown on the tip. The pressure difference required in the bubble formation is proportional to the surface tension of the solution [14]. Due to the dynamic behavior of the test method, increasing bubble lifetimes will cause lower measured surface tensions [13]. Thus, method development included determination of optimal bubble lifetime.

2.2.4 UV-measurements

Initially, the maximum absorbance of SDBS in H_2O and in aqueous filtrate containing electrolytes, such as Ca^{++} and Mg^{++} [12, 15], provided from a cement and fly ash suspension, was determined. The calibration curve of SDBS was constructed from various concentrations of SDBS in H_2O up to 0.1 g/l, which was the limit for the absorbance measurements. Different SDBS concentrations in 5, 10 and 20 vol% solutions of filtrate from a cement and fly ash suspension were prepared to study any deviation from the calibration curve based on SDBS in H_2O. All measurements were corrected by a background measurement on diluted filtrate alone corresponding to the applied solutions (5 to 20 vol%). Pharmacia Biotec Ultraspec 3000 was used as spectrophotometer.

The fly ash and cement samples were prepared similar to the surface tension measurements and the SDBS solution was added in 0.6 and 1.8 g/l concentrations. In addition, a background was prepared from adding pure water to the fly ash and cement. The resulting filtrates were diluted before the UV–measurements to get below the limit of electrolyte interference, which was determined from the calibration curve of SDBS in pure water and the SDBS in the filtrate solutions. 0.6 g/l SDBS solutions were also prepared in pure filtrates from cement and cement/fly ash samples and in the same filtrates diluted two times with water. The solutions were allowed to stand for 3 days to ensure equilibrium. The resulting precipitates were removed by filtering and the filtrates were diluted for the UV–measurements. The measured concentrations of SDBS in the filtrates were used to estimate the precipitated fraction of SDBS.

2.3 Results and Discussion

2.3.1 Foam Index Values

FI values from which the blank value of pure cement has been subtracted and spec. FI values are shown in Figs. 2.1a and 2.1b, respectively. The

results support the trends shown in past publications [1, 16, 17]: the FI tends to increase with the fly ash carbon content (Fig. 2.1a); but the unburned carbon in fly ash can show quite different adsorption capacities of AEAs (Fig. 2.1b). The FI value of the burned ash further proves how the residual carbon contributes to increased AEA requirements. The FI went from 0.26 ml/2 g fly ash (2.8 wt% carbon) to 0.04 ml/2 g fly ash when the carbon was removed, which is similar to what others have observed [2].

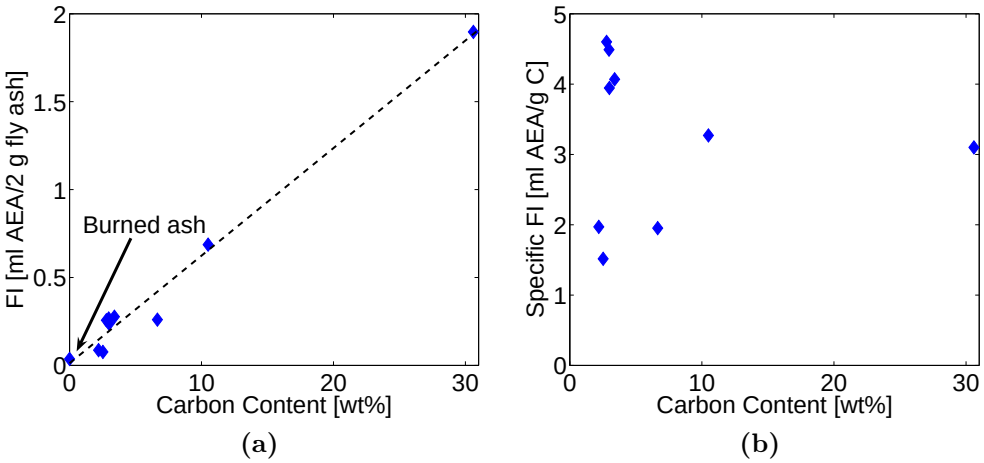

Figure 2.1: (a) FI values compared with carbon content of fly ash. (b) FI values normalized into ml AEA pr. gram of carbon in the ashes.

Attempts to carry out the FI test with SDBS as AEA substitute were done in the present work as in the study by Külaots *et al.* [2]. For unknown reasons, stable foams corresponding to the endpoint of the test could not be obtained in the experiments. The amount of foam increased with adding SDBS, but the bubbles were still bursting within the 30 seconds. Further efforts to solve this problem were not considered.

2.3.2 Optimizing Surface Tension Measurements

Applied bubble lifetime and initial concentration of SDBS in the surface tension measurements are based on the experimental data presented in Figs. 2.2a-2.3a, where the fly ash and cement suspensions have incubated with SDBS in different concentrations for 10 minutes. The results are presented as single determinations. The consequence of having an initial concentration of SDBS on 0.5 g/l is revealed in Fig. 2.2a, where only a minor difference in the measured dynamic surface tension can be detected in a wide span of bubble lifetime between two high carbon ashes. It appears as if both

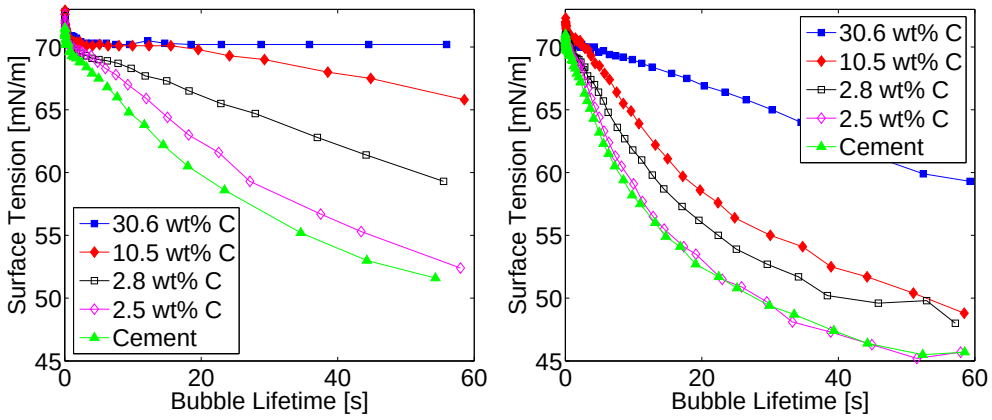

Figure 2.2: Dynamic Surface tension compared with bubble lifetime at (a) 0.5 g SDBS/l and (b) 1 g SDBS/l in initial concentration. The incubation time between surfactants and fly ash/cement was 10 minutes.

ashes have adsorbed most of the added surfactant, making it difficult to measure any difference in their adsorption capacity. On the other hand, an initial concentration of SDBS on 1.0 g/l (Fig. 2.2b) leads to similar dynamic surface tension measurements of both cement and a low carbon ash, indicating that the amount of surfactant adsorbed by the fly ash is low compared to the remaining SDBS in the solution. The CMC of SDBS may explain this observation. Normal surfactant behavior is observed below the CMC, i.e. surfactants are found as monomers and the concentration relates to the surface tension [7]. Above the CMC the hydrophobic part of the surfactant interacts with other surfactants leading to micelle formation, where only the hydrophilic part is in contact with the aqueous phase. The micelles are not surface active and hence will not contribute to changes in surface tension. Published CMC values of SDBS in H_2O range from 0.52 g/l (temperature not provided) [18] to 1.88 g/l (22 °C) [19]. The CMC was in this work determined to approximately 0.24 g/l at 30 °C in H_2O. It is noted, that the CMC for ionic surfactants typically is lowered by the presence of electrolytes [7] but this issue was not further addressed in the present work. In any case, dynamic measurement methods are suitable for concentrations above the CMC opposite to static methods [13]. This was demonstrated on different surface active compounds at temperatures ranging from 30 to 80 °C [13].

Addition of a 0.6 g/l SDBS solution gives a detectable difference between both low and high carbon ashes as shown in Fig. 2.3a. It is evident, how

utilization of a short bubble lifetime leads to similar surface tension results. Equilibrium between surfactants in the solution and at the surface are not

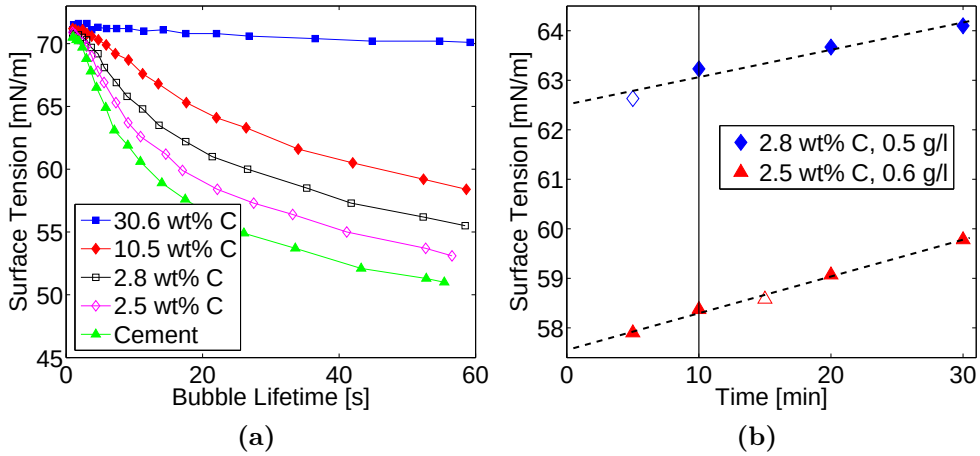

Figure 2.3: (a) Dynamic surface tension versus bubble lifetime at initial SDBS–concentration on 0.6 g/l and 10 minutes in incubation time. (b) Surface tension determined at 21.6–22.0°C (2.8 wt% C) and 22.1-22.5°C (2.5 wt% C) compared with incubation time. The unfilled and filled markers represent single and double determinations respectively. Initial concentration of SDBS = 0.5–0.6 g/l. The solid vertical line corresponds to the usual time of the FI test.

obtained due to a short age of the bubble surface (short adsorption time of the surfactants) and the surface tension of the pure solvent is measured [13], being water in this case (72.3 mN/m at 23 °C). At high bubble lifetime, the surfactants move toward equilibrium and the surface tension is lowered. Hence, any variation in surface tension between the samples can be detected. On the other hand, the difference in surface tension between the samples appears not to increase substantially when a bubble lifetime above 20 seconds is applied, making it a reasonable choice in further measurements. Moreover, testing time will significantly be extended with higher bubble lifetime because the results are based on the average of at least five measurements.

Surface tension measurements of two ashes plotted against the time between surfactant addition to the cement/fly ash sample and centrifuging of the mixture are displayed in Fig. 2.3b, where the surface tension is observed to increase with the time. The intention was to achieve equilibrium conditions, where no further surfactant adsorption took place and in this way, minimize the influence from incubation time on the measurements. The laboratory data show a continuous increase in surface tension with incubation

time likely due to a decrease in surface active compounds, in which the latter support the results reported by others [12, 16, 20]. Freeman *et al.* [16] found that more AEA was required to achieve the endpoint of the FI test with increasing testing time. The observed dynamics in this method are expressed by a higher surface tension with longer incubation time. In fact, the equilibrium is not reached within the 30 minutes, which is at least 20 minutes more than the time of the FI test. Diffusion limitations of surfactants into the carbon particle [16, 20] and formation of insoluble compounds due to presence of CO_2 in the atmosphere [12] may be the reasons. In terms of the latter, it has been suggested that carbonic acid, produced from dissolving of atmospheric CO_2, leads to formation of insoluble free surfactant acids [12], and this was to some extent supported from the present experiments as well: initially during optimizing of the bubble pressure method, the filtrate surface was in contact with atmospheric air resulting in formation of a white precipitate on top of the liquid surface during testing time. This was prevented by conducting the surface tension measurements under nitrogen (only the results in Fig. 2.2a and 2.2b is conducted in atmospheric air). It is noted that others have shown a leveling off in AEA adsorption within 10 minutes, when conducting the experiments under nitrogen [12] or in a closed system [17]. The results of the present experiments, showing a continuous increase in surface tension with time of samples mixed in a closed system, contradict these studies. Incubation time was chosen to 10 minutes corresponding to the usual time of a single FI test. The time is sufficient to detect difference in AEA requirements of the FI test and keeps the testing time of the present method low.

The sensitivity of the surface tension toward the temperature of filtrate prepared from two fly ashes is seen in Fig. 2.4a. The surface tension drops by 0.26 mN/(m °C) (2.8 wt% C) and 0.34 mN/(m °C) (2.5 wt% C) with increasing temperature and the linear decrease is consistent with the literature [7]. To avoid temperature dependency, the filtrate was placed in water bath during the surface tension measurements in order to work close to isothermal conditions within the same experimental series. It is evident that future steps in the method development could include implementation of temperature–correlation. Considering the high temperature sensitivity of the surface tension, it was questioned whether the temperature affects the FI values as well. The subject is addressed in section 2.3.5.

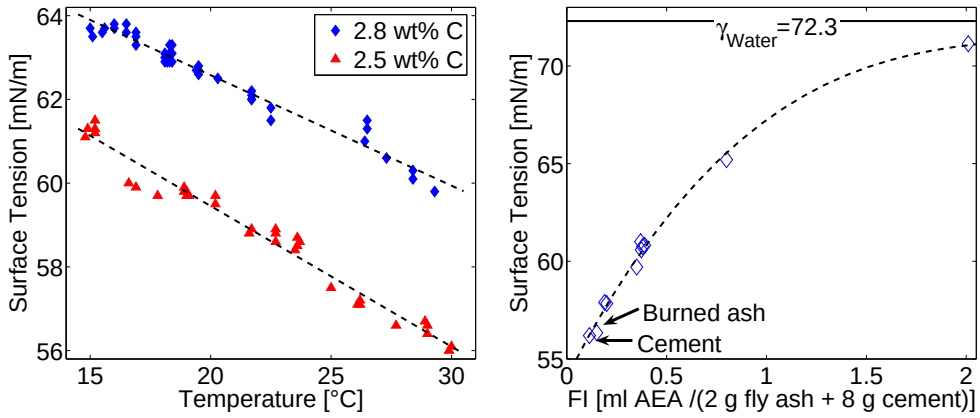

Figure 2.4: (a) Surface tension and temperature measured on the filtrate from two fly ashes (each sample prepared once). 0.6 g/l SDBS in initial concentration and 10 minutes in incubation time. (b) Surface tension of filtrate compared with FI. The temperature of the filtrate was between 22.7–22.9°C. 0.6 g/l SDBS in initial concentration and 10 minutes in incubation time.

2.3.3 Comparison of Surface Tension Measurements and Foam Index

Fig. 2.4b presents surface tension measurements on filtrate from cement/fly ash samples compared with their respective FI values. Cement is included in the evaluation and therefore, the reported FI values have not had the cement (blank) value subtracted. To reduce the influence of the previously described interfering parameters affecting the FI test, all measurements have been conducted by the same operator in one batch within the same day. The results display a good correlation between the two methods. Increasing FI of a fly ash corresponds to higher adsorptivity toward surfactants as previously discussed. In the surface tension method, the concentration of surfactants in the aqueous phase is reduced by the adsorption, leading to higher surface tensions. The correlation appears to be linear within lower adsorption capacities of fly ashes (0–6.7 wt% C). At higher adsorption capacities, the new test meets its limit under the applied conditions. It is obvious, that surface tension values can not exceed the surface tension of the pure liquid (γ_{water}). Thus, ashes with high adsorption capacities will result in filtrates with low surfactant concentrations and show surface tensions close to pure water, making it difficult to detect any variance in their adsorption capacity. Measurements on activated carbon which are highly AEA adsorptive

(FI>14 ml/2 g C) confirm this behavior. The surface tension was measured as 71.9 mN/m, indicating that the surfactants have been exhausted from the supernatant fluid completely. Therefore, in order to detect any difference in surface tension of high adsorption ashes, a greater initial concentration of SDBS must be applied. However, as Fig. 2.2a shows, the difference between ashes with lower adsorption capacities will then be more difficult to detect (section 2.3.2).

2.3.4 Evaluation of Surface Tension Method

The overall repeatability of the method was tested by preparing the same two ashes at least 10 times followed by surface tension determinations and the results are provided in Table 2.1. Given the small surface tension difference

Carbon	[wt%]	2.8	2.5
FI	[ml AEA]	0.38	0.20
No. of meas.		10	11
ST	[mN/m]	61.5	58.8
SD	[mN/m]	0.51	0.48
Range	[mN/m]	60.7–62.4	58.1–59.5
Temperature	[°C]	23.4–23.6	21.0–21.4

Table 2.1: Repeatability of two ashes, SD is the calculated standard deviation. Adsorption time = 10 minutes and initial concentration of SDBS = 0.6 g/l. The FI is given in ml AEA/(2 g fly ash + 8 g cement).

of 2.7 mN/m between the two ashes, which shows quite different FI values, the variation of the test is found to be high, making it difficult to detect small differences in adsorption capacities of ashes. Nevertheless, their 95% confidence intervals are not overlapping and this indicates a significant difference in their adsorption capacities for surfactants. The variation may be caused by the bubble tensiometer and varying ash sample properties. The former is stated to have repeatability error of 0.5 mN/m. This was checked on a 0.2 g/l SDBS solution divided into 6 samples. Surface tension was measured on each sample and was found to be 37.5 mN/m with 0.04 mN/m in standard deviation at 22.1–22.4°C. The results do not explain the poor repeatability. Particle size measurements on repeated ash and cement samples, taken from the same beaker, did not indicate any variation in the size distribution, which might have influenced the varying adsorption behavior as well. Of course, variation in surface area and porosity of the residual carbon are not revealed

from the particle size distribution.

Steps to increase the repeatability and sensitivity of the test can be taken in two directions, i.e. lower the variation within single samples and expand the surface tension scale. We suggest replacing cement with a solution containing a known electrolyte composition and alkalinity corresponding to what a cement suspension would provide. This will, as cement does, minimize the influence of various soluble ions provided by the fly ash [12] but prevent the interference of varying cement properties. As described in section 2.3.2 a white precipitate was formed on the liquid surface when conducting the surface tension measurements under atmospheric air indicating that CO_2 was dissolved in the filtrate. The observation is in contradiction with what others have proposed [2], that the alkaline "buffer" provided by the electrolytes eliminate the influence from CO_2 dissolution. To increase the surface tension scale, it is suggested to change surfactant. As results below reveal (section 2.3.6), a large fraction of SDBS precipitates due to formation of insoluble compounds with the electrolytes in the solution, as observed by others [12]. Surfactants of non-ionic character may avoid this problem, since they are less inclined to salt out [3], and they increase the solubility of metal anionic surfactant salts [21]. Higher sensitivity may also be obtained by changing the initial concentration of surfactant. For instance, if the investigated ashes are known to be within a certain adsorption capacity region, then the initial surfactant concentration could be optimized in order to detect small variations in that particular region.

A fundamental difference between this new method and the FI test is the procedure for adding surfactants. In the FI test, the surfactants are added stepwise until a stable foam is obtained, whereas in the present method, the surfactants are added in one step at the beginning of the test followed by surface tension measurements after a given incubation time. In order to obtain the same order of magnitude between results of different ashes by the two methods, the surface tension method could be based on same principle as the FI test. For instance, the surfactants could be added continuously to a stirred mixture of cement and fly ash while the surface tension of the aqueous phase is measured. The endpoint of the test will be when it reaches a defined surface tension. The rate of adding surfactants are believed to have a significant impact on the result as in the FI test [2] and will require further attention.

2.3.5 Temperature Effects on Foam Index Values

The relationship between temperature and surface tension inspired us to conduct the FI test at two temperatures corresponding to conditions in a room and in a cold outdoor environment. The experimental data are presented in Fig. 2.5a. It appears as if less AEA is required to obtain a stable foam

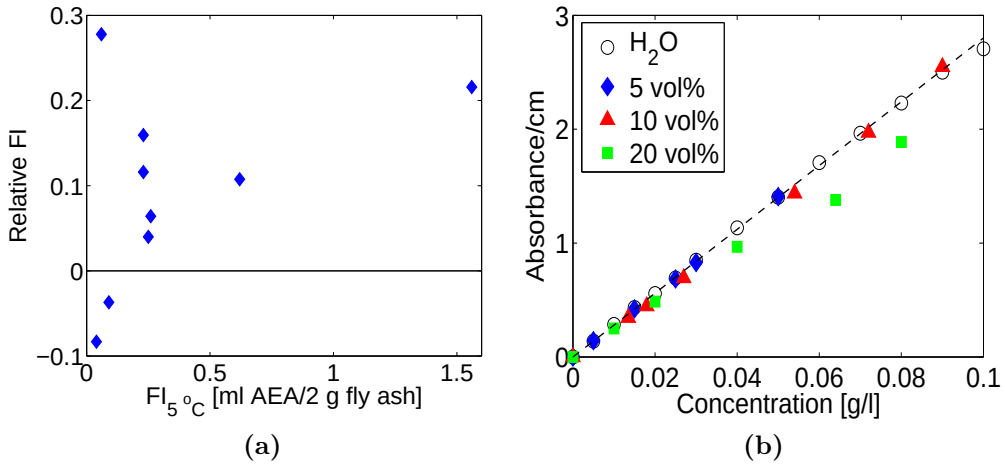

Figure 2.5: (a) Relative difference between FI carried out at 5±1 °C and 27±1 °C $\left(\text{Relative FI} = \frac{\text{FI}_{27\ °\text{C}} - \text{FI}_{5\ °\text{C}}}{\text{FI}_{5\ °\text{C}}}\right)$.
(b) Calibration curve of SDBS in 0–20 vol% aqueous solutions of cement and fly ash filtrate ($C_{SDBS} = 0.036 \cdot ABS$).

at lower temperatures. Only in case of very low FI values (burned ash and fly ash with 2.2 wt% carbon content), the opposite trend is observed, which is believed to be due to that lower values can be presented with greater uncertainties. Temperature effect on foam stability has been investigated by others [22, 23] and a similar trend was observed. Decreasing temperature gives rise to higher viscosities of the liquid phase and this lowers the drainage of the foam film. The increased viscosity may partly be caused by micelle formation, which usually is enhanced at lower temperatures [7]. Thus, the lifetime of the foam is prolonged and less AEA is required to obtain a stable foam. Furthermore, it is possible that diffusion of AEA molecules into the carbon particles is reduced due to lower temperatures (which will apply for the surface tension method as well). The results provide additional problems in standardizing the FI test. Varying testing temperatures due to location, season or even heating of sample by hand give rise to a poor comparability with earlier results.

2.3.6 UV-measurements

In the search of an explanation for the low difference in surface tension measurements between ashes having high difference in FI values, the concentration of SDBS in the cement and fly ash filtrates was determined by UV-measurements.

The maximum absorbance of SDBS dissolved in H_2O was determined to be at 222.3 nm and about 0.5 nm higher when prepared in filtrate containing electrolytes from cement and fly ash. Both samples were mixed in a closed system. The calibration curve obtained at 223 nm in Fig. 2.5b shows linearity up to 0.09 g/l. Good correlation between absorbance and SDBS concentration was obtained in 5–10 vol% solutions of filtrate, even though visible insoluble compounds, presumably being precipitated calcium surfactant salts [15], had formed in the 10 vol% solution. No visible insoluble compounds were formed in the 5 vol% solution. The good linearity could not be obtained at 20 vol% solution, which from a visual comparison had the highest turbidity. Therefore, the following UV–measurement was conducted on filtrate diluted to 10 vol% in water. Results from background measurements showed that the electrolytes only had a small contribution to the absorbance at 223 nm (0.04 at 20 vol% solution).

Table 2.2 provides the laboratory data from adding two different concentrations of SDBS to pure cement and a cement and fly ash sample. Table 2.1 summarize the properties of the fly ash (2.8 wt% carbon), while for cement the FI has been found to 0.12 ml AEA/8 g cement and the surface tension was measured to 56.2 mN/m. In order to be below the limit of electrolyte interference, all resulting filtrates were diluted 10 times before UV-measurements as described above. The results show that 7–8 % of the initial added SDBS

Sample	$C_{SDBS,0}$ [g/l]	ABS/cm	C_{SDBS} [g/l]
Cement	0.6	0.132	$4.71 \cdot 10^{-2}$
Fly ash	0.6	0.120	$4.28 \cdot 10^{-2}$
Cement	1.8	0.275	$9.82 \cdot 10^{-2}$
Fly ash	1.8	0.252	$8.99 \cdot 10^{-2}$

Table 2.2: UV-measurements at 223 nm of cement and fly ash sample (single determinations). The absorbance (ABS) is measured on a 10 times diluted sample. The concentration of SDBS is reported as the added solution ($C_{SDBS,0}$) and in the resulting filtrate (C_{SDBS}), which has been recalculated to original sample.

concentration on 0.6 g/l remains dissolved in the filtrate and only 5 % when adding 1.8 g/l SDBS solution. Considering the three times higher FI of the examined fly ash compared with pure cement, the difference in remaining SDBS concentration between the filtrates of the two samples is low for both initial concentrations of SDBS (app. 9 % of the mean value). The observation is believed to be directly related with the low difference in measured surface tension between the two samples.

The low amounts of dissolved SDBS in the filtrate may partly be explained by the results in Table 2.3, which shows the attempts to prepare a 0.6 g/l SDBS solution in pure filtrate from cement and fly ash and in the same filtrate diluted two times with water. Recalculating absorbance measurements into

Sample	Filtrate	ABS/cm	C_{SDBS} [g/l]
Cement	1:1	0.640	$1.14 \cdot 10^{-1}$
Cement/fly ash	1:1	0.672	$1.20 \cdot 10^{-1}$
Cement	1:2	0.256	$9.14 \cdot 10^{-2}$
Cement/fly ash	1:2	0.295	$1.05 \cdot 10^{-1}$

Table 2.3: Concentration of SDBS in pure filtrate (1:1) and in filtrate diluted two times (1:2) from a cement and fly ash solution. Amount of SDBS has been added corresponding to 0.6 g/l in concentration. The absorbance was measured on 5 (1:2) or 10 (1:1) times diluted samples to be below electrolyte interference, and the concentrations of SDBS are recalculated to original sample.

concentrations shows that approximately 80–85 wt% of the added SDBS is not dissolved in the aqueous phase, probably due to formation of insoluble calcium surfactant salts [12]. Others have found similar trend with other surfactants too [15]. This implies that only 15–20 wt% of SDBS will be left to detect difference in adsorption behavior of the ashes. The sensitivity of the surfactant toward the ions coming from cement may be reduced by applying a non-ionic surfactant in the surface tension measurements as discussed in section 2.3.4.

As a final comment, we believe that the parameters affecting the foam stability (described in section 2.1), may complicate the development of spectroscopic assays. Such methods will only report a surfactant concentration and not an overall contribution to foam stability.

2.4 Conclusions

The commonly employed foam index test, which determines fly ash quality for concrete utilization, has been compared with a new method based on surface tension measurements, using the bubble pressure method. The comparison has been done on pure cement, nine fly ash samples and a carbon free ash sample and good relationship was accomplished between the two methods. The new method takes away the individual operator criterion on foam stability, making the test easier to standardize. Moreover, the test can be based on using a pure surfactant instead of an air-entraining admixture, where commercial products show variation in chemical nature and concentrations.

To summarize the method we have:

- Added a standard surfactant solution to a mixture of cement and fly ash.
- Allowed it to incubate under shaking for 10 minutes, followed by centrifugation and filtration.
- Measured the surface tension of the filtrate with the bubble pressure method at a fixed temperature and bubble lifetime.

The described method is at present stage not a finished procedure, but needs further work to fulfill our goal of having a reproducible method, which is able to detect small differences in fly ash adsorption capacities of surfactants. Improvements for the method have been suggested, which should be tested in the further work. The applied anionic surfactant was found to be very sensitive to the electrolytes provided from the cement and fly ash. We suggest testing non-ionic surfactants instead, which are less sensitive to form insoluble calcium surfactant salts. In order to prevent the interference of varying cement properties in the test, while still reducing the influence of the various soluble ions provided by the fly ash, we suggest testing if the applied cement can be replaced with a well defined electrolyte solution. Effort should also be put into testing if the protocol of adding surfactants should be changed.

Finally it has been shown that changes in temperature affect the foam index test.

2.5 Acknowledgements

This work was carried at the CHEC (Combustion and Harmful Emission Control) Research Center and financially supported by Elsam A/S, Energy E2 A/S, Babcock Wilcox Vølund aps, B&W Energy A/S, the Technical University of Denmark, the Danish Technical Research Council and Nordic Energy Research. The authors thank Professor Robert H. Hurt (Division of Engineering at Brown University) for providing ashes from the U.S.

2.6 Abbreviations

AEA	air-entraining admixture
CMC	critical micelle concentration
FI	foam index
SD	standard deviation
SDBS	sodeum dodecyl benzene sulfonate
Spec. FI	specific foam index
ST	surface tension

2.7 References

[1] I. Külaots, R. H. Hurt, E. M. Suuberg, Size distribution of unburned carbon in coal fly ash and its implications, Fuel 83 (2) (2004) 223–230.

[2] I. Külaots, A. Hsu, R. H. Hurt, E. M. Suuberg, Adsorption of surfactants on unburned carbon in fly ash and development of a standardized foam index test, Cement and Concrete Research 33 (12) (2003) 2091–2099.

[3] T. M. Schmitt (Ed.), Analysis of Surfactants, 1st Edition, Marcel Dekker, New York, 1997, p. 53.

[4] E. D. Manev, R. J. Pugh, Froth stability in aqueous solutions of nonionic surfactant and inorganic eletrolyte, Journal of Colloid and Interface Science 152 (2) (1992) 582–584.

[5] E. D. Manev, R. J. Pugh, Diffuse layer electrostatic potential and stability of thin aqueous films containing a nonionic surfactant, Langmuir 7 (10) (1991) 2253–2260.

[6] S. I. Karakashev, E. D. Manev, Correlation in the properties of aqueous single films and foam containing a nonionic surfactant and or-

ganic/inorganic electrolytes, Journal of Colloid and Interface Science 259 (1) (2003) 171–179.

[7] D. J. Shaw, Introduction to colloid and surface chemistry, 4th Edition, Butterworth–Heinemann, Cornwall, 2000, pp. 69–93.

[8] D. Beneventi, B. Carre, A. Gandini, Role of surfactant structure on surface and foaming properties, Colloids and Surfaces A: Physicochemical and Engineering Aspects 189 (2001) 65 – 73.

[9] P. Juyal, D. Merino-Garcia, S. I. Andersen, Effect on molecular interactions of chemical alteration of petroleum asphaltenes. i, Energy and Fuels 19 (4) (2005) 1272–1281.

[10] R. Helmuth, Fly ash in cement and concrete, 1st Edition, Portland Cement Association, Illinois, 1987, pp. 80–82.

[11] V. H. Dodson, Concrete admixtures, 1st Edition, Van Nostrand Reinhold, New York, 1990, pp. 129–164.

[12] J. P. Baltrus, R. B. LaCount, Measurement of adsorption of air-entraining admixture on fly ash in concrete and cement, Cement and Concrete Research 31 (5) (2001) 819–824.

[13] V. B. Fainerman, R. Miller, P. Joos, The measurement of dynamic surface tension by the maximum bubble pressure method, Colloid and Polymer Science 272 (6) (1994) 731–739.

[14] L. Schulze, K. Lohmann, Physikochemie – beurteilung des zustands von wasch- und spulflussigkeiten mit neuen messmethoden für oberflachen, Tenside Surfactants Detergents 36 (6) (1999) 384–386.

[15] G. M. Bruere, Air-entraining actions of anionic surfactants in Portland cement pastes, Journal of Applied Chemistry and Biotechnology 21 (1971) 61–64.

[16] E. Freeman, Y.-M. Gao, R. Hurt, E. Suuberg, Interactions of carbon-containing fly ash with commercial air-entraining admixtures for concrete, Fuel 76 (8) (1997) 761–765.

[17] R. L. Hill, S. L. Sarkar, R. F. Rathbone, J. C. Hower, An examination of fly ash carbon and its interactions with air entraining agent, Cement and Concrete Research 27 (2) (1997) 193–204.

[18] C. Zhang, K. T. Valsaraj, W. D. Constant, D. Roy, Aerobic biodegradation kinetics of four anionic and nonionic surfactants at sub- and supracritical micelle concentrations (CMCs), Water Research 33 (1) (1999) 115–124.

[19] B. Allred, G. O. Brown, L. A. Brandvold, Enhanced animal waste management through application of surfactants to soil material: laboratory feasibility testing, Transactions of the ASAE 44 (3) (2001) 513–524.

[20] J. Yu, I. Külaots, N. Sabanegh, Y. Gao, R. Hurt, E. Suuberg, *et al.*, Adsorptive and optical properties of fly ash from coal and petroleum coke co-firing, Energy and Fuels 14 (3) (2000) 591–596.

[21] X.-J. Fan, P. Stenius, N. Kallay, E. Matijevic, Precipitation of surfactant salts. II. The effect of nonionic surfactants on precipitation of calcium dodecyl sulfate, Journal of Colloid and Interface Science 121 (2) (1988) 571–578.

[22] M. S. Pradhan, D. S. R. Sarma, K. C. Khilar, Stability of aqueous foams with polymer additives. II. effects of temperature, Journal of Colloid and Interface Science 139 (2) (1990) 519–526.

[23] A. P. Brady, S. Ross, The measurement of foam stability, Journal of the American Chemical Society 66 (1944) 1348–1356.

Chapter 3

The Effect of Combustion Conditions and Fuel Type on Adsorption Behavior of Fly Ash in Concrete

Abstract. Fly ash from pulverized coal combustion contains residual carbon that can adsorb the air-entraining admixtures (AEAs) added to control the air entrainment in concrete. This is a problem that has increased by the implementation of low-NO_x combustion technologies. In this work, pulverized fuel has been combusted in an entrained flow reactor to test the impact of changes in operating conditions and fuel type on the AEA adsorption of ash and NO_x formation.

Increased oxidizing conditions, obtained by improved fuel-air mixing or higher excess air, decreased the AEA requirements of the produced ash by up to a factor of 25. This was due to a lower carbon content in the ash and a lower specific AEA adsorptivity of the carbon. The latter was suggested to be caused by changes in the adsorption properties of the unburned char and a decreased formation of soot, which was found to have a large AEA adsorption capacity based on measurements on a carbon black. The reactor was modeled with CFD and a relationship between oxygen concentration in the early stage of combustion and the AEA adsorption properties of the ash was observed. The NO_x formation increased by up to three times with more oxidizing conditions and thus, there was a trade-off between the AEA requirements of the ash and NO_x formation. The type of fuel had high impact on the AEA adsorption behavior of the ash. Ashes produced from a Columbian and a Polish coal showed similar AEA requirements, but the specific AEA adsorptivity of the carbon in the Columbian coal ash was up

to six times higher. The AEA requirements of a South African coal ash was unaffected by the applied operating conditions and showed up to 12 times higher AEA adsorption compared to the two other coal ashes. This may be caused by larger particles formed by agglomeration of the primary coal particles in the feeding phase or during the combustion process, which gave rise to increased formation of soot.

3.1 Introduction

The adsorption of air-entraining admixtures (AEAs) of fly ash in concrete is primarily related to the amount of residual carbon present in the fly ash and its specific AEA adsorption capacity. In this work, the effect of combustion conditions and fuel type on the AEA adsorption properties of the ash is investigated. An entrained flow reactor (EFR) has been applied to simulate the conditions taking place under the combustion of pulverized coal at operating conditions leading to various NO_x formation levels. The produced ashes have been collected and have been subject for further analysis including the commonly applied foam index (FI) test. The ash properties have been compared to the operating conditions, the fuel type and the achieved NO_x concentrations. Modeling has been applied to support the achieved results.

3.2 Experimental

One medium volatile and two high volatile bituminous pulverized coals have been applied in the experiments. Moreover, a biomass (straw) has been co-fired 1:1 on weight basis with a coal (Poduff). The fuel properties are summarized in Table 3.1. Fig. 3.1 illustrates the EFR-setup. The cylindrical ceramic reactor is 2 meter long and 8 cm in diameter and is electrically heated to a wall temperature of 1300 °C in the top and 1400 °C in the bottom. A particle feeder is placed at the top of the reactor and the particles are fed together with part of the air through the water cooled feed probe into the reactor. The largest fraction of remaining air passes through a preheater having a wall temperature of 1100 °C before it enters the reactor, while a minor fraction (2–4 Nl/min) is introduced as purge gas to prevent the heating elements from being exposed to corrosive species. Part of the flue gas is sampled through a water cooled particle collection probe with a sampling diameter of 3.2 cm, located in the bottom of the reactor. The sampled particles are collected on a filter. The details for the ash sampling calculations, illustrated by an example, are found in appendix 3.A. The

	Polish Poduff	South African Kleinkopje	Columbian Cerrejon	Straw
Proximate analysis				
Ash	15.4	15.8	12.9	7.9
Volatile	27.7	24.6	35.6	73.7
Fixed carbon (diff.)	57.0	59.6	51.4	18.4
Ultimate analysis				
Carbon	71.18	71.51	70.62	44.80
Hydrogen	4.50	3.82	4.78	5.80
Oxygen (diff.)	6.88	6.55	9.23	40.20
Nitrogen	1.26	1.75	1.59	1.10
Sulphur	0.61	0.55	0.91	0.20
Net caloric value [MJ/kg]	28.14	27.07	28.13	16.99
Median (dry) [μm]	21.3	13.3	23.4	249.2

Table 3.1: Results from proximate and ultimate analysis in wt% (d.b.) unless otherwise reported.

remaining flue gas is cooled downstream of the reactor and analyzed for O_2, CO, CO_2 and NO_x (NO + NO_2) using standard gas analyzers. The monitored compounds are reported as single average values for each experimental run. An example of data acquired from a single run is found in appendix 3.B.

The effect of feed air ratio (ratio between feed air flow and total air flow, R_f), excess air ratio (λ) and fuel type on the AEA adsorption of the ash was investigated and subsequently compared with the obtained NO_x emission levels. The experimental conditions are summarized in Table 3.2 and the applied air flows are based on stoichiometric calculations. (equations are found in appendix 3.C). In order to maintain a constant mean residence time of 1.7 seconds of the gas, the total combustion air flow was kept constant while the excess air ratio was changed by varying the feed rate of the solid fuel. The mean residence time of the gas is calculated from the reactor volume of 10.1 l, an average wall temperature of 1350 °C and the estimated total flue gas flow. Applying Stoke's law on a 35 μm coal particle gives a terminal velocity about 2 orders of magnitude lower than the mean gas velocity indicating that the particle follows the gas flow.

The collected ash samples were investigated for carbon content using the loss-on-ignition method (LOI) and AEA adsorptivity using the FI test, which is described elsewhere [1]. The procedure for estimating the specific AEA adsorptivity of carbon (spec. FI) was slightly changed by including

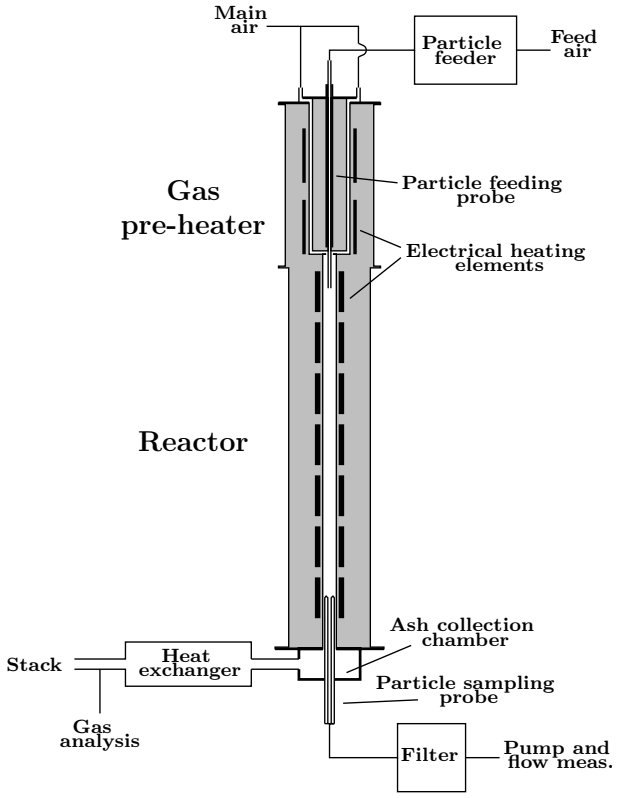

Figure 3.1: Sketch of the EFR reactor.

	Operating conditions	Fuel type
$\dot{m}_{\text{fuel}}$ [kg/h]	0.34–0.46	0.40 (0.51)
Q_{feed} [Nl/min]	6.0–17.4	6.0–15.0
Q_{total} [Nl/min]	57.3–57.7	55.6–57.7
λ	1.03–1.38	1.17–1.18

Table 3.2: Experimental conditions applied when investigating the effect of the operation conditions or the type of fuel. Only Poduff were fired when changing the operating conditions. The feed rate given in brackets is for the Poduff/straw mixture, i.e. to maintain similar aerodynamics as the coal experiments, a higher feed rate is required due to the higher oxygen content of straw compared with coal.

the contribution from the mineral part of the ash into the blank value of the

FI. Particle size measurements were carried out on a Malvern Mastersizer. Surface area was determined using BET-N_2 adsorption isotherm performed on a Micromeritics Gemini 2375. Scanning electron microscopy (SEM) was carried out on a JEOL JSM-5900, which was coupled with energy dispersive X-ray spectroscopy (EDX), model INCA from Oxford. A JEOL 3000 F FEG was applied for the Transmission Electron Microscopy (TEM). Thermal gravimetric analysis (TGA) performed on a STA 409 C from Netsch was applied to measure oxidation reactivities of coal char.

3.3 Modeling

The EFR was modeled by computational fluid dynamics (CFD) using the commercial software Fluent 6.3., where time-averaged equations for conservation of mass, momentum, energy and species are solved. Fluent requires a geometry of the EFR and it was created in three dimensions using the preprocessor tool GAMBIT 2.4. The feed probe and the pre-heater section was constructed with proper entrance length according to conventional theory for laminar [2] and turbulent flow [3] to ensure fully developed flow in the reactor. The meshed geometry contained 110000 hexahedral elements and was refined close the outlet of the feed probe.

In the modeling, the standard $k-\epsilon$ with near-wall modeling was applied as turbulence model and the two phase flow was described by the Euler-Lagrange approach. Radiation was simulated by the discrete ordinates radiation model (DO). The released volatile matter was represented by a single material and assumed to be fast burning making the reaction rate controlled by the turbulent mixing. In the present work, the eddy-break-up model was applied together with a two step-reaction scheme according to Peters and Weber [4]. The model has been found to make reasonably accurate predictions of combustion flows [4–6], but should only be applied for a one- or two-step global reaction mechanism. The specific heat capacities of the species involved in the reaction mechanism have been modified according to Rose and Cooper [7] to account for the effect of the neglected dissociated species on the flame temperature.

The volatile release was based on a single first-order reaction model [8] and the high temperature volatile yield was determined according to Neoh and Gannon [9]. The char combustion was modeled by a kinetics/diffusion surface reaction rate model [10, 11]. Table 3.3 summarizes the properties of

coal and the parameters of devolatilization and char combustion, which are mainly based on Poduff coal.

Coal	
Paricle Density [kg/m^3] [12]	1000
Particle specific heat [J/kg K] [12]	1100
Particle size distribution[a]	Rosin-Rammler
Emissivity [13]	0.9
Scattering factor [13]	0.6
Swelling coefficient [14, 15][b]	1
Volatile matter	
Molecular weight [kg/kg mol] [4]	50
Volatile yield at high temp. [wt%] (daf) [9][c]	50.4
Pre-exponential factor [s^{-1}] [8][d]	$3.8 \cdot 10^5$
Activation Energy [J/kmol] [8]	$7.4 \cdot 10^7$
Char	
Oxygen diffusion rate constant [kg/(m s Pa K$^{0.75}$)] [11]	$5 \cdot 10^{-12}$
Pre-exponential factor [kg/(m^2 s Pa)] [16]	53.6
Activation energy [MJ/kg mol] [16]	161
Stochiometric ratio [wt%,O_2/wt%,C]	2.67
Net caloric value [MJ/kg] (daf) [12]	33

Table 3.3: Properties of coal (Poduff), volatiles and char applied in the CFD modeling.
[a] $Y_d = e^{(-d/\overline{d})^n}$, $\overline{d}$=31μm, n=0.99, range: 2 – 200 μm.
[b] Coal particles may only swell 0-15% under pf-firing conditions in air [14, 15].
[c] Determined at (H+2O)/C+S)=0.90 and interpolated to 2150 K.
[d] Determined at 84.3 wt% C, daf.

The volatile matter was presented by a single material having a composition corresponding to Poduff and it was derived assuming that char consists of carbon only. The following reaction path for the volatile matter was assumed:

$$\begin{aligned} C_{2.87}H_{5.30}O_{0.51}N_{0.16} + 2.76O_2 &\rightarrow 2.36CO + 0.51CO_2 + 2.65H_2O + 0.08N_2 \\ CO + 0.5O_2 &\rightarrow CO_2 \end{aligned}$$

The fraction of volatiles that reacts directly to CO_2 was determined according to $12f_O/16f_C$, where f_O and f_C is the mass fraction of oxygen and carbon in the volatile matter [4]. The char was assumed to oxidize directly to CO_2

based on the observations by Peters and Weber [4], who argued that the size of the boundary layer around a particle, where CO is oxidized to CO_2, is small compared to the size of the turbulent eddy it is traversing through.

A fixed wall temperature has been applied as thermal boundary condition according the experimental work. The wall emissivity was set to 0.6 as applied elsewhere for a ceramic refractory wall [4].

3.4 Results

An extensive number of combustion experiments have been performed under different operating conditions and using different types of fuel. To give the reader an overview, this first section collects all the results from the EFR experiments. The following sections deal with the results produced in the experimental series of changing the operation conditions and type of fuel.

3.4.1 General Evaluation of Results and Performance

Ash Properties and Emissions

The EFR-ashes have been produced with adsorption properties and carbon contents that span over a wide range. The LOI values range from 1.6 to 34.8 wt% (Fig. 3.2a) corresponding to a burnout from 0.90 to more than 0.99, FI ranges from 0.1 to 4.8 ml AEA/2 g ash (Fig. 3.2a) and spec. FI ranges from 1.6 to 12.2 ml AEA/g C (Fig. 3.2b). The FI tends to increase

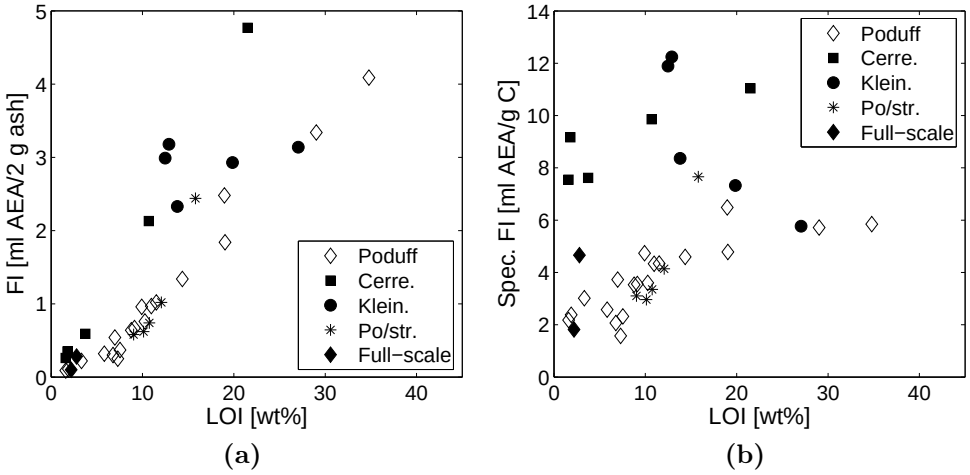

Figure 3.2: (a) FI and (b) spec. FI compared with LOI of all the produced ashes.

with the LOI (Fig. 3.2a) in agreement with results from other studies [1, 17–19] and this indicates that the AEAs are adsorbed by the residual carbon. However, the FI value of ashes with similar carbon content can differ, which is caused by the variations in specific AEA adsorptivity of the residual carbon as illustrated in Fig. 3.2b. E.g. the spec. FI of ashes about 7 wt% in LOI ranges from 1.6 to 3.7 ml AEA/g C when originating from the same coal type (Poduff), but the specific AEA adsorptivity of the residual carbon can be even higher in ashes produced from the other investigated coal types. The figures include the results of two full-scale ashes acquired from Danish coal fired power plants burning bituminous coal; Enstedværket (ENV) and Nordjyllandsværket, unit 3 (NJV3) and the results are also summarized in Table 3.4. No problems with utilizing ashes from ENV in concrete have

	ENV	NJV3
LOI [wt%]	2.2	2.8
FI [ml AEA/2 g ash]	0.1	0.28
Spec. FI [ml AEA/g C]	1.8	4.7

Table 3.4: LOI, FI and Spec. FI of two commercial fly ashes acquired from Enstedværket (ENV) and Nordjyllandsværket, unit 3 (NJV3).

been reported, whereas ashes from NJV3 have caused problems with the air entrainment [20]. The FI values of the EFR-ashes are generally higher than the full-scale ashes, which are mainly caused by the higher amounts of carbon in the EFR-ashes. Thus, most of the combustion conditions, applied in the experimental work, do not give the same degree of burnout as in modern power plants, where high combustion efficiency is required. The specific AEA adsorption capacities of the residual carbon in the EFR-ashes produced from the Poduff coal are in the same range as the measured values of the two full-scale ashes (Fig. 3.2b), while the Cerrejon and Kleinkopje coal ashes show higher spec. FI. The comparability between the full-scale ashes and the EFR-ashes being higher in LOI is addressed further below (section 3.4.1).

The applied operating conditions and fuel types lead to NO_x concentrations in the flue gas ranging from 410 to 1370 ppm at 6 vol% O_2 (Figure 3.3a to 3.4). The normalization to 6 vol% O_2 is achieved by multiplying the measured NO_x concentration with a correction factor $\frac{21\ \text{vol\%}-6\ \text{vol\%}}{21\ \text{vol\%}-O_{2,\text{obs}}}$, where $O_{2,\text{obs}}$ is the measured oxygen concentration. The obtained NO_x concentrations are in general higher than achieved when firing bituminous coal in suspension

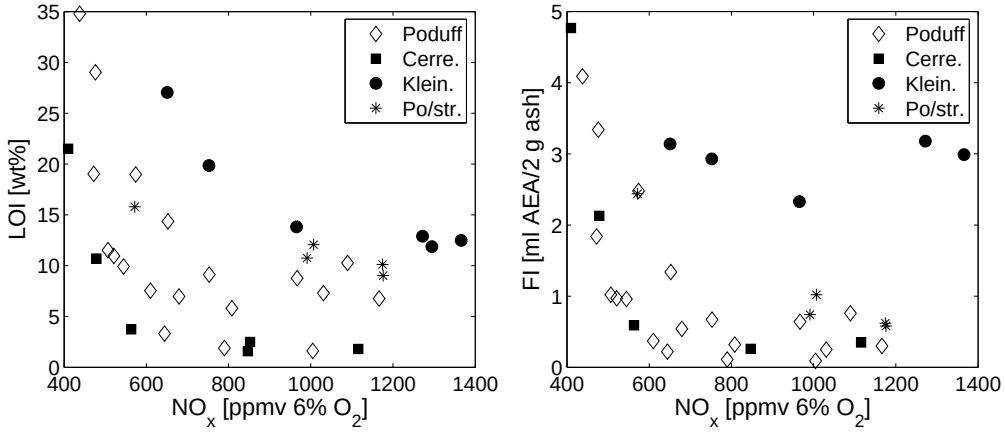

Figure 3.3: (a) LOI and (b) FI compared with NO_x of all the produced ashes.

fired boilers applying low-NO_x combustion technologies, e.g. NO_x concentrations between 210-330 ppmv (6 % O_2) [21] and 290–680 ppmv (6 % O_2) [22] have been reported. The variations in the reported NO_x concentrations may depend on factors like N-content and rank (volatile content) of the bituminous coal, furnace design and the generation of low-NO_x burners. The EFR applied in the present work does not operate with air staging techniques for NO_x control as in coal-fired boilers, e.g. low-NO_x burners and furnace air staging. However as presented below, the applied operating conditions significantly affect the NO_x formation, oxygen concentration profile in the reactor and ash adsorption properties and therefore, some relevant relationship between combustion conditions and ash properties are expected from the experimental work.

The correlation between NO_x concentration and LOI (Fig. 3.3a) or FI (Fig. 3.3b) of the ashes is poor, but the results do indicate that combustion conditions leading to higher NO_x concentrations can cause a lower LOI and FI of the produced ash, except for the Kleinkopje coal ashes where the FI values are unchanged at various NO_x concentration levels. A poor correlation between the spec. FI and NO_x concentration are found as well (Fig. 3.4) as others have reported [23]. Within each coal type, different trends between NO_x concentration and spec. FI are found varying from decreasing (Poduff), both decreasing and increasing (Cerrejon) and increasing (Kleinkopje).

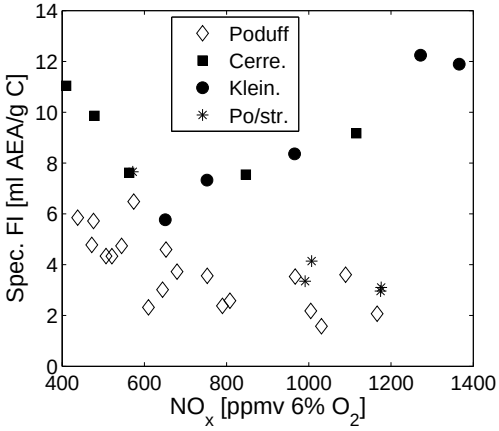

Figure 3.4: Spec. FI and NO_x of all the produced ashes.

Other Properties

The EFR-ashes were visually compared with the full-scale ashes by scanning electron microscopy (SEM). Fig. 3.5a and 3.5b show the images of a commercial ash acquired from NJV3 burning bituminous coals and an EFR-ash produced from burning Poduff coal, respectively. Most of the ash particles from the EFR are observed to be glassy and spherical in shape as the com-

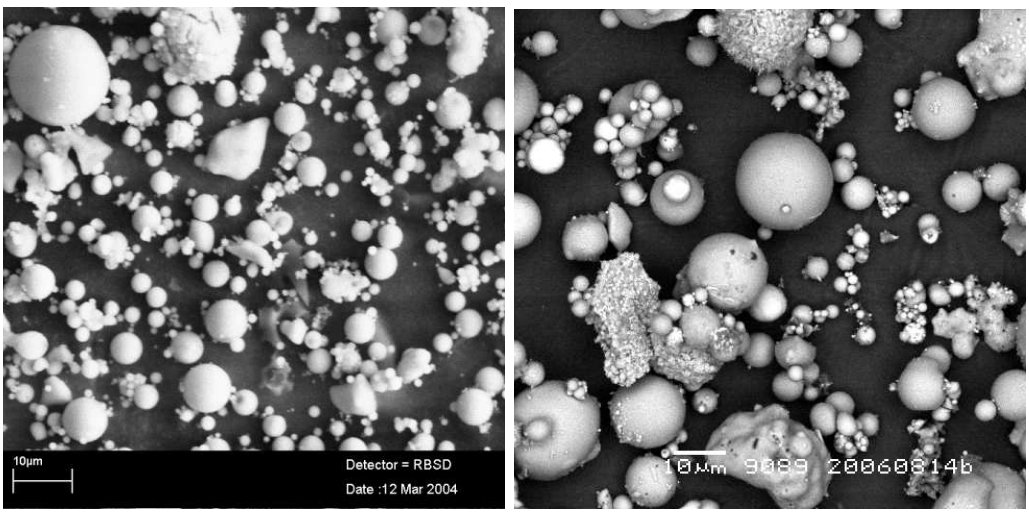

(a) **(b)**

Figure 3.5: SEM images of ashes from (a) NJV3 and (b) EFR.

mercial ash. This is a morphology usually found among inorganic fly ash particles, which have gone trough a molten phase caused by the high temperatures reached in the combustion process [24]. EDX measurements of both examined ashes reveal that the major part of the spherical particles is composed of Al, Si and O, with minor fractions of Na, Mg, K and Ca.

The comparability between full-scale and laboratory-scale ashes with focus on char morphology have been addressed by others [25], where it was found that the char morphology is influenced by the reaction temperature. High-temperature chars produced in an entrained flow reactor at 1330 °C showed a morphology similar to full-scale ashes, i.e. the chars were found to be dominated by thicker-walled morphotypes with small bubbles (crassipheres and mixed morphotype), the latter suggested to be caused by pyrolysis after swelling has ended [26]. On the other hand chars produced in a drop tube furnace at temperatures between 800-1150 °C, showed higher amounts of highly porous thin-walled morphotypes (tenuispheres). Thus, based on their work [25], it was suggested that laboratory chars produced at temperatures greater than 1300 °C combined with high heating rates are comparable with full-scale chars, as in the present case. Results from preliminary work on the EFR, which was conducted at lower wall temperatures (1150 °C), may support the findings by Rosenberg *et al.* [25]. Chars produced at wall temperatures of 1150 °C (Fig. 3.6a) appears to have a more

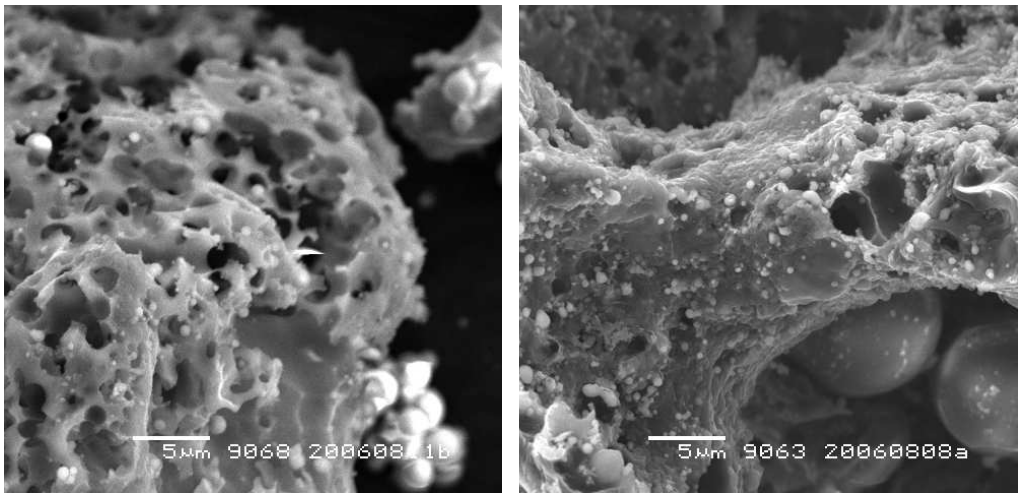

(a) **(b)**

Figure 3.6: Char produced at (a) 1150 °C, 10.8 wt% in LOI and (b) 1350 °C, 11.1 wt% in LOI.

porous structure than chars produced at 1350 °C (Fig. 3.6b) and thus, it was

decided to proceed the EFR experiments using an average wall temperature of 1350 °C.

Results from particle size measurements of a full-scale ash and an EFR-ash suspended in ethanol are presented in Fig. 3.7. Both ashes show a

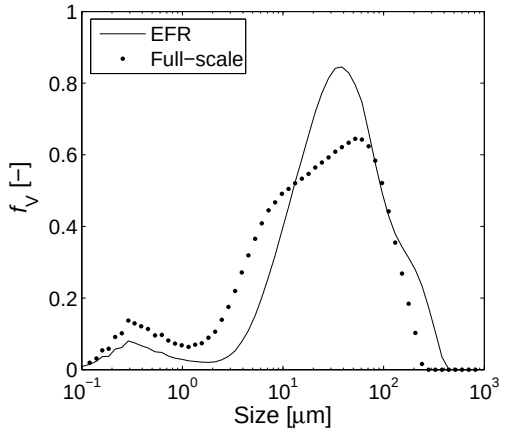

Figure 3.7: Volume distribution ,f_V, of an EFR- and full-scale ash. Measurements have been carried out in ethanol.

bimodal size distribution, but the size distribution of the EFR-ash appears to be slightly shifted toward larger particles.

The BET surface areas of five EFR-ashes with carbon contents up to 11 wt%, are measured to 3.4–11.3 m^2/g ash. The surface areas of carbon are estimated to range from 34-99 m^2/g carbon by taking the contribution from the mineral matter of 0.74 m^2/g ash into account (value based on a large series of measurements on different ashes by Yu *et al.* [27]). The carbon surface areas correspond well with areas measured on two fly ashes acquired from full-scale utilities, where the carbon surface areas are determined to 40 and 76 m^2/g carbon (LOI 2.5 wt% and 2.8 wt%, respectively). The results give further evidence that the EFR produced char are comparable with full-scale ashes. BET results are further discussed below.

The Agglomeration Problem

The applied range of feed air was restricted by some physical properties of the experimental setup. The feed air flow was limited to 17.4 Nl/min in order to avoid exceeding the maximum allowed pressure in the feed container. Contrary, a distinct agglomeration of the coal particles occurred at low feed air flows leading to formation of particles that were difficult to burn out

within the available residence time. Such a agglomeration or caking behavior can occur for bituminous coals [28] and may take place when the particle collide during the combustion process [29] or in the more dense feeding phase of the particles [30]. The agglomeration is further strengthened during the plastic phase of the pyrolysis of the coal [30]. The larger agglomerated char particles (up to app. 1 mm in size) did not follow the gas streamlines and ended up in the bottom of the reactor or in the ash sampling probe. A visual observation of the combustion process revealed larger glowing particles (up to one second) at feed air flows of 3 Nl/min, but not at 6 Nl/min and therefore, the lowest range of feed air was chosen to 6 Nl/min. However, SEM examination of an ash produced at a feed air flow of 7.5 Nl/min (Fig. 3.8) reveals a char particle larger than 200 μm in size. The particle appears to

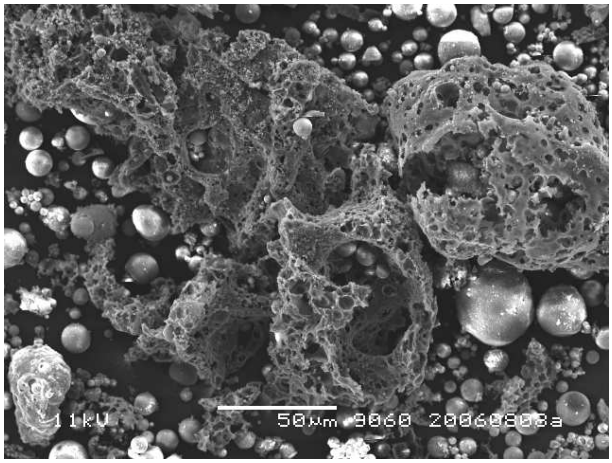

Figure 3.8: Possibly agglomerated char particles in an EFR-ash.

be comprised of several char particles, as observed elsewhere [29], suggesting that some degree of agglomeration still has occurred. In addition, the largest peak in the particle size distribution of the EFR-ash presented in Fig. 3.7 appears to overlap a small peak caused by larger particles, which may be agglomerated particles [29]. This is also observed for ashes produced at higher feed air ratios.

Consistency and Uncertainty

Statistical variance and the law of propagation of uncertainties have been applied to determine the absolute uncertainty of O_2 and NO_x concentrations and the LOI values. The estimated uncertainty is based on five double determinations at different conditions. Table 3.5 presents the results as 95 %

confidence intervals and equations are found in appendix 3.D. The uncer-

NO_x [ppmv 6 % O_2]	±44–63
O_2 [vol%]	±0.18
LOI [wt%]	±1.30

Table 3.5: Estimated 95 % confidence interval of the reported values.

tainties of the FI and spec. FI values have not been estimated due to lack of material in the double determinations to perform the FI test.

The experimentally determined degree of burnout of the coal is included in the stoichiometric calculations in order to compare the difference between theoretical and measured oxygen concentration. Table 3.6 reports the average difference with a 95 % confidence interval. Details are found in appendix 3.E. The measured oxygen concentrations are in general higher than the

$O_{2,exp}$-$O_{2,meas}$ [vol%]	0.59±0.68
False air [Nl/min]	1.5±1.8 (2.3±2.9 % of total air)

Table 3.6: Difference between theoretical and measured oxygen concentrations and the estimated amount of false air entering the system. 95 % confidence intervals are included.

theoretical caused by false air entering the reactor through small leakages when operating the reactor in sub-pressure (approximately 0.3 mbar). The amount of false air is estimated to be about 2.3 % of total added air (Table 3.6), which is found acceptable in the present experiments.

3.4.2 Operating Conditions

Both the feed air ratio and the excess air ratio affect the ash properties and NO_x concentration and thus, both is used as abscissa when presenting the results.

The AEA adsorption property of the produced ash, i.e. the FI value, is of primary concern from a practical point of view and is presented as a function of feed air (Fig. 3.9a) and total excess air ratio (Fig. 3.9b). Increases in both parameters lead to a reduced AEA adsorption capacity of the produced ash. The feed air ratio is of importance to the FI value at ratios below approximately 0.16 (Fig. 3.9a), where the FI decreases up to 9 times with increased ratio compared with the initial value at $R_f = 0.10$. At higher feed

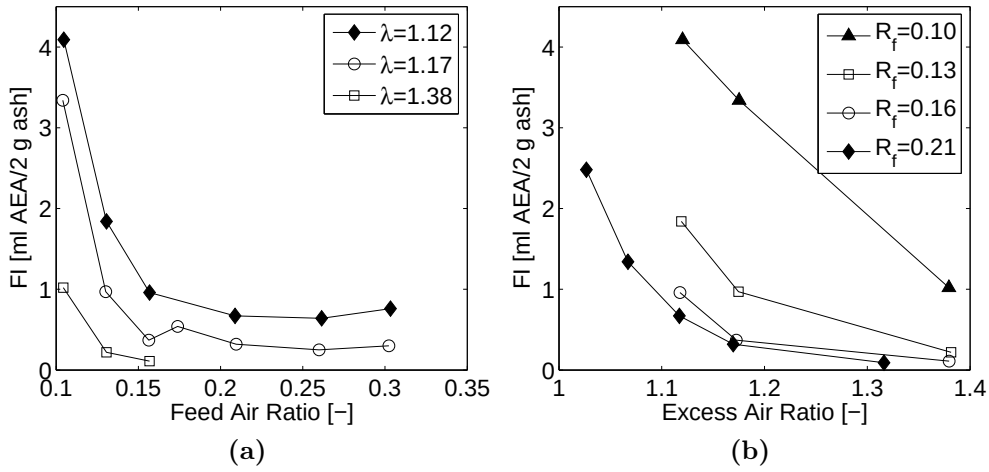

Figure 3.9: The effect of (a) feed air ratio and (b) excess air ratio on FI.

air ratios, the FI is only affected by the excess air ratio. This is also illustrated in Fig. 3.9b, where the ashes produced at feed air ratios of 0.16 and 0.21 are found to have almost similar FI values in the applied range of excess air ratio. The impact from changing the excess air ratio on the FI is highest at lower excess air ratios as well, except at a feed air ratio of 0.10. Within the applied excess air range the FI is reduced up to 25 times from the highest to the lowest value. The lowest FI values obtained of the EFR-ashes are similar to values measured on full-scale ashes. These are achieved at higher feed air ratios combined with a total excess air of 1.17 or higher.

Changing the feed air ratio or the excess air ratio has an inverse effect on the NO_x formation and thereby the NO_x concentration in the flue gas, as presented in Figs. 3.10a and 3.10b, respectively. The inverse relationship between NO_x formation and AEA adsorption agrees well with work by others [23]. The feed air ratio and NO_x concentration follows each other in an almost linear manner and the achieved concentrations range from about 440 to 1170 ppm at 6 vol% O_2. The increase in NO_x formation may be due to the increased jet velocities obtained at higher feed air rates, which increases the turbulence causing an improved mixing between coal particles and combustion air. Hereby higher O_2 concentrations occur in the early stage of combustion, which can promote the oxidation of volatile-N to NO_x [31]. Increasing O_2 concentrations with the feed air ratio in near probe region have been shown from CFD modelling presented below. Less unburned char available for the reduction of NO_x may further contribute to the increased NO_x concentration at higher feed air ratios.

The NO_x concentration increases with the excess air ratio (Fig. 3.10b).

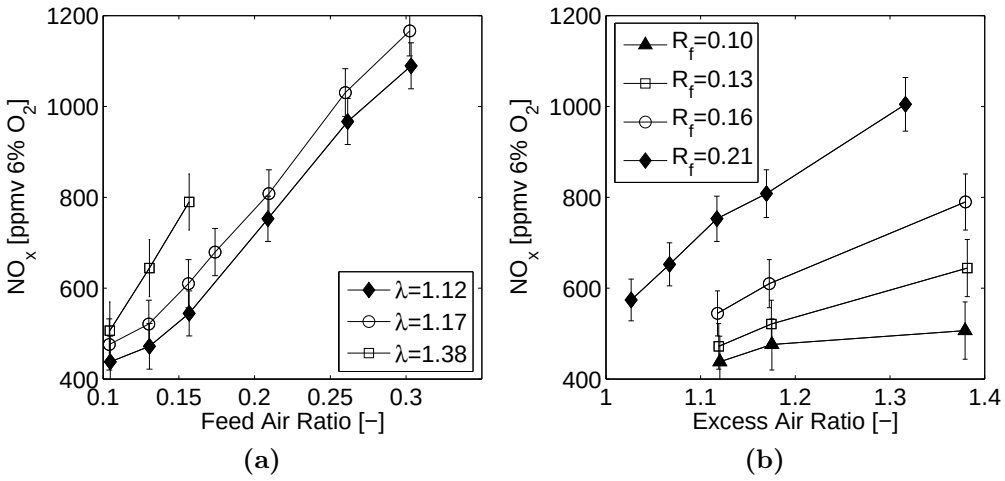

Figure 3.10: NO_x concentration as a function of (a) feed air ratio and (b) excess air ratio.

This is in good agreement with pilot scale observations for lean combustion [32] and shows that good mixing exists. The latter is explained from the fact that coal bound nitrogen in pulverized coal combustion typically contributes with more than 80 % of the NO emissions [31] and that the conversion to NO strongly depends on local stoichiometry [33]. This is also as expected since the excess air is controlled by the coal feed rate and not by changes in the mixing pattern. However, indications of some fuel rich conditions exist. Results from Spliethoff *et al.* [34] showed that the NO_x concentration increases with decreasing temperatures when burning coal under reducing conditions in an electrical heated ceramic tube reactor, while under lean conditions, lower temperatures causes lower NO_x concentrations. In the present work, preliminary EFR experiments were performed at a wall temperature of 1150 °C and this gave rise to higher NO_x concentrations in the flue gas. This and the CFD modelling presented below indicate that fuel rich conditions to some extent exist in the EFR, especially at lower feed air ratios.

The LOI values, presented as a function of feed air ratio (Fig. 3.11a) and excess air ratio (Fig. 3.11b), follows the trend of the FI values and this explains the main reason for the observed relationship between operation conditions and AEA adsorption of the ash. Increases in feed air ratio below a ratio of 0.16 results in an improved burnout of the coal particles, while the burnout remains constant at higher ratios (Fig. 3.11a). Again, lower nozzle output velocities at lower feed air ratios lead to a less violent oxidation of coal particles causing a poorer burnout. The constant carbon content found in the ash at higher feed air ratios could be a combination of improved coal/air

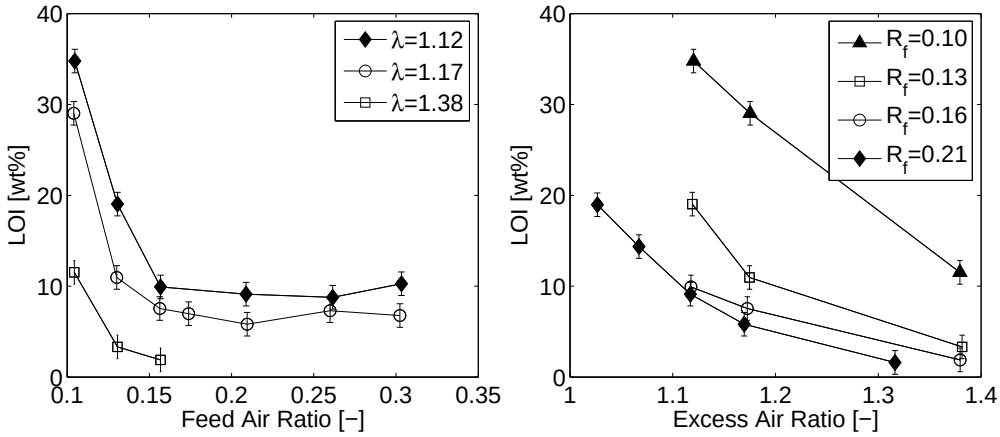

Figure 3.11: The effect of (a) feed air ratio and (b) excess air ratio on LOI.

mixing, which is compensated by reduced temperatures when applying more non-preheated feed air. Moreover, the concentration of coal particles in the combustion air may be lowered, which can result in a delayed ignition [35]. The influence of a general higher oxygen concentration in the reactor on the conversion of the carbon particles is illustrated in Fig. 3.11b, where increased excess air ratio leads to higher burnout of the coal in the whole tested range.

Fig. 3.12a shows the specific AEA adsorptivity of the residual carbon as a function of feed air ratio. The adsorptivity decreases with increasing feed air ratio indicating that the lower AEA requirements of the total ash at higher ratios are not only caused by a lower carbon content, but are due to some changes in adsorption properties of the residual carbon as well. The decline in spec. FI tends to be highest at low ratios. The percentage-wise contribution from both a reduction in LOI and spec. FI to the decrease in FI at $\lambda = 1.17$ are presented in Fig. 3.12b. At a feed air ratio of 0.26, FI is decreased to 7 % compared with the highest value (achieved at $R_{\mathrm{f}} = 0.10$) and this is caused by a reduction in LOI to 25 % and spec. FI to 28 %. Table 3.7 summarizes the maximum obtained reductions in FI, LOI and Spec. FI of the ashes produced at a total excess air of 1.12, 1.17 and 1.38. The ashes produced at $\lambda = 1.17$ shows the highest percent-wise reduction in spec. FI with the feed air ratio, but a higher reduction of the ashes produced at $\lambda = 1.38$ may have been achieved if a higher feed air ratio than 0.16 had been tested.

Increasing the total excess air results in lower surfactant adsorption capacity of the residual carbon as well (Fig. 3.13a). It is observed that the major decrease is obtained at lower total excess air ratio at feed air ratios

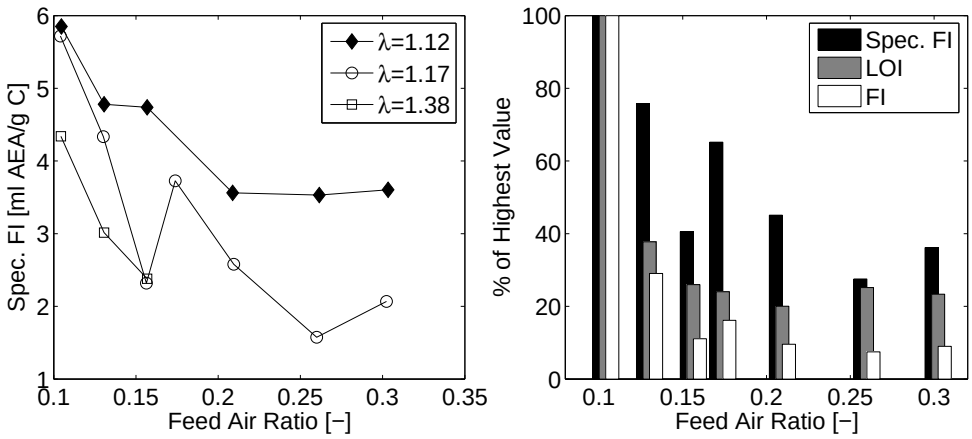

Figure 3.12: (a) The effect of feed air ratio on the Spec. FI. (b) The reduction in LOI, FI and spec. FI at $\lambda = 1.17$ compared with feed air ratio (the reduction is given in percentage of highest value at $R_f = 0.10$).

λ [-]	FI [%]	LOI [%]	Spec. FI [%]
1.12	16	25	60
1.17	7	25	28
1.38	11	16	54

Table 3.7: The maximum reduction in adsorption properties and carbon contents, given in percentage of highest value, when the feed air ratio is increased at the different applied excess air series (reductions achieved at $R_f = 0.26$ for $\lambda = 1.12$ and 1.17 and $R_f = 0.16$ for $\lambda = 1.38$).

of 0.16 and 0.21, while at lower feed air ratios, the decrease is linear. The highest percentage-wise reduction in spec. FI is at $R_f = 0.21$, where it is reduced to 33 % of highest value (Fig. 3.13b). Combined with a decrease in LOI to 8 %, the FI of the ash is reduced to 4 % of the highest value. The decrease in FI, LOI and spec. FI at the other feed air ratio series is presented in Table 3.8. The order of maximum reduction in spec. FI is found to follow the order of the reduction in LOI.

The observed reduction in specific AEA adsorptivity of the residual carbon at more oxidizing conditions, here experimentally obtained by improved mixing and increased excess air, agrees well with work from Gao *et al.* [23]. In their pilot-scale experiments, residual carbon with the highest specific

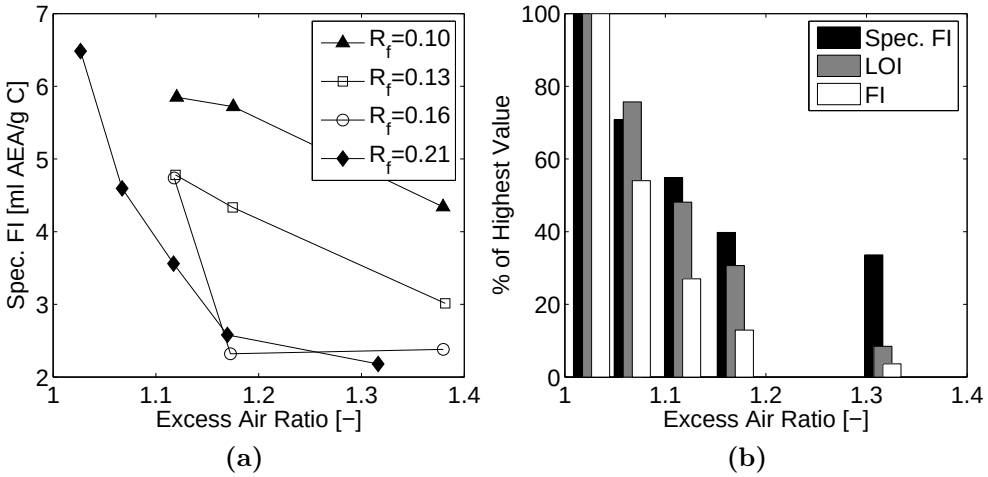

Figure 3.13: (a) The effect of excess air ratio on Spec. FI. (b) The reduction in LOI, FI and spec. FI at $R_{\mathrm{f}} = 0.21$ compared with excess air ratio (the reduction is given in percentage of highest value at $\lambda = 1.03$).

R_{f} [-]	FI [%]	LOI [%]	Spec. FI [%]
0.10	25	33	74
0.13	12	17	63
0.16	11	16	50
0.21	4	8	33

Table 3.8: The maximum reduction in adsorption properties and carbon contents, given in percentage of highest value, when the excess air ratio is increased at the feed air ratio series.

AEA adsorptivity was produced under air staged combustion causing more reducing conditions. It was also observed that the spec. FI tended to increase with the amount of carbon in the ashes and this appears to be the case in the present work as well. Whether the specific AEA adsorptivity of the carbon solely depends on its burnout level, or if the carbon properties alone can be affected by the oxidizing conditions, may be tested by grouping the ashes into degree of burnout and compare them with the NO_x concentrations as a measure for the oxidizing conditions.

Fig. 3.14a presents the spec. FI compared with the LOI of all the Poduff coal ashes and in general the specific AEA adsorptivity of the residual carbon is observed to be higher among the ashes with poor burnout. The three ellipses correspond to the burnout grouping. The spec. FI decreases to some

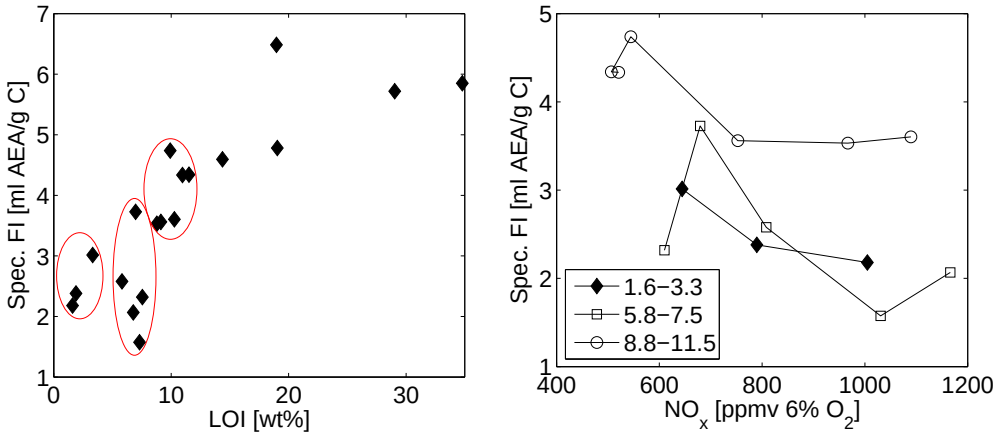

Figure 3.14: (a) Spec. FI and LOI. The ellipses correspond to the burnout grouping. (b) Spec. FI compared with NO_x concentration. The legend describes the grouping of ashes into LOI values.

extend with increasing NO_x concentration within each group of LOI values (Fig. 3.14b) indicating that the adsorption properties of carbon is not only caused by the degree of burnout. However, grouping the ashes differently do not necessarily reveal this relationship and moreover, the order of burnout of the group with LOI values from 1.6 to 3.3 wt% follows the order of spec. FI. This suggest that the specific AEA adsorptivity of the residual carbon is coupled with the degree of burnout, at least to a certain extend, and that it is hardly changed alone by conditions that significantly can affect the NO_x concentration at the applied conditions.

Three ash samples have been tested for BET-N_2 surface area and their properties are listed in Table 3.9. The surface area of the investigated ashes

	λ	R_f	NO_x [ppm 6 % O_2]	LOI [wt%]	Spec. FI [ml AEA/g C]	Total area [m^2/g ash]	Spec. area[a] [m^2/g C]
A	1.17	0.13	521	11.0	4.33	5.6	44.4
B	1.12	0.16	545	8.5	4.74	4.1	33.9
C	1.18	0.26	1031	7.3	1.57	3.4	36.4

Table 3.9: Properties of ash samples. [a]Based on a surface area of the inorganic particles of 0.74 m^2/g ash [27].

increases with the carbon content, which agrees well with the higher surface

area per mass of residual carbon compared with the inorganic part of the ash [18]. The few investigated samples do not provide sufficient data to reveal any relationship between the surface area and the specific AEA adsorptivity of the residual carbon. However, the relative difference in carbon surface area of ash B and C are small compared to their threefold difference in spec. FI indicating that BET surface area cannot alone be used as a measure for the adsorption behavior [36]. Thus, the degree of adsorption by the residual carbon is controlled by additional factors, which is suggested to include the accessibility of the surface area for the AEAs and surface chemistry as reviewed elsewhere [37]. E.g. Gao *et al.* [23] found a better correlation between specific AEA adsorptivity and non-microporous area of chars than with the total surface area. The non-microporous area was determined by applying by the Barrett-Joyner-Hallender (BJH) theory to N_2 adsorption isotherm. However, attempts to determine this area did not succeed in the present work.

3.4.2.1 Modeling

The simulation process started by solving the case with disabled reactions to obtain a cold-flow solution. When the flow pattern was established, the coal particle trajectories and reactions were solved and finally the radiation model was enabled. Initially, 1000 particles were injected, which increased to 8000 when the solution was close to convergence. From the converged solution, the fuel and feed air rates were easily changed to the values applied in the different experiments. Grid adaption was performed on selected solutions to ensure grid independence.

Some difficulties lies in validating the model toward absolute values in the experimental work, e.g. temperatures have not been measured in the reactor. Moreover, several parameters describing the coal are empirically determined or adapted from work by others. Therefore, the main purpose of the modeling is to reveal tendencies between experimental observations and relative differences in simulated combustion conditions in the reactor. Some validation of the modeled results will be included in the discussion given below.

The oxygen and temperature distribution in the upper part of the reactor for a feed air ratio of 0.10 and 0.30 and a total excess air ratio of 1.17 is shown in Figs. 3.15a and 3.15b, respectively. Operating with a low feed air ratio results in a lower oxygen concentration in the near feed probe region than operating at a high feed air ratio (Fig. 3.15a). In fact, a minimum in oxygen concentration is observed in the flame at the low feed air ratio indicating that more fuel rich conditions exists compared to at the high feed

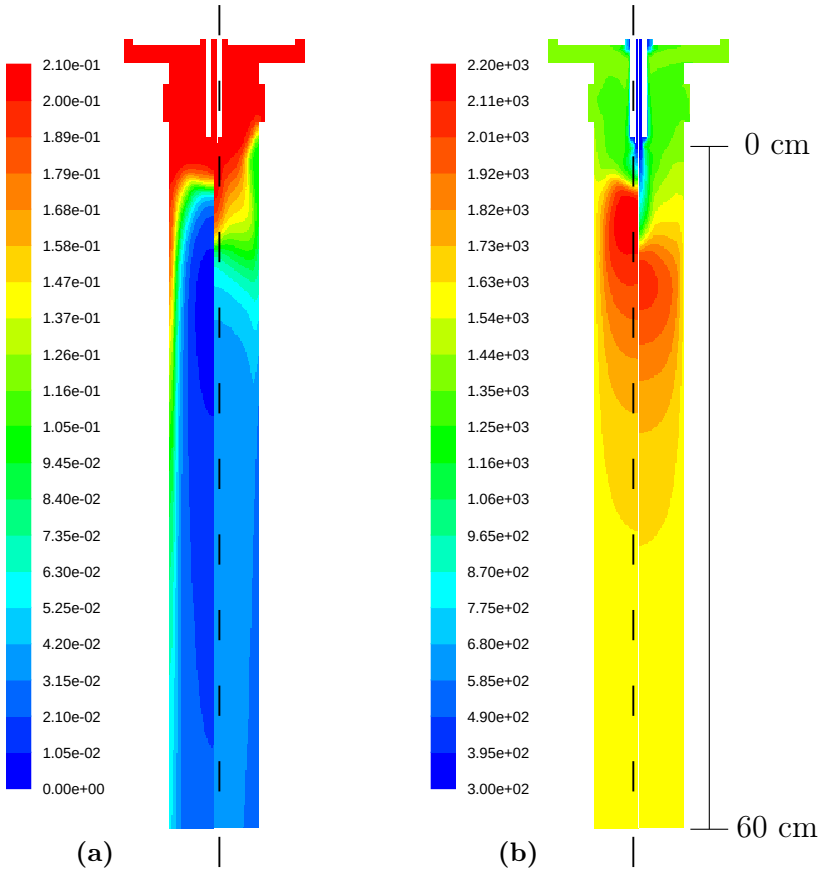

Figure 3.15: (a) Oxygen in molar fraction and (b) temperature [K] distribution in the reactor at a excess air of 1.17. Left and right images in each figure presents feed air ratios of 0.10 and 0.30, respectively.

air ratio. The oxygen distribution illustrates as well that higher feed probe inlet velocities moves the ignition point downwards and causes a recirculation of combustion gases and particles in the near probe region. The latter is observed from the lower oxygen concentration near the wall at the feed probe inlet level. The temperature distribution support that the ignition point is moved downwards in the reactor (Fig. 3.15b). The maximum combustion temperature is observed to decrease from 1912 °C at a feed rate of 0.10 to 1781 °C at a feed rate of 0.30.

The two solutions have been tested for grid independence by adapting the region near the feed probe (number of cells increased from 110.000 to 250.000). For a feed air ratio of 0.10, the maximum temperature increased 3 °C and the minimum oxygen concentration increased from 0.49 vol% to 0.50 vol% in the adapted solution, while they remained unchanged at a feed

air ratio of 0.30. The relative small changes indicate a satisfactory grid independent solution and since increases in grid size happens at costs of computational time, grid adaption was not performed in the remaining test cases.

Fig. 3.16a shows the flow field at the two different feed air ratios. The

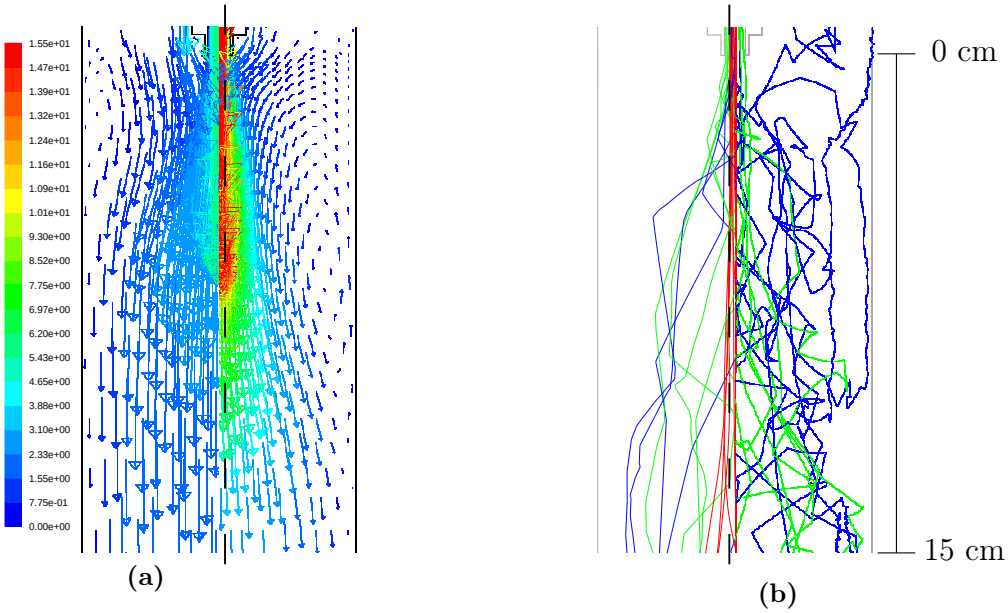

Figure 3.16: (a) Velocity vector distribution in the reactor at an excess air of 1.17. (b) Particle trajectories of three particle sizes with turbulence dispersion; 2 μm (blue), 20 μm (green), 200 μm (red), 8 injections each. Left and right images presents feed air ratios of 0.10 and 0.30, respectively.

average feed air velocity in the feed probe increases from 4.3 m/s at a feed air ratio of 0.10 to 12.4 m/s at a feed air ratio of 0.30 (maximum velocity is 15.5 m/s). Recirculation of combustion gases is observed in the near feed probe region, which is caused by a decrease in pressure near the feed probe inlet. The recirculation is intensified at higher feed air ratios.

The increased recirculation of combustion gases impacts the particle trajectories as illustrated in Fig. 3.16b. At higher feed air ratios, the smaller particles (2 μm in this case) are recirculated near the feed probe region. Combined with the high temperature provided by the main air, the recirculated particles burn near the wall in that region and cause a lower oxygen concentration as shown in Fig. 3.15a. The red trajectories in Fig. 3.16b represents 200 μm particles, which for both feed air ratios follows a more straight path along the reactor length. Hurt [38] discuss how the residual

carbon in fly ash may be presented by the largest and most dense particles, which have the shortest residence time and have passed through the coolest regions and lowest oxygen concentrations. Thus, the history of a 200 μm particle traveling through the center of the EFR furnace is believed to be coupled with residual carbon properties of the ash collected in the bottom of the reactor.

The burnout history of a 200 μm particle combusted at different feed and excess air ratios is shown in Fig. 3.17. Initially, the particle passes through

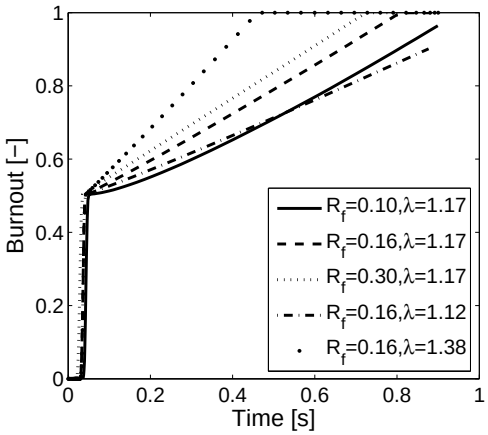

Figure 3.17: Burnout history of a 200 μm particle traveling along the centerline of the reactor at different applied conditions.

the feed probe where no combustion takes place. The steep rise in burnout at a residence of about 0.03 seconds corresponds to the release of volatiles from the coal particles and this is followed by the char burnout, which is expressed by the more moderately increase in burnout. The model predicts that increased feed air ratio and excess air ratio causes a faster burnout with the residence time of the 200 μm particle and this agrees well with a lower observed carbon content in the collected ashes. The residence time of the particle in the reactor differs from 0.8 to 0.9 seconds, with the lowest residence time at highest feed air ratio, but this does not influence the order of burnout at the axial position in the reactor.

Fig. 3.18 presents the conditions that a 200 μm particle is exposed to at different feed air ratios and a total excess air of 1.17, when having a trajectory along the centerline of the EFR. The particle produced at the lowest feed air ratio is exposed to the lowest oxygen concentration and the highest temperature in the early stage of the combustion process, while at higher feed air ratios, the oxygen concentration increases and the temperature decreases.

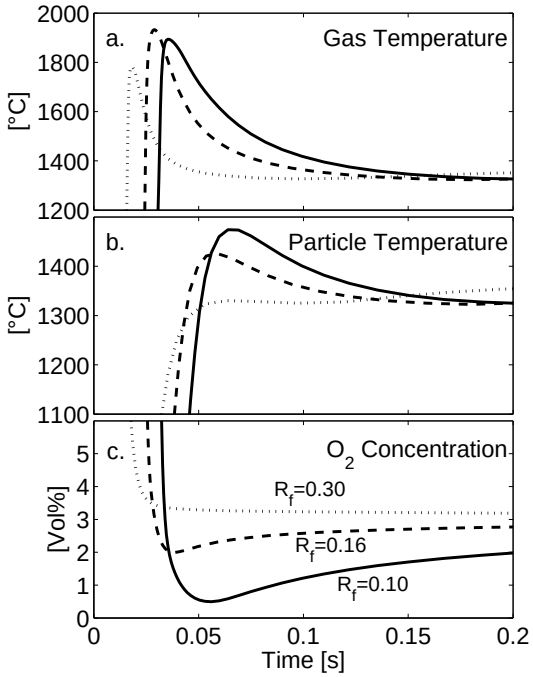

Figure 3.18: (A) Gas temperature, (b) particle temperature and (c) oxygen history as a function of particle residence time of a 200 μm particle along the centerline of the reactor at an excess air ratio of 1.17.

The faster raise in gas temperature compared to particle temperature comes from the combustion of the volatiles. Those conditions found at low feed air ratios cause a poorer burnout in the model and this is agrees well the experimental data. Moreover, they may also increase the specific AEA adsorption capacity of the residual carbon [23].

Some difficulties lies in direct comparisons between the modeled conditions and experimental results, e.g. the NO_x concentration measured in the outlet of the reactor is an integrated value emerged from the conditions existing in the whole reactor. Despite this, the following discussion attempts to draw relations between the experimental results and single spot modeled results, which are believed to be key parameters for AEA adsorption of the fly ash. Again, the focus is attended to a 200 μm particle traveling along the centerline of the reactor. Figs. 3.19a and 3.19b show the maximum flame and particle temperature and the minimum oxygen concentration that the particle is exposed to when changing the feed and excess air ratio, respectively. The results show that a decrease in oxygen concentration is obtained in the near probe region at feed air ratios below 0.20 (Fig. 3.19a). This local

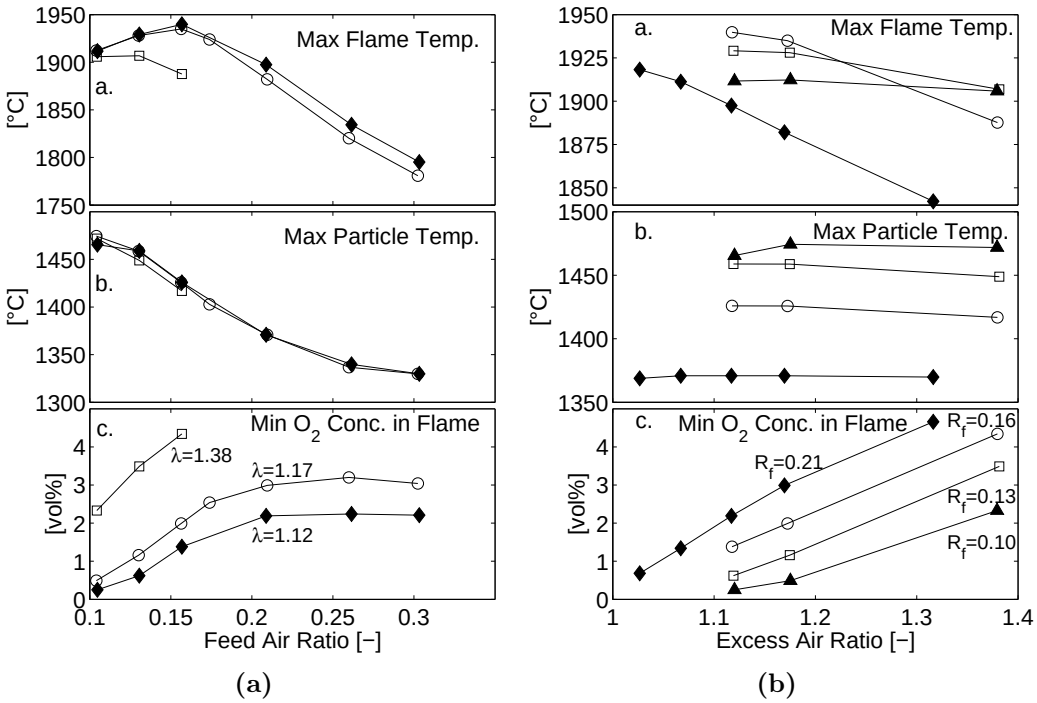

Figure 3.19: Conditions that a 200 μm is exposed to when traveling along the centerline of the reactor as a function of (a) feed air ratio and (b) excess air ratio.

decrease in oxygen concentration is not observed at feed air ratios above 0.20. Therefore, the provided values above a feed ratio of 0.20 correspond to an averaged outlet concentration that is only affected by the applied excess air ratio. The maximum flame temperature (Fig. 3.19a) is observed to initially increase with the feed air ratio at a total excess air of 1.12 and 1.17, presumably caused by the improved mixing between fuel and combustion air. At feed ratios above 0.16, the flame temperature starts to decrease as a consequence of applying higher amounts of non-preheated feed air that lowers the temperature and delays the ignition.

A linear relationship between excess air ratio and the lowest achieved oxygen concentration for the different feed air ratios is observed (Fig. 3.19b). This fits well with the fact that the excess air is controlled by the feed rate of the coal and therefore a change in coal feed rate will change the local stoichiometry in the flame. The maximum flame temperature (Fig. 3.19b) decreases with the excess air ratio and this is caused by the lower fuel load. However, the degree of impact depends on the feed air ratio indicating that the mixing between coal and air is poorer at low ratios. The observation may explain why different feed air ratios give rise to different slopes between

NO_x concentration and excess air ratio (Fig. 3.10b). The maximum particle temperature is observed to be unaffected by changes in total excess air.

Figs. 3.20a and 3.20b are prepared from the assumption that the highest influence of the oxygen concentration on the ash and carbon adsorption behavior occurs at the highest particle temperature, which is reached in the early stage of combustion. A lower oxygen concentration in the early stage

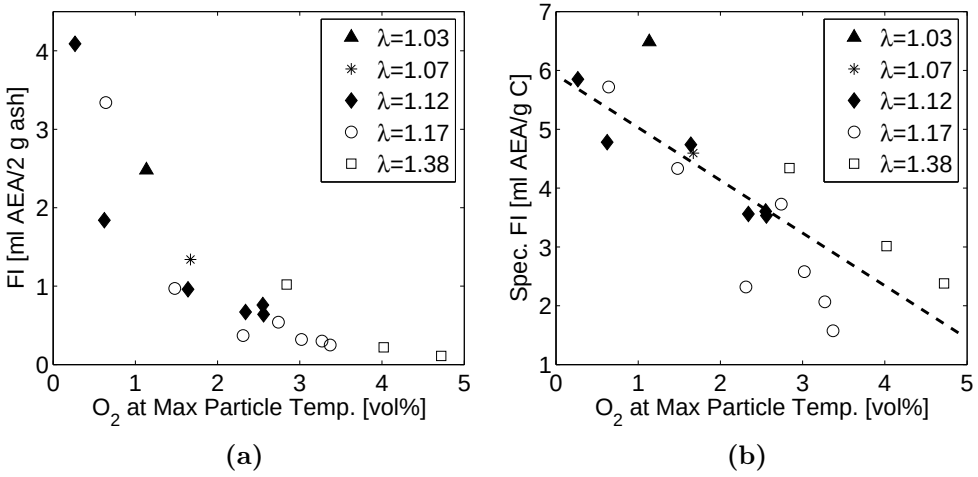

Figure 3.20: (a) FI and (b) spec. FI compared with oxygen concentration at the maximum particle temperature.

of combustion process leads to a higher FI (Fig. 3.20a) and spec. FI (Fig. 3.20b) of the produced ashes, which supports the already discussed trends. Any effect from the excess air ratio on the FI and spec. FI can not be observed, which is probably because the excess air ratio influences the oxygen concentration at maximum particle temperature as well. Regarding the particle temperature, the ashes with the highest FI and spec. FI have experienced the highest particle temperature (Figs. 3.21a and 3.21b) within each series of excess air ratio. However, the effect of oxygen concentration on the specific AEA adsorptivity of the residual carbon is repeated again: applying an excess air ratio of 1.03 gives a low oxygen concentration in the flame and downstream in the reactor, which produces an ash with a high spec. FI (Fig. 3.21b) and this is despite that the obtained maximum particle temperature is in the lower range.

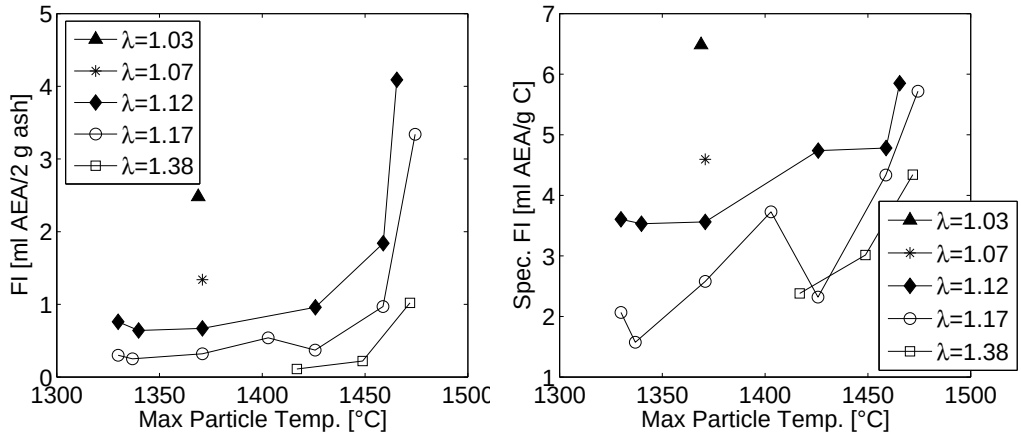

Figure 3.21: (a) FI and (b) spec. FI compared with the maximum particle temperature.

3.4.3 Type of Fuel

The fuel type influences the surfactant adsorptivity of the ash as observed in Fig. 3.22a. The Cerrejon coal ash adsorbs up to two times more AEA

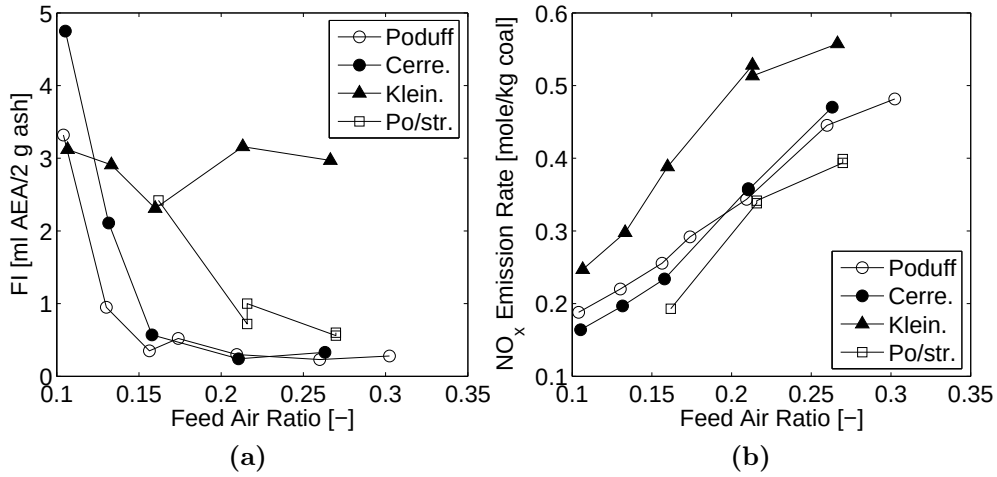

Figure 3.22: The effect of feed air ratio on (a) FI and (b) NO_x emission rate. The FI values of Poduff co-fired with straw are presented by single determination

than the Poduff ash at feed ratios of 0.10 and 0.13, but apart from that they follow the same trend and have similar FI values at higher ratios. The behavior of the Kleinkopje coal ashes is very different from the two high volatile

bituminous coal ashes. Apparently, the FI of these ashes is not affected by the feed air ratio and maintains a constant level of about 3 ml AEA/2 g ash throughout the tested range of feed air ratio, which entails that they at certain conditions obtain up 12 times higher AEA requirements compared to the Poduff ashes. Co-firing Poduff with straw produces ashes with higher AEA adsorption than firing Poduff alone. Moreover, an effect of changing the feed air ratio on the FI is still observed at higher ratios compared to firing with Poduff or Cerrejon.

The achieved NO_x concentration is converted into an emission rate (moles per kg of coal) in order to eliminate the influence of the applied combustion air flow, which differs slightly between the fuel types. Some difference in NO_x formation is observed between the fuels (Fig. 3.22b), which can be caused by several factors such as rank (volatile content), nitrogen content, particle size and char reactivity. In pulverized fuel combustion the major contribution to NO_x formation comes from fuel-N [31], which include both volatile-N and char-N. Volatile-N is mainly released as HCN and NH_3 and is further converted to NO and N_2 depending on temperature and stoichiometric conditions, i.e. more oxidizing conditions leads to higher formation of NO [39]. Therefore, volatile-N is the largest source to NO formation in unstaged combustion, while char-N is the major contributor in staged combustion [31, 39]. Thus, lower NO formation is found with increased volatile amount under staged combustion [39]. Besides the influence from the rank of the coal, the NO formation has also been found to increase with the nitrogen content under both staged and unstaged combustion [40]. The influence of particle size can go in both directions; smaller coal particles lead to increased release of fuel-N with the volatiles, which can reduce the NO_x formation [41]. On the other hand, NO is reduced on char and therefore an increased particle size, which leads to longer residence time of NO in the pores, gives a larger reduction of NO [31]. This residence time is also prolonged when the char has a lower combustion reactivity [31]. In the present work, the highest NO_x formation is found for the Kleinkopje coal. Besides having the highest nitrogen content, it has the lowest reactivity as shown below and the lowest volatile content and all contribute to a higher total NO_x formation under air staged conditions. Kleinkopje has the smallest particle size as well but the effect on the NO_x emission from this is unknown. The NO_x emission rates of Poduff and Cerrejon are similar despite Cerrejon has the highest nitrogen content (see Table 3.1). This may be due Cerrejon also contains the highest amount of volatiles, which has an inverse effect on NO_x formation at fuel rich conditions. Firing the Poduff-straw mixture decreases the NO_x formation compared to firing Poduff alone in agreement with observations made on full-scale co-firing of straw and coal [42]. Again, the lower nitrogen content

combined with higher amounts of volatile in the straw can cause the lower NO_x emission rate.

Increasing the feed air ratio decreases the LOI for all the investigated fuel ashes (Fig. 3.23a). The highest reactivity among the coals is found

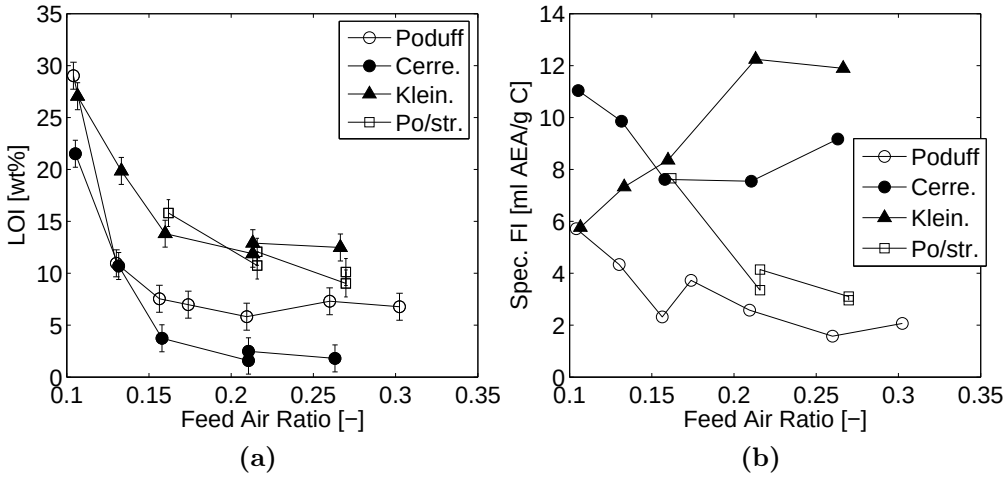

Figure 3.23: (a) LOI and (b) spec. FI compared with feed air ratio.

for Cerrejon, expressed by its high burnout, while Kleinkopje is lowest in reactivity. The reactivity of coal is known to depend on its rank and maceral composition [43]. The rank of coal is the degree of coalification of the organic plant sediment from peat to graphite-like material, the latter being highest in rank [28]. In general, the reactivity [44], oxygen content and volatile content [28] of coal decreases with the rank and studies have shown that the lower reactivity correlates with a lower oxygen content [45] and lower volatile matter to fixed carbon ratio [46]. In the present study, the order of reactivity compared to the content of volatiles and oxygen of the applied coals agrees well with these findings. The macerals are the organic components in coal, which are identifiable in a microscope and they are classified into three groups for bituminous coals: vitrinite, liptine an inertinite [28], where inertinite are the least reactive among the maceral groups [43, 44]. The inertinite content of the Kleinkopje and Cerrejon coal is counted to 74 % and 13 %, respectively, in agreement with the lower reactivity found for Kleinkopje. The maceral composition of the Polish coal has not been determined. In addition TGA measurements of the coal chars (see appendix 3.F) shows same order of reactivity as found for the coals in the EFR experiments.

Mixing Poduff with straw leads to a blend with a lower reactivity and thereby higher carbon content in the produced ash compared with firing Poduff coal alone. The particle size of biomass can control the reactivity of such

blends, where smaller biofuel particles increase burnout [47]. Thus, the significantly higher particle size of straw compared with Poduff do presumably cause the higher carbon content in the ash.

The spec. FI, presented in Fig. 3.23b, reveals that the residual carbon in the coal and biomass ashes have been produced with varying AEA adsorption capacity. The FI values of Poduff and Cerrejon ashes are approximately the same at feed air ratios above 0.16 (Fig. 3.22a), but the carbon content of the Cerrejon ash is lower, which entails that it achieves a significantly higher spec. FI. Moreover, the development in Spec. FI with increased feed air ratio of the Cerrejon ash do also partly differ from the Poduff ash by increasing at the highest feed air ratio where it becomes up to 6 times higher compared with the Poduff ash. The general difference in spec. FI between the two coal ashes may be explained from the BET-N_2 area of their residual carbon. The area is determined to 44 m^2/g C for Poduff and 98 m^2/g for Cerrejon (both produced at a feed air ratio of 0.13) and this correlates well the relative difference in spec. FI. Work performed by others on fly ashes produced from coal with different rank [18], has shown that the spec. FI and surface area is higher in ashes produced from low rank coal or lignite compared to ashes produced from higher rank coals. The present work supports these findings; Cerrejon coal is lowest in rank and shows the highest spec. FI. However, both are considered to be high-volatile bituminous coals.

The increased AEA requirements of ash produced from Poduff co-fired with straw compared with firing Poduff alone is not only caused by an increased carbon content, but also due to a higher specific AEA adsorptivity of the residual carbon (Fig. 3.23b). This result may be explained by the larger particle size of straw, and by straw being a fuel of low rank.

The spec. FI of the Kleinkopje ashes are high as well and inversely affected by the feed air ratio compared with the other fuel types. Similar to applying a low feed air flow, larger agglomerated char particles were observed in the collected ash indicating a higher caking behavior of the Kleinkopje coal compared with Poduff and Cerrejon. Because of their large size, oxygen may not penetrate the particles within the available residence time and therefore, they will not represent the actual combustion conditions. In the preliminary work, such particles were also formed at a feed air flow of approximately 1 Nl/min and the produced ashes showed more than two times higher spec. FI than ashes produced at a feed air flow of 12 Nl/min. These ashes produced at 12 Nl/min had similar carbon contents, but did not contain visible signs of agglomerated particles. Therefore, the formation of such particles is believed to promote an adsorption of AEAs, which may explain the high spec. FI of the Kleinkopje ashes. The observed increase in spec. FI with higher ratios indicates that the relative impact from the formation of the agglomerated

particles becomes larger. The agglomeration behavior of Kleinkopje coal may be explained from its smaller particle size compared to Poduff and Cerrejon, which can promote the agglomeration between particles [48]. The moisture content of Kleinkopje was less than 1 wt% and is not believed to cause its caking behavior.

3.4.4 Influence of Soot

The formation of soot in coal combustion plays an important role, e.g. it increases the radiative heat transfer [49]. Soot is usually formed from the volatile matter by secondary reactions under fuel rich conditions at high temperatures [49] and can have a lower reactivity than unburned char [29]. Bituminous coals have been found to show higher sooting tendency compared to lignite or anthracite [50]. Soot in fly ash can lower its performance in concrete due to its higher AEA adsorptivity compared with char. This was suggested by Gao *et al.* [51] based on adsorption measurements on carbon blacks; being in the form as a fine particulate carbon material, it provides easy accessibility to the AEAs [51]. In the present work, the spec. FI of a carbon black from Cabot Corporation (M1300, 13 nm in primary particle size) is estimated to approximately 30 ml AEA/g C, which is more than 15 times higher than the spec. FI of the commercial fly ash from ENV. Gao *et al.* [51] have reported up to similar differences between carbon blacks and power plant ashes, but the difference is strongly influenced by the particle diameter of the carbon black and suggested to be an external surface area effect.

Various observations made on the EFR indicate that increased soot formation takes place at lower feed air flows. The flame structure in combustion experiments performed on saw dust at a feed air flow of 1.5 Nl/min is shown in Fig. 3.24a [52]. It is clearly seen that soot is formed and escapes the flame and this was not observed at higher feed air flows. In addition, the preliminary work on the FI test procedure involved reuse of test glass cleaned in water. Testing ash samples with high spec. FI (often produced at low feed air ratios) could cause formation of a black film on the glass surface, which could be collected by ultrasonic suspension in ethanol. TEM examination of this material revealed that it was agglomerated particles composed of multiple primary particles in agreement with soot [53]. Fig. 3.24b illustrates such a primary particles and the observed shell/core structure is a possible nanostructure for soot particles [54]. The adhesion of soot on reused glass surfaces may be related to the added AEAs. In concrete mixtures, certain soaps can act as hydrophobic agents when they react with calcium ions and precipitates [24]. Some of these precipitates may stick to test glass surface,

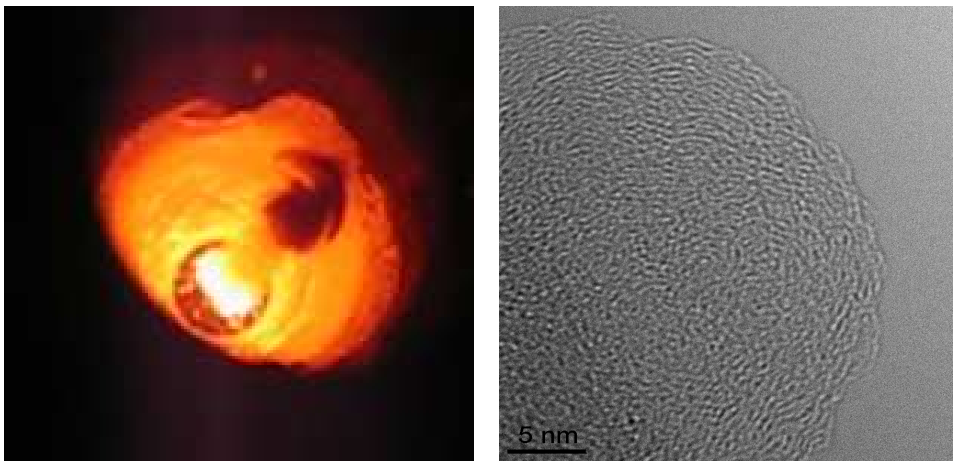

(a) **(b)**

Figure 3.24: (a) Flame structure of burning saw dust at a feed air flow of 1.5 Nl/min (saw dust feed rate of 0.5 kg/h and excess air rate of 1.17) [52]. (b) Primary soot particles from an EFR-ash.

which changes its hydrophilic character to be more hydrophobic and thus becomes capable of adsorbing the non-polar soot particles. The contact angle of water was higher on a reused test glass surface than a non-used indicating that it had gained a more hydrophobic character.

The Kleinkopje ashes formed a black film on the test glass surface as well, indicating that the coal has increased sooting tendency under combustion. Larger particles show higher sooting tendency than smaller particles [50]. In their study [50], 80 μm coal particles combusted in a lean methane/air flame (35 % excess air) were surrounded by a volatile jet, which produced small solid particles believed to be soot. The jet was not observed for 40 μm particles. Thus, the larger agglomerates formed from firing Kleinkopje coal may increase the soot formation and cause an increased spec. FI of the ash.

3.5 Discussion

Based on this work it is evident that combustion conditions and type of fuel influences the AEA adsorption of the produced ash.

3.5.1 The Effect of Operating Conditions

Increasing the oxidizing conditions in the EFR by improved mixing or increased excess air produces ashes with lower AEA requirements, mainly

caused by an increase in burnout, but also due to a lower specific AEA adsorptivity of the residual carbon. A general observation for the Poduff coal is that the ashes with high burnout contain residual carbon with lower specific AEA adsorptivity (Fig. 3.14a) and that the percent-wise reduction in spec. FI within certain operating conditions follows the reduction in LOI (Table 3.8). The modeling results indicate that the chars with poor burnout have been exposed to the lowest oxygen concentrations and, in most cases, the highest particle peak temperatures in the early stage of combustion (see Fig. 3.19). These early interactions can decrease the reactivity of the fuel due to thermal deactivation [55] and drive off surface oxides, thus creating a less polar carbon surface that has a higher affinity to AEAs [23]. The often slow fuel-air mixing applied at these conditions may further screen the particles from the oxygen by the cloud of volatiles released under the pyrolysis and lead to increased formation of soot, which has a high adsorption capacity of AEAs [51]. The development in surface area and porosity of char, which are properties that affects the AEA adsorption as well, is influenced by the oxygen concentration under the pyrolysis. Others have found that the surface area of coal chars both increases [56, 57] and decreases [57] with the oxygen concentration under pyrolysis. Moreover, the study from Gale *et al.* [57] observed that increased particle temperatures under pyrolysis caused both a higher and lower porosity of the chars. These char properties have not been given further attention in the present work and therefore it is not known how they develop under the applied conditions. Nevertheless, total available carbon surface area decreases with the burnout [58] and thus less adsorption sites will be available for the AEAs in the total ash.

Comparing the NO_x concentrations with the FI values (Fig. 3.25a) reveals an interesting behavior. Apparently, a trade-off exists between the NO_x formation, here expressed by the NO_x concentration, and the FI of the produced EFR-ashes. Below a NO_x concentration of 550-650 ppm, even small changes in the oxidizing conditions have a large impact on the AEA adsorption of the ash. On the other hand, above this threshold, a further change in combustion conditions mainly lead to higher NO_x concentration with less impact on the AEA adsorption behavior of the ash. The specific AEA adsorptivity of the residual carbon compared with the NO_x concentration (Fig. 3.25b) supports the results by Gao *et al.* [23]; the residual carbon produced at lower NO_x concentration tends to have increased AEA adsorptivity, though the measured NO_x concentration can not solely be used as an indicator for the adsorption behavior of the residual carbon.

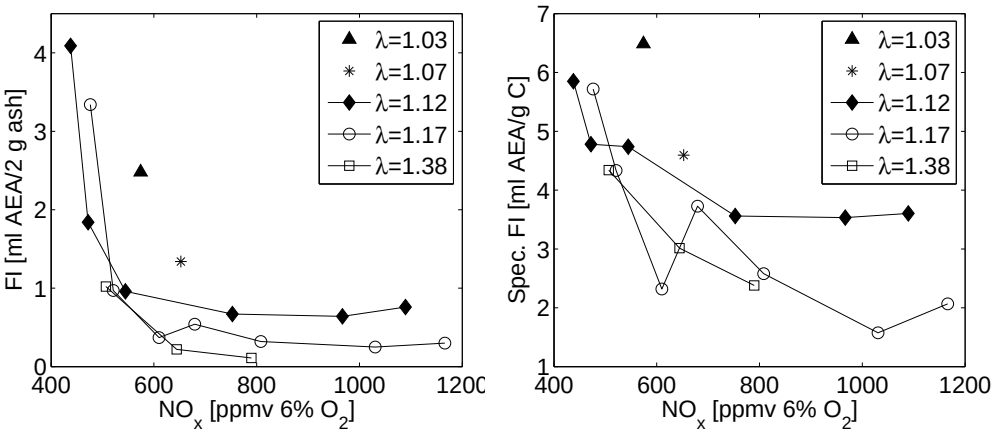

Figure 3.25: (a) FI and (b) spec FI compared with the NO_x concentration achieved at different total excess air.

3.5.2 The Effect of Fuel Type

The type of fuel has impact on the AEA requirements of the produced ash in addition to the combustion conditions (Fig. 3.22a). Moreover, the absolute difference in specific AEA adsorptivity of the residual carbon can be higher between burning different types of fuel compared to changing the feed air ratio on the EFR (Fig. 3.23b). Despite this, it may not be revealed by the FI of the total ash, e.g. the residual carbon of the Cerrejon ash has from 2 to 6 times higher specific AEA adsorptivity compared with the carbon in Poduff ash at feed air ratios above 0.16, but shows the same FI due to its lower carbon content. However, the consequences of increasing carbon content in the Cerrejon ash will be worse compared with Poduff ash as discussed elsewhere [18].

The observed behaviour of Kleinkopje coal is interesting. An important question is wether significant agglomeration takes place at full-scale conditions and if it cause a poor performance of the ash in concrete. Agglomeration of coal occurs in blast furnaces when pulverized coal replaces coke [29]. It has been observed under combustion of single pulverized coal char particles [48] and in drop tube furnace experiments under inert conditions [29], but can generally be ignored at pulverized fuel combustion with respect to burnout [59]. The latter remains unanswered in the present work, but the results suggest that agglomeration can have an impact on the AEA adsorption of the ash due to formation of some highly AEA adsorptive residual carbons (see Fig. 3.23b). These carbons may partly be in the form of soot, since larger particles have higher sooting tendency [50]. Moreover, the larger char

particles may be exposed to lower oxygen concentrations due to a screening effect from the volatiles. This effect increases with the particle size [56] and is also observed for lower rank coals. Thus, in addition to the higher surface area of the Cerrejon ash, such conditions may lead to the higher spec. FI of the Cerrejon ash compared to the Poduff ash.

3.5.3 The Effect of Soot

The sooting tendency observed at low feed air rates or when burning the Kleinkopje coal indicates that the adsorption properties of ash is not related to the char properties alone. Furthermore, soot formation complicates the comparison between experimental results and modeling, where soot formation is not taken into account. It has been suggested, that soot concentrations in power plant ashes are too low to significantly affect air entrainment in concrete [51]. Veranth *et al.* [60] separated a high carbon ash into a fine and coarse fraction suggested to be soot and char, respectively. The average fraction of soot in four power plant ashes was estimated to be about 16 % of the total carbon. Based on the spec. FI values of the full-scale ashes (Table 3.4) and the spec. FI of the investigated carbon black (30 ml AEA/g C), the following scenario can be outlined: a 16 % soot content of the total carbon in the ENV ash will increase the spec. FI from 1.8 to 6.5 ml AEA/g C, which make the FI of the total ash increase from 0.10 to 0.31 ml AEA/2 g ash. Thus, the ENV ash would obtain higher AEA requirements than the NJV ash of 0.28 ml AEA/2 g ash suggesting that soot can have an influence on the AEA requirements of the fly ash. As a note to this, the level of polycyclic aromatic hydrocarbons (PAHs), precursors for soot, have been found higher in fly ash from NJV3 compared to fly ash from a power plant [61] that to the authors knowledge do not cause problems when it is utilized in concrete.

3.5.4 Practical Problems

A coupling of the mechanisms that contributes to the specific AEA adsorptivity of the residual carbon is still an unresolved issue. The results presented here support what others have shown that surface area alone does not control the adsorption. A main focus of the present work was to produce ashes with carbon contents within the same order of magnitude as full-scale ashes. This does on the other hand lead to an ash that is mainly composed of inorganic material, which can highly interfere with methods used for further analysis, e.g. mercury porosity determination. Recovering carbon from the ash samples by separating techniques, does not remove all carbon from the sample and may still leave a mineral fraction containing carbon with large

AEA adsorptivity [23]. Determination of char surface chemistry by for instance time-of-flight secondary ion mass spectrometry (TOF-SIMS) is also problematic due to the irregular shape of the char and the presence of inorganic compounds in its structure. Eventually, the presence of soot can cause increased AEA requirements of the ash, but the sticky nature of soot makes it difficult to completely separate it from the ash.

3.6 Practical Implementation

Based on the results from the EFR experiments, we can point out some relevant parameters, which may be altered for a beneficial operation of a power plant, where the marketability of the fly ash is an important factor in a cost effective power generation.

Our findings suggest that the AEA requirements of fly ash can be lowered by changing the operating conditions toward more oxidizing conditions in the early stage of combustion. In a power plant applying furnace air staging such conditions can be achieved by operating with more burner air and less over burner air and over fire air at constant overall stoichiometry (see chapter 4). In the EFR experiments, the more oxidizing conditions decrease the unburned carbon content in the ash as well as its specific AEA adsorptivity (per gram of carbon), but they give rise to increased NO_x formation, i.e. there is a trade-off between the AEA requirements of the ash and the NO_x formation. The latter can be compensated by increased removal in a downstream $DeNO_x$ process by increasing the NH_3 injection (see chapter 4). A further benefit from increasing the oxidizing conditions in the early stage of combustion is that it can decrease the formation of soot. Results indicated that soot can have high adsorption capacity of AEAs, and therefore its formation in the coal flame should be minimized. At full-scale conditions, formed soot may be destroyed further downstream by effective mixing with remaining combustion air.

Changing the type of fuel can be an alternative to adjust the operation conditions. It can improve the burnout, which for certain fuels have a positive effect on AEA requirements of the produced ash. However, for some fuels the improved burnout does not necessarily cause a lower total FI, if the resulting ash contains carbon with a higher AEA adsorptivity. Some fuels should be totally avoided, either due to a poor burnout, but also because the residual carbon of the ash can have a very high specific AEA adsorption capacity. The negative impact of a single poor coal on the AEA adsorption of the fly ash may be however diluted by blending coals of different types. Other benefits from coal blending includes lower costs, lower SO_2 emissions and improved

combustion performance [62].

3.7 Summary

The AEA adsorption of an ash utilized in concrete is primarily related to the amount of residual carbon present in the ash and its AEA adsorption capacity. In the present work, pulverized bituminous coals and a straw have been combusted in an entrained flow reactor with the aim of testing the impact of operating conditions and fuel type on AEA adsorption properties of the ash and the NO_x formation. The experimental results have been compared with the combustion conditions predicted by CFD modeling.

The oxidizing conditions in the reactor are controlled by the feed air ratio or the excess air ratio, where an increase in both decreases the AEA requirements of the produced ash by up to a factor of 25. This is caused by a decrease in the carbon content combined with a lower specific AEA adsorptivity of the carbon. The results indicate that the ashes with the poorest burnout and highest specific AEA adsorptivity of the residual carbon are produced at the lowest oxygen concentrations in the early stage of the combustion. These conditions occur at the lowest feed air ratio, where the rate of mixing between coal particles and combustion air is lowest. Combining this with a decrease in excess air that further lowers the oxygen concentration, ashes with high carbon contents and high specific AEA adsorptivities are produced. Operating the EFR to produce ash with lower AEA requirements increases the NO_x formation by up to three times due to the higher oxidizing conditions in the early stage of the combustion, i.e. there is a trade-off between these two parameters.

Three types of bituminous coal and one coal/straw mixture were fired in the EFR. Ash produced from a Columbian coal being lowest in rank contains carbon having two to six times higher specific AEA adsorptivity compared to an ash produced from a Polish coal. However, due to the lower carbon content of the Colombian ash, the AEA requirements of the total ash are similar to the Polish ash, which contains a larger amount of carbon. The BET-N_2 surface area of the residual carbon in the Colombian coal ash is at one operating condition about two times higher than in the ash produced from the Polish coal and this may partly explain its increased AEA adsorptivity. A South African coal being highest in rank shows diverging behavior, i.e. the feed air ratio does not affect the AEA requirements of the ash, which therefore at certain operating conditions are up to 12 times higher compared to the two other coal ashes. Apparently, the South African coal has higher tendency to agglomerate leading to larger particles. This enhances the for-

mation of a residual carbon having a high AEA adsorptivity. Part of this carbon could be in the form of soot, which has a high adsorption capacity of AEAs. Visual flame observations and TEM examination of an ash produced from the Colombian coal, indicates that increased soot formation occurs at lower feed air ratios as well. Co-firing straw with coal increases the AEA requirements of the total ash compared to firing coal alone. This is partly caused by a higher carbon content in the ash, presumably related to the larger particle size of straw compared to the coal, but the higher AEA requirements are also due to a higher specific AEA adsorptivity of the residual carbon.

In conclusion, we have suggested some relevant parameters, which may be altered for an improved operation of a power plant. These include rearranging of combustion air in the furnace in order to achieve more oxidizing conditions in the early stage of combustion and avoid or blend fuels, which give rise to the formation of ashes with high AEA requirements.

3.8 Acknowledgements

The CHEC Research Centre is co-funded by the Technical University of Denmark, DONG Energy A/S, FLSmidth A/S, The Hempel Foundation, Vattenfall A/S, Haldor Topsøe A/S, Energinet.dk, the Danish National Advanced Technology Foundation, the Danish Technical Research Council, the Danish Energy Research Programme, Nordic Energy Research, the European Union, and several other industrial partners.

3.9 Abbreviations

AEA	air-entraining admixture
BET	Brunauer-Emmet-Teller
BJH	Barrett-Joyner-Hallender
CFD	computational fluid dynamics
EDX	X-ray spectroscopy
ENV	Enstedværket
EFR	entrained flow reactor
FI	foam index
LOI	loss-on-ignition
NJV3	Nordjyllandsværket, unit 3
SEM	scanning electron microscopy
Spec. FI	specific foam index
TEM	transmission electron microscopy
TGA	thermogravimetric analysis

3.10 References

[1] K. H. Pedersen, S. I. Andersen, A. D. Jensen, K. Dam-Johansen, Replacement of the foam index test with surface tension measurements, Cement and Concrete Research 37 (6) (2007) 996–1004.

[2] R. B. Bird, W. E. Steward, E. N. Lightfoot, Transport Phenomena, 2nd Edition, John Wiley & Sons, New York, 2002, p. 51.

[3] S.-S. Hsieh, C.-Y. Lin, C.-F. Huang, H.-H. Tsai, Liquid flow in a microchannel, Journal of Micromechanics and Microengineering 14 (4) (2004) 436–445.

[4] A. A. F. Peters, R. Weber, Mathematical modeling of a 2.4 MW swirling pulverized coal flame, Combustion Science and Technology 122 (1-6) (1997) 131.

[5] B. F. Magnussen, B. H. Hjertager, On mathematical modeling of turbulent combustion with special emphasis on soot formation and combustion, in: Proceedings of the Combustion Institute, Vol. 16, 1976.

[6] T. Asotani, T. Yamashita, H. Tominaga, Y. Uesugi, Y. Itaya, S. Mori, Prediction of ignition behavior in a tangentially fired pulverized coal boiler using CFD, Fuel 87 (4-5) (2008) 482–490.

[7] J. W. Rose, J. R. Cooper, Technical Data on Fuel, 7th Edition, Scottish Academic Press, Edinburgh, 1977.

[8] S. Badzioch, G. W. Hawksly, Kinetics of thermal decomposition of pulverized coal particles, Ind Eng Chem Process Des Develop 9 (4) (1970) 521–30.

[9] K. G. Neoh, R. E. Gannon, Coal volatile yield and element partition in rapid pyrolysis, Fuel 63 (10) (1984) 1347–1352.

[10] M. M. Baum, P. J. Street, Predicting the combustion behaviour of coal particles, Combustion Science and Technology 3 (1971) 231–243.

[11] M. A. Field, Rate of combustion of size-graded fractions of char from a low-rank coal between 1200 °K and 2000 °K, Combustion and Flame 13 (3) (1969) 237–252.

[12] K. J. Knill, T. F. J. Maalman, M. E. Morgan, Development of a combustion characterization technique for high volatile bituminous coals, report of the CC 4 trials, Tech. Rep. F 88/a/10, International Flame Research Foundation, IJmuiden, The Nederlands (1989).

[13] R. Backreedy, L. Fletcher, L. Ma, M. Pourkashanian, A. Williams, Modelling pulverised coal combustion using a detailed coal combustion model, Combustion Science and Technology 178 (4) (2006) 763–787.

[14] P. T. Jensen, R. E. Mitchell, High temperature char reactivity measurements in the sandia laminar flow reactor. part 1: Text, Energy Research Project No. 1323/87-16, Ministry of Environment, Geological Survey of Denmark, Copenhagen, Denmark (1993).

[15] C. J. Lawn (Ed.), Principles of combustion engineering for boilers, 1st Edition, Academic Press, London, 1987, pp. 238–239.

[16] A. Williams, R. Backreedy, R. Habib, J. Jones, M. Pourkashanian, Modelling coal combustion: the current position, Fuel 81 (5) (2002) 605–618.

[17] E. Freeman, Y.-M. Gao, R. Hurt, E. Suuberg, Interactions of carbon-containing fly ash with commercial air-entraining admixtures for concrete, Fuel 76 (8) (1997) 761–765.

[18] I. Külaots, R. H. Hurt, E. M. Suuberg, Size distribution of unburned carbon in coal fly ash and its implications, Fuel 83 (2) (2004) 223–230.

[19] R. L. Hill, S. L. Sarkar, R. F. Rathbone, J. C. Hower, An examination of fly ash carbon and its interactions with air entraining agent, Cement and Concrete Research 27 (2) (1997) 193–204.

[20] M. T. Hasholt, Afklaring af problemer med NJV-flyveaske. Trin 2: Undersøgelse af asken vha. foam index-metoden, Tech. Rep. 2, Danish Technological Institute, Taastrup, Denmark (2003).

[21] R. P. van der Lans, P. Glarborg, K. Dam-Johansen, P. Knudsen, G. Hesselmann, P. Hepburn, Influence of coal quality on combustion performance, Fuel 77 (12) (1998) 1317–1328.

[22] B. R. Stanmore, S. P. Visona, Prediction of NO emissions from a number of coal-fired power station boilers, Fuel Processing Technology 64 (1-3) (2000) 25–46.

[23] Y. Gao, I. Külaots, X. Chen, E. M. Suuberg, R. H. Hurt, J. M. Veranth, The effect of solid fuel type and combustion conditions on residual carbon properties and fly ash quality, in: Proceedings of the Combustion Institute, Vol. 29, 2002, pp. 475–483.

[24] P. C. Hewlett (Ed.), Lea's chemistry of cement and concrete, 4th Edition, Elsevier Butterworth-Heinemann, Oxford, 1998, pp. 480–485, 889-890.

[25] P. Rosenberg, H. I. Petersen, E. Thomsen, Combustion char morphology related to combustion temperature and coal petrography, Fuel 75 (9) (1996) 1071–1082.

[26] J. F. Unsworth, D. J. Barratt, P. T. Roberts, Coal Quality and Combustion Performance, Vol. 19 of Coal Science and Technology, Elsevier, Amsterdam, 1991.

[27] J. Yu, I. Külaots, N. Sabanegh, Y. Gao, R. Hurt, E. Suuberg, *et al.*, Adsorptive and optical properties of fly ash from coal and petroleum coke co-firing, Energy and Fuels 14 (3) (2000) 591–596.

[28] K. L. Smith, L. D. Smoot, T. H. Fletcher, R. J. Pugmire, The structure and reaction processes of coal, 1st Edition, Plenum Press, London, 1994, p. 9.

[29] W. H. Chen, S. W. Du, T. H. Yang, Volatile release and particle formation characteristics of injected pulverized coal in blast furnaces, Energy Conversion and Management 48 (7) (2007) 2025–2033.

[30] S.-W. Kang, A. F. Sarofim, J. M. Beèr, Agglomerate formation during coal combustion: A mechanistic model, Combustion and Flame 86 (3) (1991) 258–268.

[31] P. Glarborg, A. D. Jensen, J. E. Johnsson, Fuel nitrogen conversion in solid fuel fired systems, Progress in Energy and Combustion Science 29 (2) (2003) 89–113.

[32] D. W. Pershing, J. O. L. Wendt, Pulverized coal combustion: the influence of flame temperature and coal composition on thermal and fuel NO_x, in: Proceedings of the Combustion Institute, Vol. 16, 1976, pp. 389–399.

[33] J. Tomeczek, Coal combustion, Krieger Publishing Company, Malabar, Florida, 1994, Ch. 3.

[34] H. Spliethoff, U. Greul, H. Rüdiger, K. R. G. Hein, Basic effects on NO_x emissions in air staging and reburning at a bench-scale test facility, Fuel 75 (5) (1996) 560–564.

[35] L. S. Xiao, J. F. Cheng, H. C. Zeng, Effects of bluff-body burner and coal particle size on NO_x emissions and burnout, Journal of the Institute of Energy 72 (493) (1999) 112–116.

[36] R. Hill, R. Rathbone, J. C. Hower, Investigation of fly ash carbon by thermal analysis and optical microscopy, Cement and Concrete Research 28 (10) (1998) 1479–1488.

[37] K. H. Pedersen, M. S. Skjøth-Rasmussen, A. D. Jensen, K. Dam-Johansen, A review of the interference of carbon containing fly ash with air entrainment in concrete, Progress in Energy and Combustion Science 34 (2) (2008) 135–154.

[38] R. H. Hurt, Structure, properties, and reactivity of solid fuels, in: Proceedings of the Combustion Institute, Vol. 27, 1998, pp. 2887–2904.

[39] R. P. van der Lans, P. Glarborg, K. Dam-Johansen, Influence of process parameters on nitrogen oxide formation in pulverized coal burners, Progress in Energy and Combustion Science 23 (4) (1997) 349–377.

[40] S. L. Chen, M. P. Heap, D. W. Pershing, G. B. Martin, Influence of coal composition on the fate of volatile and char nitrogen during combustion, in: Proceedings of the Combustion Institute, Vol. 19, 1982, pp. 1271–1280.

[41] H. Maier, H. Spliethoff, A. Kicherer, A. Fingerle, K. R. G. Hein, Effect of coal blending and particle size on NO_x emission and burnout, Fuel 73 (9) (1994) 1447–1452.

[42] L. S. Pedersen, H. P. Nielsen, S. Kiil, L. A. Hansen, K. Dam-Johansen, F. Kildsig, J. Christensen, P. Jespersen, Full-scale co-firing of straw and coal, Fuel 75 (13) (1996) 1584–1590.

[43] B. N. Nandi, T. D. Brown, G. K. Lee, Inert coal macerals in combustion, Fuel 56 (2) (1977) 125–130.

[44] J. C. Crelling, N. M. Skorupska, H. Marsh, Reactivity of coal macerals and lithotypes, Fuel 67 (6) (1988) 781–785.

[45] S. Charpenay, M. A. Serio, P. R. Solomon, Prediction of coal char reactivity under combustion conditions, in: Proceedings of the Combustion Institute, Vol. 24, 1992, pp. 1189–1197.

[46] G. Liu, R. C. Erbar, Characterizations of reactivity of coals and chars, Petroleum Science and Technology 11 (3-4) (1993) 463.

[47] H. Rudiger, A. Kicherer, U. Greul, H. Spliethoff, K. R. G. Hein, Investigations in combined combustion of biomass and coal in power and plant technology, Energy and Fuels 10 (3) (1996) 789.

[48] R. Hurt, K. Davis, Percolative fragmentation and spontaneous agglomeration, Combustion and Flame 116 (4) (1999) 662–670.

[49] T. H. Fletcher, J. Ma, J. R. Rigby, A. L. Brown, B. W. Webb, Soot in coal combustion systems, Progress in Energy and Combustion Science 23 (3) (1997) 283–301.

[50] W. R. Seeker, G. S. Samuelsen, M. P. Heap, J. D. Trolinger, Thermal decomposition of pulverized coal particles, in: Proceedings of the Combustion Institute, Vol. 18, 1981, pp. 1213–1226.

[51] Y.-M. Gao, H.-S. Shim, R. H. Hurt, E. M. Suuberg, N. Y. C. Yang, Effects of carbon on air entrainment in fly ash concrete: The role of soot and carbon black, Energy and Fuels 11 (2) (1997) 457–462.

[52] W. Lin, Department of Chemical Engineering, Technical University of Denmark, Personal communication (Oct 2007).

[53] J. Ma, T. H. Fletcher, B. W. Webb, Thermophoretic sampling of coal-derived soot particles during devolatilization, Energy and Fuels 9 (5) (1995) 802–808.

[54] R. H. Hurt, G. P. Crawford, H. S. Shim, Equilibrium nanostructure of primary soot particles, in: Proceedings of the Combustion Institute, Vol. 28, 2000, pp. 2539–2546.

[55] H.-S. Shim, R. H. Hurt, Thermal annealing of chars from diverse organic precursors under combustion-like conditions, Energy and Fuels 14 (2) (2000) 340–348.

[56] D. Alvarez, A. G. Borrego, The evolution of char surface area along pulverized coal combustion, Energy and Fuels 21 (2) (2007) 1085–1091.

[57] T. K. Gale, T. H. Fletcher, C. H. Bartholomew, Effects of pyrolysis conditions on internal surface areas and densities of coal chars prepared at high heating rates in reactive and nonreactive atmos pheres, Energy and Fuels 9 (3) (1995) 513.

[58] K. A. Davis, R. H. Hurt, N. Y. C. Yang, T. J. Headley, Evolution of char chemistry, crystallinity, and ultrafine structure during pulverized-coal combustion, Combustion and Flame 100 (1995) 31–40.

[59] R. W. Shampine, R. D. Cohen, Y. Bayazitoglu, C. F. Anderson, Effect of agglomeration on pulverized-coal combustion, Combustion and Flame 101 (1-2) (1995) 185–191.

[60] J. M. Veranth, T. H. Fletcher, D. W. Pershing, A. F. Sarofim, Measurement of soot and char in pulverized coal fly ash, Fuel 79 (9) (2000) 1067–1075.

[61] B. Sander, DONG Energy A/S, Denmark, Personal communication (June 2004).

[62] A. M. Carpenter, Coal blending for power stations, Tech. Rep. IEACR/81, International Energy Agency (IEA) Coal Research, London, UK (1995).

[63] P. G. Saffman, The lift on small sphere in slow shear flow, Journal of Fluid Mechanics 22 (1965) 385–400.

[64] K. Dam-Johansen, P. Glarborg, note, Department of Chemical Engineering (2002).

[65] L. Brøndum, J. D. Monrad, Statistik II, Anvendt statistik, 5th Edition, Den private ingeniørfond, København, 1998, pp. 402–416.

[66] S. Katta, D. L. Keairns, Effect of time/temperature history on char reactivity, Canadian Journal of Chemical Engineering 64 (6) (1986) 994–1000.

[67] H.-Y. Cai, A. J. Güell, I. N. Chatzakis, J.-Y. Lim, D. R. Dugwell, R. Kandiyoti, Combustion reactivity and morphological change in coal chars: effect of pyrolysis temperature, heating rate and pressure, Fuel 75 (1) (1996) 15–24.

[68] A. Zolin, A. Jensen, L. S. Pedersen, K. Dam-Johansen, A comparison of coal char reactivity determined from thermogravimetric and laminar flow reactor experiments, Energy and Fuels 12 (2) (1998) 268–276.

[69] S. Dutta, C. Y. Wen, Reactivity of coal and char 2. in oxygen-nitrogen atmosphere, Ind Eng Chem Process Des Dev 16 (1) (1977) 31–37.

[70] A. Zolin, Ph.D. thesis, Department of Chemical and Biochemical Engineering , Technical University of Denmark (2000).

Appendices

3.A Ash Sampling Calculations

Isokinetic gas sampling was intended in order to collect a representative size distribution of the particles from the flue gas stream. The required sampling flow is based on the calculated flue gas flow and the sampling probe factor. The sampled volume is determined by a gas flow meter. Table 3.10 presents data for an experiment performed at feed air ratio of 0.16 and excess air ratio of 1.38.

Gas flow meter, start	8633	l
Gas flow meter, end	9261	l
Time	21.9	min
Temperature in gas meter	300	K
Pressure in gas meter	25	mbar
Flue gas flow[a]	56.3	Nl/min
Probe factor ($d^2_{\text{probe}}/d^2_{\text{reactor}}$)	0.16	
Ash collected	7.0	g
Coal consumed	124	g
Ash content of coal	15.4	wt%
LOI of ash	1.9	wt%

Table 3.10: Data for and experiment performed with Poduff coal, $R_f = 0.16$ and $\lambda = 1.38$.
[a]Estimated from equations presented in appendix 3.C

The desired sampling velocity is based on laminar flow in the reactor (Re < 400), which gives a parabolic flow profile where the center flow velocity is two times higher than the average velocity [2]. The calculations, based on an example, are shown in Table 3.11. The higher obtained sampling flow rate compared

Sampled flow	:	$\frac{9261\ \text{l} - 8633\ \text{l}}{21.9\ \text{min}}$	=	28.7	l/min
Adjusted flow	:	(The pump contribute with 1.5 l/min of false air)	=	27.2	l/min
Normalized flow	:	$27.2\ \text{l/min} \cdot \frac{273.15\ \text{K}}{300\ \text{K}} \frac{1038\ \text{mbar}}{1013\ \text{mbar}}$	=	25.4	Nl/min
Expected flow[a]	:	$0.160 \cdot 56.3\ \text{Nl/min} \cdot 2$	=	18.0	Nl/min
% of desired flow	:	$\frac{25.4\ \text{Nl/min}}{18.0\ \text{Nl/min}} \cdot 100\%$	=	141	%

Table 3.11: Sampled volume flow calculations.
[a]Based on a parabolic flow profile and sampling in the center of the reactor, not compensated for that the probe spans over a larger area.

to the theoretical is explained from a wrongly assumed sample probe diameter. Initially, the sampling flow rate was dimensioned to a probe diameter of 3.9 cm, but later inspection of the sampling probe inlet revealed that the diameter was only 3.2 cm. In order to maintain consistency throughout the experimental work, the applied sampling flow was maintained. In addition, a high sampling flow is beneficial for achieving sufficient amounts of ash for further analysis. Table 3.12 presents the achieved sampled flow rates given in percentage of desired flow. The wide span of the range comes from the

% sampled flow of expected flow	130	(96 - 147)
Amount of ash [g]	8.9	(2.8 - 21.1)
% ash of expected amount	75	(46 - 109)

Table 3.12: Particle sampling flows and collected ash amount presented as an average value. The range is given brackets.

coal/straw co-firing experiments, where the sampling probe was often blocked by larger particles giving rise to a lower gas sampling flow.

Table 3.12 includes the collected ash amounts given as a total value and percentage of expected. Again the lowest ash amounts are found among the coal/straw co-firing experiments. An example of the calculations is found in Table 3.13. The ash particles are assumed to be evenly distributed in the gas phase and follow the streamlines of the gas. The collected amounts fulfill the

Total ash produced	:	$\frac{124\ \text{g}\cdot 0.154}{(100-1.9\ \text{wt\%})/100}$	=	19.4	g
Expected ash collected	:	$19.4\ \text{g}\frac{25.4\ \text{Nl/min}}{56.3\ \text{Nl/min}}$	=	8.7	g
% of desired amount	:	7.0 g/8.7 g$\cdot$ 100 %	=	80	wt%

Table 3.13: The calculations involved in comparing expected and actual collected ash amount.

requirements for further analysis, but are lower than estimated. The too high sampling flow may explain this observation; the gas streamlines are bend into the nozzle at higher sampling flows than at isokinetic sampling and this will cause that some particles will pass the nozzle due to their inertia. Therefore, the size distribution may be shifted toward a smaller particle diameter. The parabolic flow profile may also give rise to a lift on the particles making them migrate toward the reactor wall [63].

3.B Example of Experimental Data

Figs. 3.26 and 3.27 shows the experimental data for a run with Poduff coal in atmospheric air at a feed air ratio of 0.16 and total excess air of 1.38.

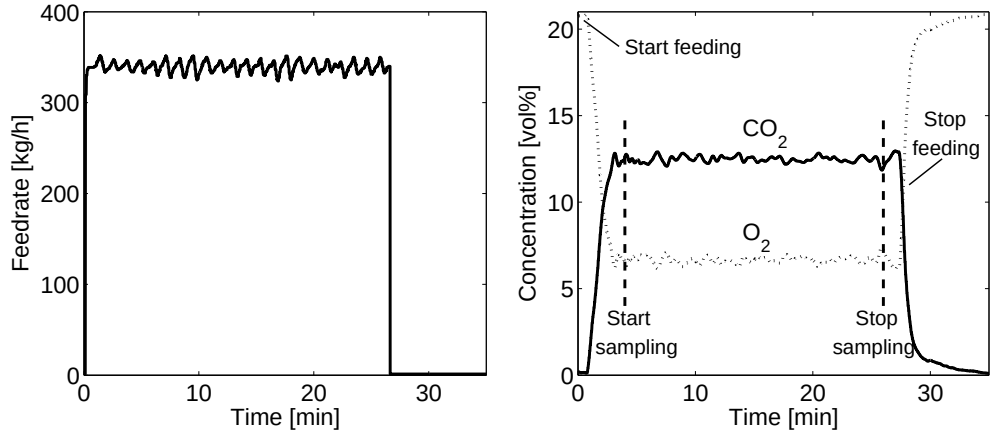

Figure 3.26: Left: feedrate. Right: O_2 and CO_2.

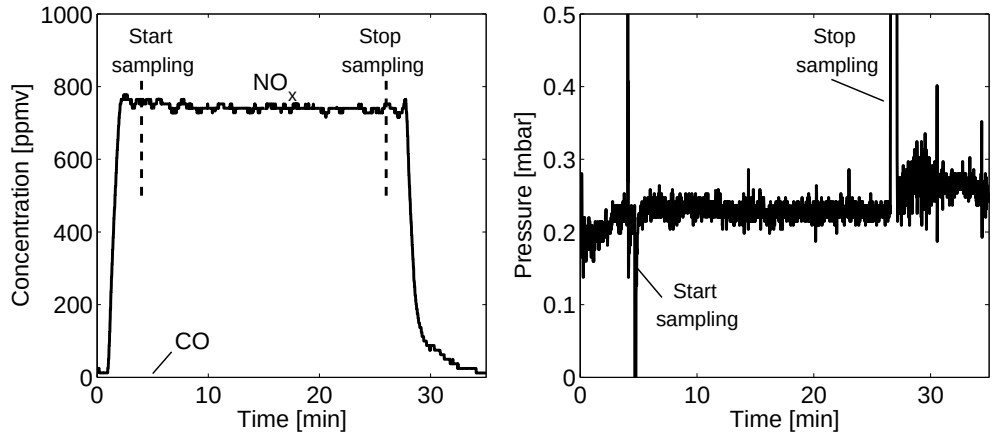

Figure 3.27: Left: NO_x and CO. Right: relative reactor pressure.

The Figs. are provided with comments to illustrate the operation of the particle feeder and gas sampling in a run. The reported concentrations represent the average value of the measurements. The relative reactor pressure is 0.4 mbar higher than the pressure measured by an U-manometer, i.e. the reactor was operated in sub-pressure to avoid the release of harmful emissions to the surroundings.

3.C Stoichiometric Calculations

The stoichiometric equation for the combustion of coal having a molar composition of $C_\alpha H_\beta S_\gamma N_\delta O_\phi \cdot (H_2O)_\mu$(s) is written as [64]:

$$C_\alpha H_\beta S_\gamma N_\delta O_\phi \cdot (H_2O)_\mu(s) + (\alpha + \beta/4 + \gamma + \delta/2 - \phi/2)O_2 \rightarrow \alpha CO_2 + (\beta/2 + \mu)H_2O + \gamma SO_2 + \delta NO$$

where the molar composition, e.g. carbon is estimated from $\alpha = X_C/M_C$, X_C is gram carbon/kg fuel and M_C is the molar mass of carbon.
The min. amount of O_2 and air in moles/kg fuel is calculated according to

$$N_{O_2,\min} = \alpha + \beta/4 + \gamma + \delta/2 - \phi/2 \qquad \text{and} \qquad N_{\text{air},\min} = \frac{N_{O_2,\min}}{x_{O_2}^{\text{air}}}$$

where $x_{O_2}^{\text{air}}$ is the molar fraction of oxygen in the combustion air.
The excess air ratio is related to $N_{\text{air,min}}$ and the applied combustion air, N_{air}.

$$\lambda = \frac{N_{\text{air}}}{N_{\text{air},\min}}$$

The flue gas is given in total amount, N_{FG}, and total dry amount, $N_{\text{FG,dry}}$.

$$\begin{aligned} N_{\text{FG},\min} &= N_{\text{air},\min} + \beta/4 + \mu + \delta/2 + \phi/2 \\ N_{\text{FG}} &= N_{\text{FG},\min} + (\lambda - 1)N_{\text{air},\min} \\ N_{\text{FG,dry}} &= (1 - x_{H_2O}^{\text{air}})\lambda N_{\text{air},\min} - \beta/4 + \delta/2 + \phi/2 \end{aligned}$$

The amount of dry flue gas is used to calculate the theoretical oxygen concentration at complete burnout of the coal particles.

$$x_{O_2}^{FG_d} = \frac{(\lambda - 1)N_{\text{air},\min}}{N_{\text{FG,dry}}}$$

Table 3.14 presents some selected results from the stoichiometric calculations.

	Poduff	Kleinkopje	Cerrejon	Poduff+straw
$N_{\text{air,min}}$ [mol air/kg fuel]	328	322	326	252
[Nl/kg fuel]	7353	7215	7307	5646
$N_{\text{FG,min}}$ [mol/kg fuel]	342	334	341	273
[Nl/kg fuel]	7664	7489	7652	6129

Table 3.14: Results from stoichiometric calculations.

3.D Uncertainty Calculations

Statistical Variance

One-sided variance analysis is a statistical method to compare more than two mean values and can be applied to estimate a pooled uncertainty [65]. Table 3.15 presents observations, x_{ij}, from r experiments with n repetitions

x_{11}, x_{12},... x_{1n}	$\overline{x_{1.}}$
x_{21}, x_{22},... x_{2n}	$\overline{x_{2.}}$
$\vdots$	
x_{r1}, x_{r2},... x_{rn}	$\overline{x_{r.}}$

Table 3.15: Observations in variance analysis.

where $\overline{x_{i.}}$ is the mean value of the different experiment. The variance, s_i^2, of the mean values is estimated from the sum of squares, SSQ.

$$s_i^2 = \frac{\sum_{j=1}^{n}(x_{ij} - \overline{x_{i.}})^2}{n-1} = \frac{\mathrm{SSQ}_i}{n-1} \quad , i \in \{1, 2, ..., r\}$$

A pooled variance of the total system, s_o^2, is given by

$$s_o^2 = \frac{\sum_{i=1}^{r} \mathrm{SSQ}_i}{r \cdot (n-1)} = \frac{\mathrm{SSQ}_o}{f_o}$$

where f_o is the degrees of freedom for SSQ_o.
The 95 % confidence interval is determined from the pooled variance

$$\overline{x_{i.}} \pm t_{0.975}(f_o) \cdot \sqrt{\frac{s_o^2}{n}}$$

where the standard deviation, SD, corresponds to $= \sqrt{\frac{s_o^2}{n}}$.

Law of propagating of uncertainties

The simplified law of propagating of uncertainties is used to calculate the NO_x concentration normalized to a reference O_2 concentration.
A function consisting of several variables can be written as

$$x = g(x_1, x_2, ..., x_n)$$

where x is the function value and x_i is the independent variables.
The uncertainty of the function value is estimated according to

$$\mathrm{SD}(x) = \sqrt{\sum_{i=1}^{n} \left(\frac{\partial x}{\partial x_i}\right)^2 \cdot \mathrm{SD}^2(x_i)}$$

where SD is the standard deviation of the function value.

3.E Check of Consistency

Theoretical oxygen concentration
The theoretical oxygen concentration, presented in appendix 3.C, assumes complete burnout of the coal particles. However, this is not achieved in the EFR and thus, must be included in the estimation of the oxygen conc.
The burnout, b, is calculated according to

$$b = \frac{100 - w_{\text{ash,coal}} \cdot (1 + \frac{\text{LOI}}{100-\text{LOI}})}{100 - w_{\text{ash,coal}}}$$

were $w_{\text{ash,coal}}$ is the ash content of the dry coal (wt%).
The burnout is included in the calculation of the total amount of dry flue gas (see appendix 3.C)

$$N_{\text{FG,b,dry}} = (1 - x^{\text{air}}_{\text{H}_2\text{O}})\lambda N_{\text{air,min}} + b\left(-\frac{\beta}{4} + \frac{\delta}{2} + \frac{\phi}{2}\right)$$

and from a molar balance, the burnout is included in theoretical oxygen concentration

$$x^{\text{FG}_\text{d}}_{\text{O}_2,\text{b}} = \frac{(\lambda - b)N_{\text{O}_2,\text{min}}}{N_{\text{FG,b,dry}}}$$

False air
The amount of false air entering the reactor is estimated from a volume balance where the difference between theoretical oxygen concentration, $x^{\text{FG}_\text{d}}_{\text{O}_2}$, and the measured oxygen concentration, $x^{\text{meas}}_{\text{O}_2}$, is taken into account.

$$Q^{\text{in}}_{\text{FG}_\text{d}} x^{\text{FG}_\text{d}}_{\text{O}_2} + Q_{\text{false air}} x^{\text{air}}_{\text{O}_2} = Q^{\text{out}}_{\text{FG}_\text{d}} x^{\text{meas}}_{\text{O}_2}$$

$Q^{\text{in}}_{\text{FG}_\text{d}}$ is the theoretical flue gas flow subtracted the flow removed by the sampling probe (observations indicated that the leaks were located further downstream of the sampling probe position, $Q_{\text{false air}}$ is the flow of false air, $x^{\text{air}}_{\text{O}_2}$ is the molar fraction of oxygen in air (0.21) and $Q^{\text{out}}_{\text{FG}_\text{d}} = Q^{\text{in}} + Q_{\text{false air}}$).
Thus by rearranging we obtain

$$Q_{\text{false air}} = Q^{\text{in}}_{\text{FG}_\text{d}} \frac{x^{\text{meas}}_{\text{CO}_2} - x^{\text{FG}_\text{d}}_{\text{O}_2}}{x^{\text{air}}_{\text{O}_2} - x^{\text{meas}}_{\text{CO}_2}}$$

3.F Thermogravimetric Analysis

The reactivities of the chars from the three fired coals were determined by non-isothermal thermogravimetric analysis (TGA), where the samples were heated in an oxidizing environment and the weight loss was measured as a function of time and temperature.

The apparatus was operated at atmospheric pressure and applied both to prepare the char samples, i.e. pyrolysis, and the oxidation of the char. The char preparation was performed by heating 7–8 mg of coal sample under N_2 at 5 °C/min to 900 °C. The temperature was maintained for 5 min and the char was then cooled down to 200 °C. Subsequently, the char was oxidized in a mixture of 4 vol% O_2 in N_2 at a heating rate of 5 °C/min to 900 °C. It may be noted that the heating rate of the pyrolysis affects the char reactivity, e.g. faster heating rates increases the reactivity due to changes in pore structure and active surface area [66]. Typically pyrolysis is conducted in an entrained flow reactor, where heating rates in the same order as full-scale pulverized fuel combustion can be achieved (10^5 K/s) [67]. The TGA applies much lower heating rates, but this should not influence the order of reactivity between different coals [67, 68].

Fig. 3.28a presents the mass loss of the three investigated coals (double determinations). The first mass loss is from the pyrolysis and the difference corresponds well with the content of volatiles in the coals. The second mass loss is from the char oxidation.

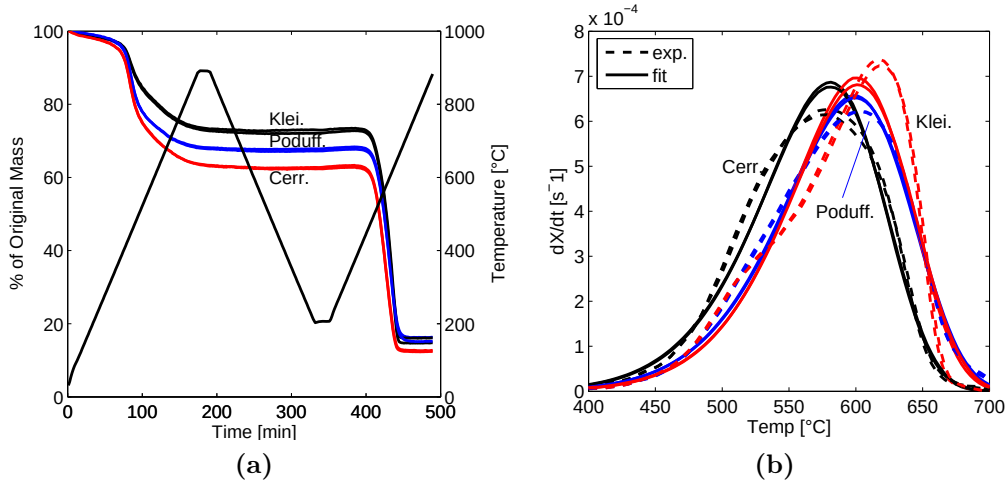

Figure 3.28: (a) Mass loss in percentage and temperature compared with time. (b) Experimental and fitted data of the char conversion rate.

The reaction between char and oxygen are assumed to kinetic controlled

and can at constant oxygen concentration be expressed by [69]:

$$\frac{dx_c}{dt} = k(1 - x_c)$$

where the rate constant, k, is described by the Arrhenius law, $k = k_0 e^{-Ea/RT}$, and the char conversion (daf) is given by $x_c = 1 - w/w_0$, w_0 is the initial weight of the char. The rate expression was fitted to the experimental data by a code developed elsewhere [70]. By applying a constant activation energy for all coal chars, the pre-exponential factor, k_0, can be used as a measure for the difference in reactivity between the chars. Initially, the program was provided with start guesses of the rate constant, activation energy and a temperature. The program returns the fitted rate constant at the given temperature and the activation energy. They are all applied to estimate the pre-exponential factor. Results are presented in Table 3.16 and the modeled data are shown in Fig. 3.28b. The activation energies are in the same order

	k_0 [s^{-1}]	E_a [kJ/mol]	k_0 [s^{-1}][a]
Cerrejon	$9.64 \cdot 10^4$	126	$11.91 \cdot 10^4$
Poduff	$6.28 \cdot 10^4$	126	$7.74 \cdot 10^4$
Kleinkopje	$6.52 \cdot 10^4$	133	$7.44 \cdot 10^4$ ($5.21 \cdot 10^4$)

Table 3.16: Estimated pre-exponential factors and activation energies. [a]Pre-exponential factor determined at E_a = 128 kJ/mol (value in bracket: see text for explanation).

of magnitude as found on two bituminous coals by Dutta *et al.* [69]. The refitted pre-exponential factor from the assumption of a common activation energy of 128 kJ/mol is included in Table 3.16 as well.

Cerrejon shows the highest pre-exponential factor in agreement with its high burnout in the EFR experiments. The similar pre-exponential factor determined for Poduff and Kleinkopje do not agree with EFR observations where the highest burnout was found for Poduff. However, the char conversion rate of Kleinkopje (Fig. 3.28b) appears to be comprised of two overlapping peaks, which may caused by the presence of compounds with different reactivity in the char sample. This complicates a proper fit of the rate expression with experimental data. Fitting only the large peak of the experimental data for Kleinkopje coal results in a lower pre-exponential factor ($k_0 = 5.21 \cdot 10^4$ s^{-1}), which agrees better with the order of burnout between Poduff and Kleinkopje coal. It is noted, that the lower peak may be catalytic induced [36].

Chapter 4

The Effect of Combustion Conditions in a Full-Scale Low-NO_x Coal Fired Unit to Fly Ash Properties for Its Application in Concrete Mixtures

Abstract. The wide implementation of low-NO_x combustion technologies in pulverized coal combustion can lead to higher levels of carbon in fly ash and increase the adsorptivity toward surfactants of the carbon. Consequently, the air-entraining admixture (AEA) requirements of the fly ash used for concrete production increases, which can complicate the stabilization of entrained air. In this study, a low-NO_x tangential fired 875 MW_{th} power plant burning bituminous coal have been operated under extreme conditions in order to test the impact of the operating conditions on fly ash adsorption behavior and NO_x formation. It was found that the AEA adsorption of the fly ash was reduced up to five times compared to reference operation, when the plant was operated with minimum furnace air staging, three levels of burners instead of four and without recycled flue gas. The lower AEA requirements of the fly ash at these conditions were primarily caused by a reduction in total carbon content, while the AEA adsorptivity of the residual carbon was lowered to about 60 % of reference value. The tested operation mode, however, increased the NO_x level in the flue gas before the $DeNO_x$ plant by 60 % compared to reference operation.

4.1 Introduction

Nordjyllandsværket Unit 3 is an 875 MW_{th} low-NO_x fired power plant, which started operation in October 1998. The plant is burning bituminous coal and typically the carbon content of the produced fly ash is significantly below the regulation of 5 wt% for a category A fly ash allowed for concrete production (European Standard EN-450 [1]). Despite the low carbon content, the fly ash has been reported to negatively affect the air entrainment in concrete to unacceptable levels since the first day of operation. In the present work, the power plant has been operated under extreme operating conditions, with the aim of testing what impact they have on the air-entraining admixture (AEA) requirements of the produced fly ash and the NO_x formation. Both are parameters that should be minimized in efficient power production. Moreover, the effect of changing the combustion conditions on the AEA adsorption properties of the residual carbon will be investigated.

4.2 Experimental

The boiler of Nordjyllandsværket, Unit 3, is of Benson tower type (12 m × 12 m × 70 m) and is tangentially fired through 16 Burmeister & Wain Energy low-NO_x burners in four levels. The boiler is designed to operate at full load using three levels of burners. The airflow to the burners is divided into primary (through the coal mills), secondary and tertiary air and each burner is provided with an over burner air nozzle (OBA). Additional furnace air staging is achieved by adding over fire air (OFA) through eight ports in two levels above the upper level of burners. Part of the flue gas is recirculated (FGR) and introduced through the OBA and OFA ports for boiler temperature control [2]. A selective catalytic reduction (SCR) DeNO_x reactor is used for NO_x control. In this technique, NO is reduced to N_2 over a catalyst after injecting ammonia in the flue gas. Fly ash is removed in two electrostatic precipitators (ESP), each consisting of four sections with two bins in the bottom. The power plant operates with hourly fluctuations in load and is typically reduced in load over night due to a lower power demand.

A mixture of three high volatile bituminous coals was fired during the test days: 35 % Polish, 35 % South African and 30 % Russian coals on weight basis. The proximate and ultimate analysis of the coal mixture is presented in Table 4.1. The power plant switched to this coal mixture four days before the tests took place. The produced fly ash was sampled continuously by a screw conveyor into a small container in the first section of the ESP (eastern) at a rate of approximately 300 g ash/h. The container was replaced every

Proximate analysis	
Ash	16.1
Volatile	31.0
Fixed carbon (diff.)	52.9
Ultimate analysis	
Carbon	62.2
Hydrogen	3.7
Oxygen (diff.)	5.6
Nitrogen	1.5
Sulphur	0.6
Net calorific value [MJ/kg]	27.1

Table 4.1: Results from proximate and ultimate analysis in wt% (d.b.).

hour in the last part of a test run, where the combustion conditions were close to steady state. The collected fly ash samples were analysed for carbon content using an ELTRA model CS-800 apparatus. The AEA requirements of the ashes were measured by the foam index (FI) test. It is a simple titration method, where a commercial AEA (5 vol% aqueous solution of Conplast 316 AEA from Fosroc) is added to a suspension of 8 g of cement and 2 g of fly ash particles. The amount of AEA added to produce stable foam on top of the liquid surface corresponds to the FI value of the sample. Further details are found elsewhere [3]. However, the contribution from the mineral matter part of the fly ash was included in the blank value when estimating the AEA adsorptivity of carbon (spec. FI). The FI of the mineral matter part was measured to 0.02 ml AEA/2 g mineral ash. Its contribution will be of greater importance when estimating the AEA requirements of residual carbon at lower FI values. The ammonia content in fly ash was determined by the Lange Cuvette Test applying a Dr. Lange XION 500 spectrophotometer. The concentrations of O_2, CO and NO_x were measured by the gas analysers used to monitor the daily operation of the plant. The measurements were done on flue gas sampled through six probes located immediately after the economizer in the top of the furnace. Moreover, SO_2 was measured just before the desulphurization plant to verify a constant coal mixture composition.

A three-day test program was planned and conducted. An overview is given below and more details are found in Table 4.2.

Reference: The power plant was operated with furnace air staging (OBA and OFA), FGR and fluctuating load conditions. All four levels of burners were in operation.

Test run 1: The power plant was operated at constant load without FGR and with minimal furnace air staging. All four levels of burners were in operation. *Test run 2:* Same as test run 1, but with three upper levels of burners in operation.

Test run 1 and 2 took place in the daytime at day two and three, respectively and the relevant adjustments to the operation were initiated in the morning. The residual carbon content in the regularly collected fly ash was determined and used as measure for the achievement of stable conditions and thereby representative samples. Soot blowing of the boiler was avoided during the daytime.

Test	Ref.	1	2
Plant load [%]	85-100	90	90
Primary air [%]	24.3 ± 1.1	27.1 ± 0.4	22.1 ± 0.2
Burner air[a] [%]	66.0 ± 1.5	70.0 ± 0.5	75.1 ± 0.2
OBA	+	none	none
OFA [%]	9.7 ± 1.1	2.9 ± 0.1	2.8 ± 0.1
FGR [%][b]	15.6 ± 4.9	none	none
O_2 in flue gas [vol%]	2.8 ± 0.4	3.0 ± 0.1	3.0 ± 0.2
Burners in operation (level)	1-4	1-4	2-4

Table 4.2: Plant parameters provided with 95 % confidence intervals, which represents the variations in the measurements. Operating with 3 vol% O_2 corresponds to an excess air ratio of about 1.17. At reference operation the excess air rate in the burner region was about 1.04.
[a] secondary and tertiary air (and OBA if added).
[b] percentage of total FGR and combustion air. The value is not corrected for air leakage in the regenerative air heater.

4.3 Results

The measured NO_x concentration is significantly affected by the operating conditions of the plant. In summary, the concentration increases with 36 % in test run 1 and 60 % in test run 2 compared with the reference condition, where the lowest NO_x concentration is obtained due to the application of air staging (OBA and OFA) and FGR. The latter may reduce the NO_x formation as well [4, 5] through a reburning effect. The increase in NO_x concentration of 36 % at test run 1 compared to the reference condition is the result of operating the plant without furnace air staging and FGR. This is mainly due to a

higher oxygen concentration in the burner belt which favours NO_x formation [5]. The further increase in NO_x concentration measured at test run 2 (60 % compared to reference) is obtained by operating the boiler with the three upper levels of burners. Splitting the load on fewer burners combined with having the combustion process taking place in a smaller volume (less cooling furnace wall area) will increase the combustion intensity which leads to local temperature increases in the burner region. This, in combination with the more air rich conditions due to the removal of furnace air staging increases the NO_x formation [5, 6], as observed.

The measured carbon contents in the fly ashes collected during the three test days are shown in Fig. 4.1. The typical carbon content in the fly ash,

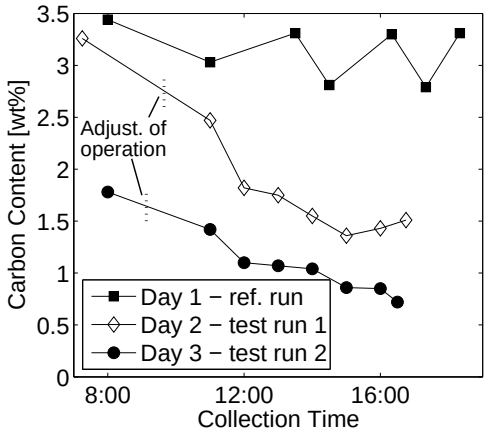

Figure 4.1: Residual carbon in the fly ash collected at the reference operation and test run 1 and 2. The values are given at the collection time of the actual day. The vertical dotted line represent the adjustment time for the relevant operation mode.

produced by firing the applied coal mixture at reference operation, is observed to be around 3 wt%, which is significantly lower than the 5 wt% allowed for a category A fly ash [1]. The more oxidizing conditions applied in test runs 1 and 2 produce fly ash with lower carbon content. The lowest content is achieved with three levels of burners in operation (test run 2), where a four times reduction is observed compared to the reference conditions. The fly ash samples representing the actual combustion conditions at test runs 1 and 2 were started to be collected after approximately 5 hours after changing from reference operation. This was decided despite the results indicate that longer time may have been necessary to reach complete steady state conditions, presumably caused by a long stabilization time of the temperature profile in

the furnace and the residence time of ash in the ESP. However, the O_2 and NO_x concentrations were unchanged during the ash sampling period. The variations in carbon content of the ash acquired at reference operation may arise from the fluctuating load conditions as reported by others [7].

Ten fly ashes were tested for adsorption properties of AEAs; four collected at the reference conditions and three samples in the last part of each test run. The results are presented in Fig. 4.2 along with the carbon content. The

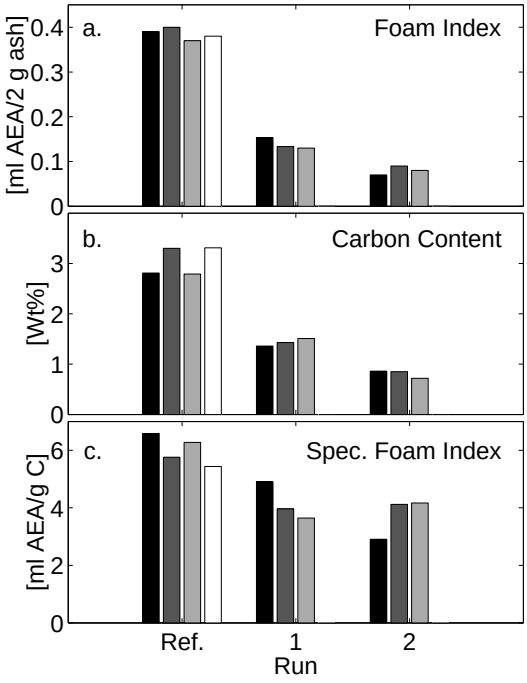

Figure 4.2: FI, carbon content and spec. FI of the investigated ashes at the different runs.

adsorption property of the fly ash, expressed by the FI value (Fig. 4.2a.), is significantly reduced at the operating conditions applied in test runs 1 and 2 with up to five times for test run 2 compared to the reference value (average value). In case the carbon content had been brought down to a "steady state" level in test run 2, the FI may have been measured even lower. The decrease in FI is higher than the four times reduction in carbon content (Fig. 4.2b.). This indicates that part of the lower FI value of the ashes produced in test run 2 is caused by a lower AEA adsorptivity of the residual carbon (Fig. 4.2c.). However, the spec. FI is only reduced to about 60 % of reference value and thus the lower FI of the ash is primarily caused by a lower carbon content. The lower adsorptivity of carbon may emerge

from the more oxidizing conditions in the early stage of combustion, which changes the char properties such as accessible surface area and carbon surface polarity [8]. It is noted that the trend for the spec. FI values, especially for the ashes collected at test run 2, is not conclusive because the low FI values may be associated with greater uncertainties [9].

For the power producers it is interesting that rearrangement of combustion air in the boiler significantly lowers the AEA adsorption of the fly ash. Unfortunately, such conditions do in the experiments presented here have an inverse effect on the NO_x concentration as illustrated in Fig 4.3. The

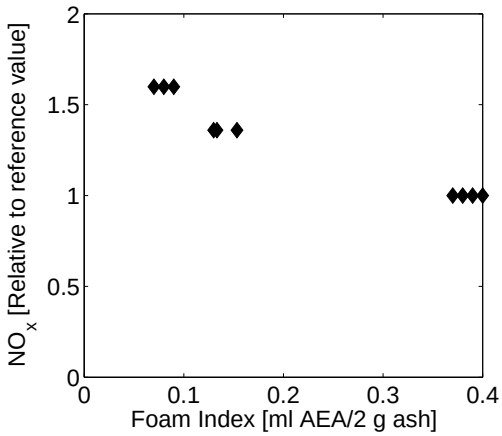

Figure 4.3: Relative NO_x concentration compared with FI.

FI of the fly ash has been brought down to a level corresponding to values measured on fly ashes, which have been reported not to cause problems with air entrainment (0.08–0.09 ml AEA/2 g fly ash [3]). However, the AEA adsorption per gram of carbon is still up to two times higher in the present case than in ashes investigated in our previous work [3]. The spec. FI values determined in our past work are even lower if the contribution from the mineral part to the FI blank is taken into account.

The observed difference in AEA adsorptivity between carbon in ashes from the present study compared to carbon in ashes from our previous work can be due to several factors such as design and operation of boiler and burners, type of coal [10] and maybe even soot formed in the combustion process [11]. The latter is suggested to show higher adsorption capacity of AEAs than char because its area is located on the surface of the particles and therefore is easily accessible for the AEAs [8]. Soot structure has been identified in fly ashes from Nordjyllandsværket, Unit 3, by transmission electron microscopy in our previous work [12]. Moreover, the level of polycyclic

aromatic hydrocarbons (PAHs), precursors for soot, have been found higher in fly ash from the present power plant [13] compared to fly ash from a power plant that to the authors knowledge do not cause problems when utilized in concrete.

4.3.1 Discussion

The experimental results indicate a potential for improving the fly ash quality produced by the power plant with respect to utilization in concrete. However, the benefits of producing fly ash with a low AEA adsorption capacity have to be compared with the costs of changing the operating conditions. In test run 2, which is considered to be an extreme case and where fly ash with the lowest AEA adsorption capacity was produced, the following major effects on plant performance was observed:

- The ammonia consumption in the SCR DeNO$_x$ process increased about 56 % from reference value. According to Danish regulations, the maximum permissible value of NO$_x$ in the flue gas emitted to the atmosphere is 200 mg/Nm^3 at 6 % O$_2$ [14]. The DeNO$_x$ plant maintained the NO$_x$ concentration in the flue gas below the limit.

- Improved conversion of coal from about [(100 - 13.4 · (1 + 3.0/(100 - 3.0)))/(100 - 13.4)] = 0.995 or 99.5 % (3.0 wt% carbon in ash) to 99.9 % (0.72 wt% carbon in ash).

- The flue gas recirculation fan was taken out of operation, resulting in decreased auxiliary power.

- Reduced boiler efficiency due to less convective heat transfer efficiency, i.e. operating the boiler without recycled flue gas lowers the flue gas velocity (lower temperatures were observed in the second intermediate pressure superheater).

Modern coal fired power plants, like Nordjyllandsværket, operate with a high conversion of coal and the results illustrate that improvements in burnout is marginal. The reduced boiler efficiency was compensated by the lower auxiliary power consumption and therefore, the gross overall efficiency of the plant was unaffected. Thus, the primary impact on the process costs when operating as in test run 2 comes from the increased ammonia consumption. Regarding this, ammonia added in SCR DeNO$_x$ processes can deposit on fly ash and cause a release of ammonia odor when it is utilized concrete [8]. The properties of the concrete are not altered [15]. It has been reported that ammonia contents below 50 ppm [16] and 100 ppm [15] in fly ash should not

be problematic for its utilization. Moreover, concrete produced from a fly ash containing 63 ppm ammonia has been shown to be below the threshold limit of an indoor environment after 28 days from production [17]. In the present work, the ammonia content of an ash produced at test run 2 was measured to 5.3 ppm. Therefore, the fly ash is not believed to give rise to ammonia related problems when being utilized in concrete.

The benefits of producing fly ash suitable for concrete application depends on local conditions, e.g. in the present case the produced fly ash is used as raw material for cement production, making the benefits of operating the plant in an extreme mode as in test run 2 minimal. However, such favourable conditions may not exists for other power plants optimised for low-NO_x combustion. In a worst case scenario, the benefits of producing fly ash suitable for concrete application are comprised of the difference between disposal costs and sales value of the fly ash [18], e.g. disposal costs of fly ash in Denmark (2005) ranged from 130 to 500 kr/ton [19], while the sales value of fly ash is 285 kr/ton delivered [20]. However, other options exist; low quality fly ash may be used for soil stabilization or fillers [18], but they are less economic attractive than utilizing the fly ash in the production of concrete.

Thus, the economy of a power plant can be affected by the marketability of fly ash as discussed by others [21]. Future design and operation of cost effective solid fuel fired power plants should therefore include the quality of the produced fly ash as an operation parameter, possibly related to the costs of operating with increased NO_x formation as well. In the present case, the results provide valuable knowledge to the operation of the present plant; in situations where fly ash quality with low AEA adsorption capacity is required, e.g. for concrete production, the plant can be operated under extreme conditions to fulfil those requirements. However, the few tested operating conditions do not reveal if the quality of the fly ash can be significantly improved with less negative consequences on the NO_x formation than observed in the present study. Estimation of optimal conditions between fly ash quality and NO_x formation will require attention in future work. It may not be necessary to aim at such low FI values as obtained in test run 2. In case a higher FI value of the ash is satisfactory for a good performance in concrete, the plant may be operated with more air staging and thus lower NO_x formation. Nevertheless, aiming at fly ash produced with a low FI reduces the negative influence from fluctuating load conditions, which causes variations in ash quality that gives rise to problems with correct dosage of AEAs in the concrete production [22]. The loss of air in concrete over time is also lower when fly ash with low AEA requirements is added than adding fly ash with higher AEA requirements [23]. Finally, the AEA adsorptivity of

carbon in the fly ash from the present plant is still higher compared to previous investigated ashes indicating that further improvements in ash quality may be achieved. The air staging taking place at the burners, which creates fuel rich zones, may still lead to a lower fly ash quality and changes in this configuration could be attended in future work.

As a final remark, the outcome of this work has led to a later experiment, where a larger amount of fly ash was produced under similar operating conditions as applied in test run 2. The concrete manufacturer reported that no significant difference in air content could be measured between concrete produced from this test fly ash and concrete produced from a fly ash considered to be normal. This shows that it is possible to run the power plant in a way where an ash that is applicable in concrete manufacture is obtained.

4.4 Summary

The air-entraining admixture (AEA) requirements in concrete are unacceptably high when adding fly ash produced at the Danish coal fired power plant, Nordjyllandsværket, Unit 3. This is a typical problem which can occur at pulverized fuel fired power plants applying low-NO_x combustion technologies such as low-NO_x burners and furnace air staging.

The present study has shown that the AEA requirements of the produced fly ash can be reduced up to five times compared to a reference value when the power plant is operated with minimum furnace air staging, removal of recycled flue gas and with three levels of burners instead of four. The lower AEA requirements were mainly caused by an improved conversion of the coal, but the results showed that the AEA adsorptivity of the residual carbon (i.e. per gram of carbon) was lowered to about 60 % of reference value. This may be because less air staging gives more oxidizing conditions in the early stage of the combustion process, which causes a change in accessible surface area and polarity of the residual carbon. The tested conditions increased the NO_x concentration by up to 60 % in the flue gas before the $DeNO_x$ plant compared to reference value. However, the $DeNO_x$ plant reduced the NO_x concentration to a value below the regulation in the emitted flue gas by adding more ammonia to the SCR $DeNO_x$ process. The ammonia content in the fly ash was kept at an acceptable level.

Despite operating the power plant with less air-staging, the AEA adsorption capacity of the residual carbon was found to be significantly higher than of previously investigated ashes from other plants suggesting that further changes in combustion conditions, with the aim of improving the residual carbon properties, may be possible.

4.5 Acknowledgements

The CHEC Research Centre is co-funded by the Technical University of Denmark, DONG Energy A/S, FLSmidth A/S, Hempel's Fond, Vattenfall A/S, Haldor Topsøe A/S, Energinet.dk, the Danish National Advanced Technology Foundation, the Danish Technical Research Council, the Danish Energy Research Programme, Nordic Energy Research, the European Union, and several other industrial partners.

4.6 Abbreviations

AEA	air-entraining admixture
ESP	electrostatic precipitator
FGR	flue gas recirculation
FI	foam index
OBA	over burner air
OFA	over fire air
SCR	selective catalytic reduction
Spec. FI	specific foam index

4.7 References

[1] European Committee for Standardization, Brussels, Fly ash for concrete - Part 1: Definition, specifications and conformity criteria (EN 450–1) (2005).

[2] H. Liu, R. Zailani, B. M. Gibbs, Comparisons of pulverized coal combustion in air and in mixtures of O_2/CO_2, Fuel 84 (7-8) (2005) 833–840.

[3] K. H. Pedersen, S. I. Andersen, A. D. Jensen, K. Dam-Johansen, Replacement of the foam index test with surface tension measurements, Cement and Concrete Research 37 (6) (2007) 996–1004.

[4] K. Okazaki, T. Ando, NO_x reduction mechanism in coal combustion with recycled CO_2, Energy 22 (2-3) (1997) 207–215.

[5] R. P. van der Lans, P. Glarborg, K. Dam-Johansen, Influence of process parameters on nitrogen oxide formation in pulverized coal burners, Progress in Energy and Combustion Science 23 (4) (1997) 349–377.

[6] H. Spliethoff, U. Greul, H. Rüdiger, K. R. G. Hein, Basic effects on NO_x emissions in air staging and reburning at a bench-scale test facility, Fuel 75 (5) (1996) 560–564.

[7] R. Helmuth, Fly ash in cement and concrete, 1st Edition, Portland Cement Association, Illinois, 1987, pp. 61–64.

[8] Y. Gao, I. Külaots, X. Chen, E. M. Suuberg, R. H. Hurt, J. M. Veranth, The effect of solid fuel type and combustion conditions on residual carbon properties and fly ash quality, in: Proceedings of the Combustion Institute, Vol. 29, 2002, pp. 475–483.

[9] K. H. Pedersen, M. S. Skjøth-Rasmussen, A. D. Jensen, K. Dam-Johansen, A review of the interference of carbon containing fly ash with air entrainment in concrete, Progress in Energy and Combustion Science 34 (2) (2008) 135–154.

[10] I. Külaots, R. H. Hurt, E. M. Suuberg, Size distribution of unburned carbon in coal fly ash and its implications, Fuel 83 (2) (2004) 223–230.

[11] Y.-M. Gao, H.-S. Shim, R. H. Hurt, E. M. Suuberg, N. Y. C. Yang, Effects of carbon on air entrainment in fly ash concrete: The role of soot and carbon black, Energy and Fuels 11 (2) (1997) 457–462.

[12] K. V. Pedersen, Application of fly ash in concrete, Master's thesis, Department of chemical engineering, Technical University of Denmark (2004).

[13] B. Sander, DONG Energy A/S, Denmark, Personal communication (June 2004).

[14] Revision af miljøgodkendelsen af Nordjyllandsværket, Nordjyllands amt, Aalborg, Denmark) (January 2006).

[15] P. Necker, Experience gained by Neckarwerke from operation of SCR $DeNO_x$ units, Symposium on Stationary Combustion Nitrogen Oxide Control 2 (1989) 6A–19 to 6A–38.

[16] M. Novak, H. G. Rych, Design and operation of SCR-type NO_x-reduction plants at the Dürnohr power station in Austria, Symposium on Stationary Combustion Nitrogen Oxide Control 2 (1989) 7A–1 to 7A–26.

[17] J. Bødker, Afdampning fra beton, Tech. Rep. 18, Danish Environmental Protection Agency, Danish Ministry of Environment, Copenhagen, Denmark (2006).

[18] R. H. Hurt, Structure, properties, and reactivity of solid fuels, in: Proceedings of the Combustion Institute, Vol. 27, 1998, pp. 2887–2904.

[19] Modtagepriser (excl. statsafgift) 2005 - deponeringsanlæg, Videnscenter for affald, Miljøstyrelsen, Denmark.
URL http://www.affaldsinfo.dk/affald+i+danmark/\%C3\%B8konomi/\newlinemodtagepriser/deponeringspriser

[20] Prisblad ved levering til betonindustrien i Danmark fra 1. juli 2007 (B4-standard), Emineral A/S, Denmark.
URL http://www.emineral.dk/filer/Emineral_prisblad_010707.pdf

[21] M. L. Hall, W. R. Livingston, Fly ash quality, past, present and future, and the effect of ash on the development of novel products, Journal of Chemical Technology and Biotechnology 77 (3) (2002) 234–239.

[22] E. Freeman, Y.-M. Gao, R. Hurt, E. Suuberg, Interactions of carbon-containing fly ash with commercial air-entraining admixtures for concrete, Fuel 76 (8) (1997) 761–765.

[23] S. Gebler, P. Klieger, Effects of fly ash on the air-void stability of concrete, in: Proceedings of the Canmet/ACI. First International Conference on the Use of Fly Ash, Silica Fume, Slag and Other Mineral By-Products in Concrete, Vol. 1, 1983, pp. 103–142.

Chapter 5

Post Treatment of Fly Ash by Ozone in a Fixed Bed Reactor

Abstract. The residual carbon in fly ash produced from pulverized coal combustion can adsorb the air-entraining admixtures (AEAs) added to enhance air entrainment in concrete. This behavior of the ash can be suppressed by exposing the fly ash to oxidizing species, which oxidizes the carbon surface and thus prevents the AEA to be adsorbed. In the present work, two fly ashes have been ozonated in a fixed bed reactor and the results showed that ozonation is a potential post treatment method that can lower the AEA requirements of a fly ash up to six times. The kinetics of the carbon oxidation by ozone was found to be fast. A kinetic model has been formulated describing the passivation of carbon and it includes the stoichiometry of the ozone consumption (0.8 mol O_3/kg C) and an ineffective ozone loss caused by catalytic decomposition. The simulated results correlated well with the experimental data.

5.1 Introduction

The adsorption of air-entraining admixtures (AEAs) of fly ash in concrete can be suppressed by post treatment methods. These methods may be based on a carbon separation technique or an oxidizing process, where the latter comprises carbon removal or carbon passivation. The passivation of carbon can be achieved from dry or wet methods that oxidize the carbon surface. The oxidation increases the surface polarity, which prevents the AEAs to be adsorbed. Dry methods are preferred in order to avoid the costs of drying the treated ashes and loss of pozzolanic activity [1]. Hurt and co-workers [1–3] have successfully applied a dry method based on ozone as reacting agent.

This is a method that further benefits from having a potential to remove ammonia added in post flame NO_x-reduction methods [4].

In the present work, fly ashes acquired from a Danish power plant, which is known to produce fly ash that negatively affects the air entrainment in concrete (see chapter 4), have been exposed to ozone in a fixed bed reactor. The ozonation was carried out at various concentrations and treatment times and a kinetic model of the process has been developed.

5.2 Experimental Section

The ozone treatment was performed on fly ashes produced from burning bituminous coal and their carbon contents and AEA adsorption measured by the foam index (FI, see below) are listed in Table 5.1. The carbon content in

Ash	Carbon [wt%]	FI [ml AEA/2 g ash]
A	2.97	0.24
B	2.57	0.36

Table 5.1: Carbon content and FI of treated samples. Ash A is produced from 90 % Columbian Coal and 10 % South African coal, while ash B is produced from 90 % Polish Coal and 10 % South African coal.

the two fly ashes represents typical values from the investigated power plant. The experimental setup is sketched in Fig. 5.1. The ozone was produced by an ozone generator from an oxygen stream. The ozone generator was a BMT Messtechnik, model BMT 803 that produces the ozone by a corona discharge. The ozone concentration was further diluted by adding an oxygen flow after the generator. The applied concentrations ranged from 500 ppm to 1.2 vol%. A flow of 0.7 L/min (standard conditions) was sampled from the main flow and introduced in the top of the glass reactor. Inside the glass reactor, a glass filter acted as a support for a fixed bed of fly ash particles (10 g). The ozone stream was then allowed to flow downwards through the ash bed. This configuration was applied in order to prevent the formation of channels in the bed, which could happen at an upward flow. Treatment times up to 20 minutes were applied. The outlet stream was on-line analyzed for ozone by UV-absorption spectroscopy (ozone analyser model BMT 964, also from BMT Messtechnik). The ozone was destroyed further downstream by a destruction unit.

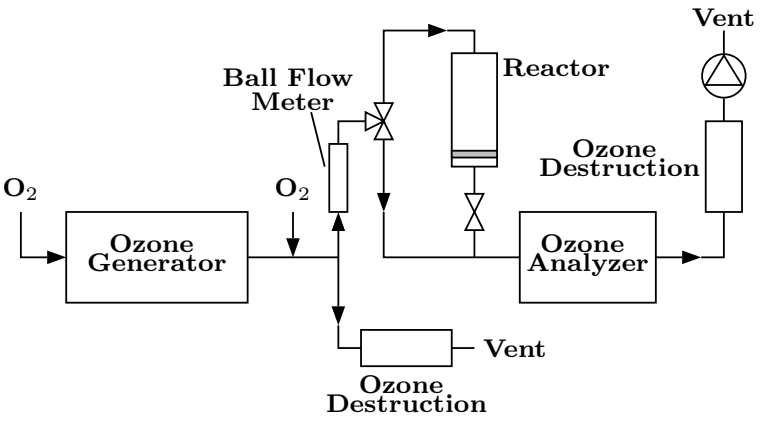

Figure 5.1: Outline of the ozone setup.

The treated samples were analyzed for AEA adsorption by the FI test as described elsewhere [5]. A 5 vol% aqueous solution of Conplast 316 AEA from Fosroc was added in the test. Carbon contents were measured by an ELTRA model CS-800 apparatus or by loss-on-ignition (LOI). BET-N_2 surface areas were determined by a Micromeritics ASAP 2000. In a few runs the off gas stream was analyzed for CO and CO_2 using standard gas analyzers.

5.3 Results

5.3.1 Experimental Part

The change of the ozone concentration with time in the outlet of the reactor filled with fly ash A is compared with the dynamics of the empty reactor in Fig. 5.2a. The reaction rate of ozone with fly ash is high in the beginning of the experiments, where almost all ozone is consumed under the applied conditions. The rate of reaction then gradually decreases until the ozone concentration reaches a constant level. The steady state level is slightly below the inlet concentration indicating that some ozone loss, which does not contribute to a lower AEA adsorption, takes place on the fly ash. This ineffective ozone loss can be due to catalytic decomposition on the mineral oxides [6] or the oxidized carbon surfaces.

The effect of exposing fly ash sample A to ozone on its AEA requirements is presented in Fig. 5.2b. It can be seen that ozone can suppress the AEA adsorption of the fly ash in agreement with Gao *et al.* [1]. The FI of the fly ash is reduced more than three times within the applied treatment time

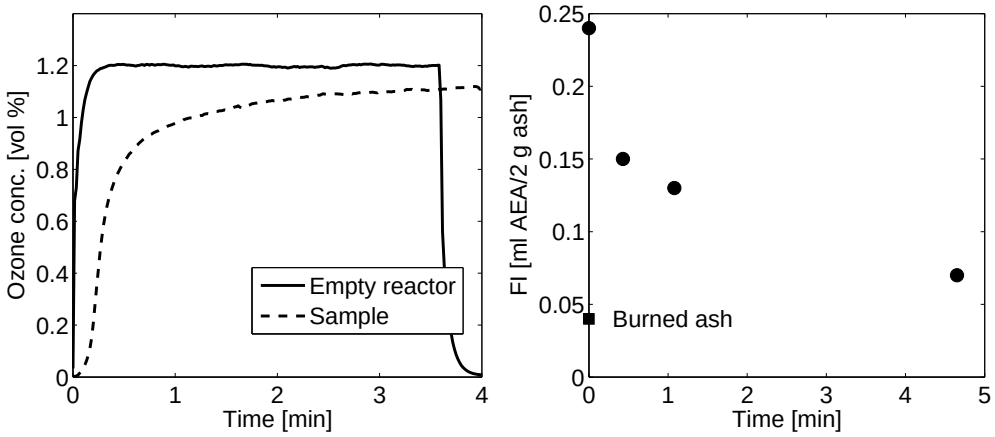

Figure 5.2: (a) Change in ozone concentration with time of an empty reactor and the reactor containing fly ash A. (b) FI compared with treatment time of fly ash. The inlet concentration of ozone was 1.2 vol% in both (a) and (b).

of about 5 minutes, with the fastest reduction occurring in the early phase of the treatment process. The lowest achieved FI of the ozone treated ash is close to the FI of the burned ash, where all carbon has been removed by heating the sample for two hours at 740 °C in air. Moreover, the FI value is below the FI of an ash that does not cause problems with air entrainment in concrete (0.08–0.09 ml AEA/2 g fly ash [5]) suggesting that ozone treatment is an efficient method to improve fly ash quality. Exposing the fly ash to oxygen alone does not change its AEA requirements, which indicates that ozone is the reacting reagent and not the oxygen at room temperature.

The reduced AEA adsorption of fly ash exposed to ozone is explained from changes in the AEA adsorptivity of the residual carbon, presumably related to changes in the surface chemistry [3]. Our results support these findings, e.g. in our preliminary work [7] a fly ash exposed to about 1 vol% ozone for 20 hours decreased in AEA requirements, but increased 4 % in LOI, revealing that the lower AEA requirements was not caused by a decrease in the carbon content. This was in the present work supported by the observation that no CO and CO_2 could be measured in the off gas stream. The small increase in sample weight may come from the chemisorbed oxygen on carbon or some mineral oxidation [1]. The BET-N_2 surface area of the ash decreased, but nowhere near enough to explain its lower AEA adsorption in agreement with observations by Gao *et al.* [1]. This, together with results on carbon blacks, where surface oxidation by ozone [2, 8] or wet processes

[9] lead to insignificant changes in BET-N_2 area, indicate that changes in surface chemistry play a key role in the adsorption suppression of the ashes treated by ozone. Moreover, it has been suggested that the non-microporous area, which is considered to be accessible for the AEAs, is not easily blocked by surface oxides [2, 3].

In order to obtain treatment times in the order of minutes, the inlet concentration of ozone is lowered to 500 – 4000 ppm. The achieved FI values are calculated to a fractional FI decrease by

$$X = \frac{\mathrm{FI}_0 - \mathrm{FI}_t}{\mathrm{FI}_0 - \mathrm{FI}_\mathrm{b}} \tag{5.1}$$

where FI_0 corresponds to the FI of the non-treated ash, FI_t is the FI at time, t and FI_b is the FI of the burned ash. Thus, the fractional decrease ranges from a value of 0 corresponding to the initial FI to a value of 1, which is the maximum reduction in FI assumed to be the value of the burned ash. Fig. 5.3a shows the fractional decrease of FI with time at concentrations ranging from 500 to 4000 ppm of fly ash B. Increasing the inlet ozone concentration gives a faster decrease of FI, except between 500 and 1000 ppm, which for unknown reasons show similar fractional FI decrease with time. The relatively fast fractional decrease achieved at 4000 ppm suggests that the low FI value obtained at an ozone concentration of 1.2 vol% may have been reached before the 5 minutes (see Fig. 5.2b).

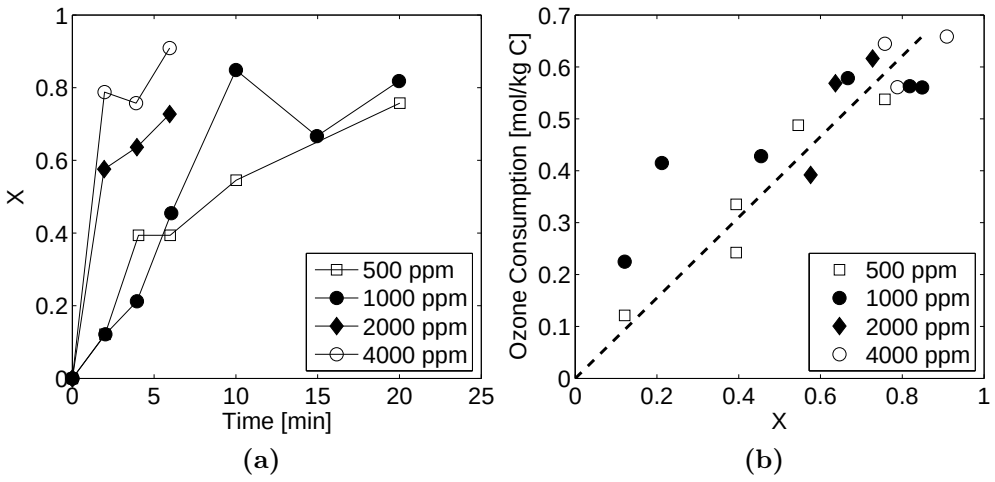

Figure 5.3: (a) Fractional FI decrease compared with time of ash B at 500 to 4000 ppm in ozone inlet concentration. (b) Fractional FI decrease compared with ozone consumption of ash B at 500 to 4000 ppm.

The ineffective ozone loss on fly ash appears from the final steady state outlet level of ozone compared to the inlet level. It can be given as a conversion according to

$$X_{\mathrm{O_3,S}} = \frac{C_{\mathrm{O_3,0}} - C_{\mathrm{O_3,S}}}{C_{\mathrm{O_3,0}}} \tag{5.2}$$

where $C_{\mathrm{O_3,0}}$ and $C_{\mathrm{O_3,S}}$ is the inlet and steady state concentration of ozone, respectively. Table 5.2 provides the estimated steady state ozone losses on fly ash A and B at different inlet concentrations. The ineffective decomposition

Ash	1000 ppm	2000 ppm	4000 ppm	12000 ppm
A	0.075	0.088	-	0.064
B	0.135	-	0.118	-

Table 5.2: Conversion of ozone caused by the ineffective ozone loss on fly ash A and B (steady state conditions).

of ozone over the samples is not notably affected by the inlet concentration and thus, the ozone loss may follow a first-order reaction. This will be applied in the present work, despite that ozone destruction on minerals is a complex process and may not be treated as a first-order reaction [10]. The general difference in steady state ozone loss on ash A and B can be caused by variations in their mineral oxide composition, e.g. iron oxides have higher ozone decomposition rate than alumina- and silica oxides [10].

The ozone requirement of the carbon in the ash, $n_{\mathrm{O_3}}$, is based on a simple approach where the difference between inlet concentration and outlet concentration, $C_{\mathrm{O_3}}$, adjusted by the ineffective ozone loss, is integrated over time according to

$$n_{\mathrm{O_3}} = \frac{v}{Ww} \int_0^t \left(C_{\mathrm{O_3,0}} - \frac{C_{\mathrm{O_3}}}{1 - X_{\mathrm{O_3,S}}} \right) dt \tag{5.3}$$

where v is the volumetric flow rate ($\mathrm{m^3/s}$), W is the mass of ash (kg) and w is the weight fraction of carbon in the ash. The ozone requirement is given in mol $\mathrm{O_3}$/kg C assuming that the fly ash carbon counts for the effective ozone consumption. By comparing the fractional decrease of FI with the ozone consumption of carbon (Fig. 5.3b) a linear relationship is revealed, though with some scattering in the data, which may be attributed with some experimental uncertainty of the FI test. An overall stoichiometric ratio of ozone to a complete decrease of FI, f, is estimated from linear regression to

0.78 mol O_3/kg C. The estimated value lies within the extremes of assuming that carbon consumes all the ozone (0.92 mol O_3/kg C) or assuming that the maximum ineffective ozone loss (Table 5.2) occurs in the whole treatment time (0.68 mol O_3/kg C). A parameter study of these two extremes does not significantly influence the modeling results and thus, the accuracy of the estimated stoichiometric ratio is considered to be acceptable.

5.3.2 Modeling

The reaction of ozone with the carbon particles in fly ash may be controlled by surface kinetics, pore diffusion resistance in the interior of the particle and film diffusion resistance in the surrounding gas film. Preliminary calculations according to Mears' criterion for external diffusion and Weisz-Prater criterion for internal diffusion suggest that the diffusion is not the rate limiting step in the carbon oxidizing process (see Appendix 5.A). Thus, the rate of reaction is believed to be controlled by kinetics.

The fixed bed reactor is treated as a tank-in-series model according to Weinell *et al.* [11]. An estimated reactor Peclet number of 10 indicates that axial dispersion is present in the bed ($Pe = UL/D_{O_3}$, where U is the actual gas velocity in the bed, L is the bed thickness and D_{O_3} is the ozone diffusion coefficient). The required number of well-mixed reactors that should be applied in the model in order to account for the axial dispersion, is estimated from comparing the residence time distribution (RTD), given by the dispersion model for a closed system, with the RTD of the tanks-in-series model [12]. A Peclet number of 10 is found to be equivalent to about 7 well-mixed reactors.

In the modeling, it is assumed that the passivation process of the carbon surface with respect to adsorption of AEAs depends on the ozone concentration and number of sites available for the AEAs:

$$-\frac{dN_i}{dt} = k'_{ox} C^m_{O_3,i} N^n_i \qquad i = 1, ..., P \tag{5.4}$$

where N_i is the number of sites on the carbon surface that can adsorb the AEAs in the ith reactor (sites/m^2), k'_{ox} is the reaction rate constant of the carbon oxidation by ozone ((m^3/mol)^m(m^2/sites)$^{n-1}$s^{-1}), $C_{O_3,i}$ is the concentration of ozone at reactor number i (mol/m^3), m and n is the reaction order with respect to ozone concentration and number of sites, respectively, and P is the number of reactors. The actual number of sites is not known, but if it is normalized with the number of sites in an non-treated carbon, N_0, it can be related to the fractional decrease of the FI by $X = 1 - N/N_0$, which

rearranges equation (5.4) to

$$\frac{dX_i}{dt} = k_{\mathrm{ox}} C_{\mathrm{O_3},i}^{m} (1 - X_i)^n \qquad i = 1, ..., P \tag{5.5}$$

where $k_{\mathrm{ox}} = k'_{\mathrm{ox}} N_0^{n-1}$ ($(\mathrm{m^3/mol})^m \mathrm{s}^{-1}$). The mole balance for ozone at each reactor is described as a transient mixed flow reactor

$$\frac{dC_{\mathrm{O_3},i}}{dt} = r_{\mathrm{O_3},i} + (C_{\mathrm{O_3},i-1} - C_{\mathrm{O_3},i}) \frac{v}{V_i} \qquad i = 1, ..., P \tag{5.6}$$

with v as the volumetric gas flow rate ($\mathrm{m^3/s}$). The volume of the gas phase, V_i, in the ash bed in each reactor is given by:

$$V_i = \epsilon \frac{W_i}{\rho} \tag{5.7}$$

where W_i is the mass of ash in the ith reactor (kg), ρ is the bulk density of the ash particles ($\mathrm{kg/m^3}$) and ϵ is the porosity of the ash bed. The volumetric reaction rate, $r_{\mathrm{O_3},i}$ ($\mathrm{mol/m^3\ s}$), is described by both a carbon oxidation rate, $r'_{\mathrm{O_3,ox},i}$, and a rate for the ineffective ozone loss, $r'_{\mathrm{O_3,de},i}$. They are based on mass of carbon and mass of fly ash, respectively and is related to the volumetric reaction rate by $r_{\mathrm{O_3}} = r'_{\mathrm{O_3}} W/V$. Thus

$$r_{\mathrm{O_3},i} = (w \cdot r'_{\mathrm{O_3,ox},i} + r'_{\mathrm{O_3,de},i}) \frac{\rho}{\epsilon} \tag{5.8}$$

where w is the weight fraction of carbon in the sample. The carbon oxidation rate (mol $\mathrm{O_3}$/kg C s) is proportional to the fractional FI decrease according to

$$\frac{dX_i}{dt} = \frac{1}{f}(-r'_{\mathrm{O_3,ox},i}) \tag{5.9}$$

with f as the stoichiometric ratio between ozone consumption and fractional decrease of FI (mol $\mathrm{O_3}$/kg C). The reaction rate of the ineffective ozone loss is assumed to be a first-order expression as discussed above and is given by

$$-r'_{\mathrm{O_3,de},i} = k'_{\mathrm{de}} C_{\mathrm{O_3},i} \tag{5.10}$$

k'_{de} is the reaction rate constant given in $\mathrm{m^3/kg}$ ash s. It is determined from assuming steady state plug flow in the reactor (the difference between tanks-in-series model and plug flow model is insignificant at low conversion):

$$\frac{V}{v} = C_{\mathrm{O_3}} \int_0^{X_{\mathrm{O_3,S}}} \frac{dX_{\mathrm{O_3}}}{-r_{\mathrm{O_3,de}}} \tag{5.11}$$

Rearranging to a mass-based expression and applying equation (5.10) followed by integrating, yields:

$$k'_{\mathrm{de}} = -\frac{v}{W}\ln(1 - X_{\mathrm{O_3,S}}) \tag{5.12}$$

In total, equation (5.6) becomes.

$$\frac{\epsilon}{\rho}\frac{dC_{\mathrm{O_3},i}}{dt} = -k_{\mathrm{ox}}C^m_{\mathrm{O_3},i}(1 - X_i)^n fw - k'_{\mathrm{de}}C_{\mathrm{O_3},i} + (C_{\mathrm{O_3},i-1} - C_{\mathrm{O_3},i})\frac{v}{W_i} \tag{5.13}$$

The solution is obtained by solving equation (5.5) and (5.13) as a system of ordinary differential equations (ODEs). This results in a time-dependent fractional FI decrease, $X_i(t)$, and ozone concentration, $C_{\mathrm{O_3},i}(t)$ for reactor number i. The ozone concentration at time t in the outlet of the reactor corresponds to the concentration at reactor number P, while the total fractional decrease of FI, $X(t)$, is the mean value of the fractional decrease in all reactors

$$X = \frac{\sum_{i=1}^{P} W_i X_i}{W} \tag{5.14}$$

The model results, using parameters from Table 5.3, are compared with the experimental values of the outlet ozone concentration and the fractional FI decrease in Fig. 5.4a and 5.4b, respectively. Being a chemisorption

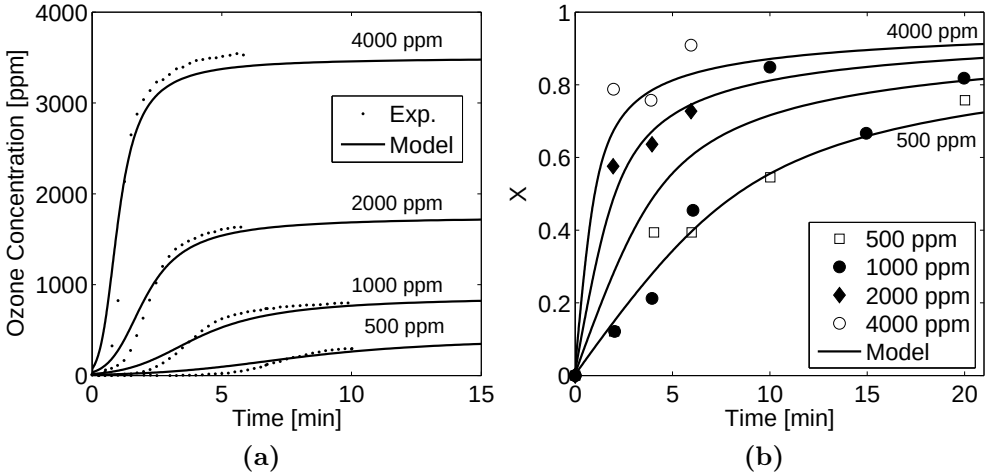

Figure 5.4: Experimental and simulated results of the (a) ozone concentration and (b) conversion of FI compared with time. Table 5.3 provides the parameters applied in the simulation.

f [mol O_3/kg C]	0.78
k_{ox} [m^3/mol s]	0.35
k'_{de} [m^3/kg ash s]	$1.69 \cdot 10^{-4}$
m	1
n	3
P	7
T [K]	293
v [Nl/min]	0.7
w	0.0257
W [kg]	0.01
$X_{O_3,S}$	0.126
ϵ	0.5
ρ [kg/m^3]	1000

Table 5.3: Parameter values for ash B used in the simulation.

reaction, m is assumed to be 1 and only n and k_{ox} were visually fitted. The simulated results agree well with the experimental data, but some difference between the simulated and experimental ozone profile is observed, particularly at lower ozone inlet levels. It was possible to obtain a better fit by increasing the number of reactors and therefore, the exact number should be experimentally determined in future work. A deviation from the fractional decrease of FI achieved at 1000 ppm is observed as well indicating that they may have been measured too low.

5.4 Discussion

Two fly ashes have been exposed to ozone, which have reduced their total AEA requirements in concrete up to one sixth of initial value after six minutes of treatment at an ozone inlet concentration of 4000 ppm (corresponds to $X = 0.9$ of the carbon). A model, describing the reaction in a fixed bed reactor, has been established. Apparently, the best fit for the rate expression describing the fractional decrease of FI (equation (5.5)) is found for $n = 3$.

The estimated ozone requirement by carbon was corrected by the ineffective ozone loss, but for costs analysis, the total consumption of ozone in the treatment process must be considered. Including the ineffective ozone loss results in a stoichiometric ratio of 0.0237 mol O_3/kg ash (0.92 mol O_3/kg C$\times$ 0.0257 kg C/kg ash) and if a fractional FI decrease of 0.7 is required (equal to a three times reduction in AEA requirements of the total ash), then the ozone consumption becomes 0.80 g O_3/kg ash for ash B. The result is in the same order of magnitude as results from Gao *et al.* [1]. In connection

to this, it is noted that the linear relationship between ozone consumption and fractional decrease of FI is not followed at high values of fractional FI decrease because of the continuous ineffective ozone loss. Given a production yield of ozone in air of 19 kWh/kg O_3 [13] results in a power consumption of 15 kWh/ton ash. On-site electricity costs are much lower than the market price of electricity, which in Denmark is approximately 2 DKK/kWh. Thus, the electricity costs of the ozonation process can be substantially lower than the expenditures of having a fly ash unsuitable for concrete production as concluded by Gao *et al.* [1] as well. In the worst case scenario, this will be comprised of a difference between disposal costs (130-500 DKK/ton in 2005 [14]) and sales value of fly ash (285 DKK per ton delivered [15]). It is noted that oxygen, which has been used as bulk gas in the experimental work, entails additional process costs. For a commercial implementation of the ozonation process, the ozone should be produced from air and this will require attention in future work.

Attempts to investigate the effect of temperature on the ozonation process in this study were complicated by an increasing influence of oxygen [16]. No sign of changes in FI was observed when exposing the fly ash to oxygen alone at room temperature, but increasing the temperature to 70 °C led to a fractional FI decrease of 0.42 after 10 minutes of treatment. Same conditions and treatment time, but with 1000 ppm ozone in the oxygen stream, further changed the fractional FI decrease to 0.70. Overall, the initial change in fractional FI decrease was faster at higher temperatures, but the ineffective ozone loss increased as well, i.e. ozone was not detected in the outlet of the reactor at temperatures of 70 °C and above despite the fractional decrease of FI was close to a final value. Nevertheless, the effect of oxygen on the fly ash adsorption behavior at slightly increased temperatures is interesting and may open for an alternative treatment process of fly ash using oxygen instead of ozone. Temperatures between 60 – 100 °C have been measured in the bottom of the electrostatic precipitators [17] and thus, it may be convenient to implement such an oxygen based treatment method in that part of a power plant.

The parameters in the model are fitted for ash B only and it is not known if they are generally applicable, e.g. ashes produced from other fuel types or which have been exposed to various conditions during the combustion process, may show a different reactivity toward ozone. This should be tested in further work.

Regarding the practical implementation, Hurt *et al.* [18] suggests that ozone treatment can be performed using a pneumatic conveyor, a fluidized bed or a storage silo for fly ash. However, the latter may be inefficient due to the ineffective ozone loss on fully treated ash. An alternative could be to add

ozone in the fly ash bin of the electrostatic precipitator. The developed model could be applied to determine the optimal type of reactor for the treatment process.

5.5 Summary

The AEA adsorption of fly ashes acquired from a Danish power plant, known to produce fly ash that negatively affect air entrainment in concrete, has been lowered by exposing them to ozone in a fixed bed reactor. The kinetics of the carbon oxidation by the ozone is observed to be fast and a six times decrease in AEA requirements within six minutes of treatment time has been observed at an ozone inlet concentration of 4000 ppm. A kinetic model has been developed to describe the passivation of the fly ash in the fixed bed reactor and it includes the stoichiometry of the ozone consumption and an ineffective ozone loss. The modeled results agree well with the experimental data. The estimated ozone requirement of about 0.8 g O_3/kg ash in order to achieve a three times reduction in FI value indicate that the treatment process can be a feasible way to lower the AEA requirements of fly ash.

5.6 Acknowledgements

The CHEC Research Centre is co-funded by the Technical University of Denmark, DONG Energy A/S, FLSmidth A/S, Hempel's Fond, Vattenfall A/S, Haldor Topsøe A/S, Energinet.dk, the Danish National Advanced Technology Foundation, the Danish Technical Research Council, the Danish Energy Research Programme, Nordic Energy Research, the European Union, and several other industrial partners.

5.7 Nomenclature

f	stoichiometric ratio of ozone and FI (mol O_3/kg C)
C_{O_3}	concentration of ozone (mol/m^3)
D_{O_3}	ozone diffusion coefficient (m^2/s)
FI_0	initial foam index value (ml AEA/2 g ash)
FI_b	foam index of the burned ash (ml AEA/2 g ash)
FI_t	foam index at time t (ml AEA/2 g ash)
i	reactor number
k'_{ox}	rate constant of the carbon oxidation ((m^3/mol)^m(m^2/site)$^{n-1}$s^{-1})
k_{ox}	rate constant of the carbon oxidation ((m^3/mol)^{m}s^{-1})
k'_{de}	mass-based reaction rate constant of the ozone destruction (m^3/kg ash s)
L	bed thickness (m)
m	reaction order of ozone concentration
n	reaction order of number of sites
n_{O_3}	ozone requirement of the carbon in the ash (mol O_3/kg C)
N	number of sites for AEA adsorption (sites/m^2)
P	number of reactors
Pe	reactor Peclet number
r_{O_3}	volumetric reaction rate of ozone (mol/m^3 s)
$r'_{O_3,ox}$	mass-based reaction rate of carbon oxidation (mol/kg C s)
$r'_{O_3,de}$	mass-based reaction rate of ozone destruction (mol/kg ash s)
t	time (s)
U	actual gas velocity in the bed (m/s)
v	volumetric gas flow rate (m^3/s)
V	volume of gas phase in reactor (m^3)
w	weight fraction of carbon in ash
W	mass of ash (kg)
X	fractional FI decrease
$X_{O_3,S}$	conversion of ozone at steady state conditions
ϵ	porosity of ash bed
ρ	bulk density of the ash particles (kg/m^3)

5.8 References

[1] Y. Gao, I. Külaots, X. Chen, R. Aggarwal, A. Mehta, E. M. Suuberg, *et al.*, Ozonation for the chemical modification of carbon surfaces in fly ash, Fuel 80 (5) (2001) 765–768.

[2] Y. Gao, I. Külaots, X. Chen, E. M. Suuberg, R. H. Hurt, J. M. Veranth, The effect of solid fuel type and combustion conditions on residual car-

bon properties and fly ash quality, in: Proceedings of the Combustion Institute, Vol. 29, 2002, pp. 475–483.

[3] X. Chen, M. Farber, Y. Gao, I. Kulaots, E. M. Suuberg, R. H. Hurt, Mechanisms of surfactant adsorption on non-polar, air-oxidized and ozone-treated carbon surfaces, Carbon 41 (8) (2003) 1489–1500.

[4] Y. Gao, X. Chen, G. Fujisaki, A. Mehta, E. Suuberg, R. Hurt, Dry and semi-dry methods for removal of ammonia from pulverized fuel combustion fly ash, Energy and Fuels 16 (6) (2002) 1398–1404.

[5] K. H. Pedersen, S. I. Andersen, A. D. Jensen, K. Dam-Johansen, Replacement of the foam index test with surface tension measurements, Cement and Concrete Research 37 (6) (2007) 996–1004.

[6] F. Hanisch, J. N. Crowley, Ozone decomposition on Saharan dust: an experimental investigation, Atmospheric Chemistry and Physics 3 (2003) 119–130.

[7] F. Al-Nakeeb, Post treatment of fly ash from solid fuel combustion to improve its quality for concrete utilization, Master's thesis, Department of Chemical and Biochemical Engineering, Technical University of Denmark (2006).

[8] I. Sutherland, E. Sheng, R. Bradley, P. Freakley, Effects of ozone oxidation on carbon black surfaces, Journal of Materials Science 31 (21) (1996) 5651–5655.

[9] N. V. Beck, S. E. Meech, P. R. Norman, L. A. Pears, Characterisation of surface oxides on carbon and their influence on dynamic adsorption, Carbon 40 (4) (2002) 531–540.

[10] F. Karagulian, M. J. Rossi, The heterogeneous decomposition of ozone on atmospheric mineral dust surrogates at ambient temperature, International Journal of Chemical Kinetics 38 (6) (2006) 407–419.

[11] C. E. Weinell, P. I. Jensen, K. Dam-Johansen, H. Livbjerg, Hydrogen chloride reaction with lime and limestone. kinetics and sorption capacity, Industrial and Engineering Chemistry Research 31 (1) (1992) 164–171.

[12] O. Levenspiel, Chemical Reaction Engineering, 3rd Edition, John Wiley & Sons, New York, 1999, Ch. 12-13.

[13] W. Samaranayake, T. Namihira, S. Katsuki, Y. Miyahara, T. Sakugawa, R. Hackam, H. Akiyama, Pulsed power production of ozone using nonthermal gas discharges, IEEE Electrical Insulation Magazine 17 (4) (2001) 17–25.

[14] Modtagepriser (excl. statsafgift) 2005 - deponeringsanlæg, Videnscenter for affald, Miljøstyrelsen, Denmark.
URL `http://www.affaldsinfo.dk/affald+i+danmark/\%C3\%B8konomi/\newlinemodtagepriser/deponeringspriser`

[15] Prisblad ved levering til betonindustrien i Danmark fra 1. juli 2007 (B4-standard), Emineral A/S, Denmark.
URL `http://www.emineral.dk/filer/Emineral\_prisblad\_010707.pdf`

[16] M. Casanovas Melià, Ozonation of fly ash, Master's thesis, Department of Chemical and Biochemical Engineering, Technical University of Denmark (2007).

[17] A. Klitgaard, Vattenfall A/S, Personal communication (March 2007).

[18] R. Hurt, E. Suuberg, Y.-M. Gao, A. Burnett, Apparatus and method for deactivating carbon in fly ash, U.S. patent no. 6,136,089, Brown University Research Foundation (Providence, RI) (October 2000).

[19] S. Fogler, Elements of Chemical Reaction Engineering, 4th Edition, Pearson Education, Massachusetts, 2006, pp. 839–841.

[20] W. Ranz, W. Marshall, Jr., Evaporation from drops, Chemical Engineering Progress 48 (4) (1952) 173–180.

[21] A. Zolin, A. Jensen, K. Dam-Johansen, Coupling thermal deactivation with oxidation for predicting the combustion of a solid fuel, Combustion and Flame 125 (4) (2001) 1341–1360.

[22] K. Kadoya, N. Matsunaga, A. Nagashima, Viscosity and thermal conductivity of dry air in the gaseous phase, Journal of Physical and Chemical Reference Data 14 (4) (1985) 947–970.

[23] W. J. Massman, A review of the molecular diffusivities of H_2O, CO_2, CH_4, CO, O_3, SO_2, NH_3, N_2O, NO, and NO_2 in air, O_2 and N_2 near STP, Atmospheric Environment 32 (6) (1998) 1111–1127.

Appendix

5.A Controlling Mechanism

The controlling mechanism in the carbon oxidation is determined according to the Weisz-Prater criterion for internal diffusion and Mears criterion for external diffusion.

Mears' Criterion
External diffusion for the char particles can be neglected if Mears criterion is fulfilled [19].

$$\frac{-r'_{\mathrm{A}}\rho_{\mathrm{b}}Rn}{k_{\mathrm{c}}C_{\mathrm{Ab}}} < 0.15 \tag{5.15}$$

The maximum reaction rate is found at the highest concentration and lowest conversion of the FI, thus for a first-order kinetics of the carbon oxidation is given $-r'_{\mathrm{A}} = k_{\mathrm{ox}}C_{\mathrm{Ab}}f$ and equation (5.15) becomes

$$\frac{k_{\mathrm{ox}}f\rho_{\mathrm{b}}Rn}{k_{\mathrm{c}}} < 0.15 \tag{5.16}$$

where the mass transfer coefficient, k_{c}, is estimated according to Ranz and Marshall [20] and is based on the whole bed properties.

$$\frac{k_{\mathrm{c}}d_{\mathrm{p}}}{D_{\mathrm{O_3}}} = 2 + 0.6\left(\frac{Ud_{\mathrm{p}}\rho}{\mu}\right)^{1/2}\left(\frac{\mu}{\rho D_{\mathrm{O_3}}}\right)^{1/3} \tag{5.17}$$

The mass transfer coefficient is calculated to 1.13 m/s, which gives a Mears criterion of $5 \cdot 10^{-3}$ at all conditions. Therefore external mass transport can be neglected.

Weisz-Prater Criterion
Internal diffusion for the char particles can be neglected if the Weisz-Prater parameter is fulfilled [19].

$$\frac{-r'_{\mathrm{A}}\rho_{\mathrm{c}}R^2}{D_{\mathrm{e}}C_{\mathrm{As}}} << 1 \tag{5.18}$$

where C_{As} is the ozone concentration at the surface of carbon (=C_{Ab}). Again, the maximum reaction rate is found at the highest concentration and lowest conversion of the carbon, thus for a first-order kinetics for the carbon oxidation, equation (5.18) becomes.

$$\frac{k_{\mathrm{ox}}f\rho_{\mathrm{c}}R^2}{D_{\mathrm{e}}} << 1 \tag{5.19}$$

The effective diffusion coefficient, D_e, is estimated according to [21], where the tortuosity factor τ is embedded.

$$D_e = \epsilon^2 D_{O_3} \tag{5.20}$$

The effective diffusion coefficient is calculated to $8.4 \cdot 10^{-6}$ m^2/s giving a Weisz-Prater criterion of approximately 0.2 and thus, transport limitations within the particle can be neglected.

Bulk density of char, ρ_b [kg/m^3][a]	430
Char particle radius, R [μm]	50
Reaction order, n	1
Inorganic particle diameter, d_p [μm]	30
Rate constant of the carbon oxidation, k_{ox} [m^3/mol s]	0.35
Ozone diffusion coefficient, D_{O_3}[m^2/s][b]	$1.6 \cdot 10^{-5}$
Actual gas velocity, U [m/s][c]	0.02
Density of air, ρ [kg/m^3]	1.2
Viscosity of air, μ [kg/m s][22]	$18.7 \cdot 10^{-6}$
Specific density of char particles, ρ_c [kg/m^3] [21]	2000
Char porosity, ϵ [-][a]	0.726

Table 5.4: Data for Weisz-Prater/Mears Criterion. Actual conditions based on a temperature of 20°C.
[a] Char derived from high volatile bituminous coal [21].
[b]Modeled diffusivity O_3 in O_2 at 20°C and 1 atm [23].
[c]Based on a flow of 0.7 Nl/min, bed area of $1.3 \cdot 10^{-3}$ m^2 and bed porosity of 0.5.

Chapter 6

Conclusions and Suggestions for Further Work

6.1 Conclusions

Fly ash from solid fuel combustion is a useful additive in the production of concrete, but the residual carbon in the ash can adsorb the air-entraining admixtures (AEAs) added to enhance air entrainment. The present thesis has dealt with three areas within this field: 1) testing of the AEA adsorption of fly ash; 2) the influence of combustion conditions and fuel type on the adsorption behavior of ash; 3) post treatment of fly ash to lower its AEA requirements.

The foam index test is commonly employed to determine the AEA requirements of a fly ash, but the test has a low reproducibility although the repeatability is acceptable. An alternative method has been developed and compared with the foam index test and the results revealed a good relationship between the two methods. In summary, the new method was based on surface tension measurements, which removes the individual operator criterion on foam stability. Moreover, it applied an anionic surfactant as a substitute for the commercial AEA that can vary in chemical nature and concentration. However, the new method has a low sensitivity toward small variations in AEA adsorption between different fly ashes and it requires further work before a finished procedure is accomplished.

Combustion of pulverized fuel in an entrained flow reactor showed that increased oxidizing conditions achieved by improved fuel-air mixing or higher excess air decreased the AEA adsorption of the produced ash by up to a factor of 25. This was due to a decrease in the carbon content combined with a lower specific AEA adsorptivity of the carbon. The latter could be caused

by changes in accessible surface area and surface polarity of the char and a lower soot formation. Soot was visually observed at low mixing rates between coal and combustion air. The reactor was modeled with CFD and a relationship between oxygen concentration in the early stage of combustion and the AEA adsorption properties of the ash was observed. The increased oxidizing conditions increased the NO_x formation up to three times, i.e. a trade-off between AEA adsorption of the ash and NO_x formation was observed. The fuel type had influence on the AEA adsorption of the produced ash as well. A South African coal, being highest in rank, produced ash with the largest amount of carbon and the carbon showed the highest specific AEA adsorptivity. Moreover, the AEA requirements of the ash were unaffected by the applied operating conditions and was up to 12 times higher at certain conditions compared to ashes produced from a Columbian and a Polish coal. This observation may be explained from its agglomerating behavior, which apparently caused an increased soot formation under combustion.

Full-scale experiments were conducted at Nordjyllandsværket, Unit 3, which is a power plant applying low-NO_x burners and furnace air staging in order to reduce the formation of NO_x. The power plant is known to produce fly ash that can interfere with the air entrainment in concrete. By operating the plant with minimum furnace air staging, removal of recycled flue gas and with three levels of burners instead of four resulted in a five times decrease in AEA requirements of the fly ash compared to a reference case. The lower AEA requirements were primarily caused by a lower carbon content, while the specific AEA adsorptivity of the carbon decreased to about 60 % of reference value. The tested operating conditions increased the NO_x concentration by 60 %.

The AEA adsorption of fly ash was lowered up to six times by oxidizing the carbon surface with ozone in a fixed bed reactor and the kinetics of the reaction was found to be fast. The required amount of ozone, in order to lower the AEA adsorption of the fly ash about three times, was estimated to 0.8 g O_3/kg ash. A kinetic model, describing the reaction in the fixed bed reactor, was developed and it agreed well with the experimental data. The developed model could be used for process optimization.

6.2 Suggestion for Further Work

In order to increase the sensitivity of the new method, the following steps may be taken: Electrolytes provided by the cement and fly ash interfered with the applied anionic surfactant and therefore a non-ionic surfactant, which is less sensitive to salt out, should be tested instead. Cement was added to

minimize the influence of various soluble ions provided by the fly ash, but may be replaced with a defined electrolyte solution in order to avoid the varying properties of the cement itself. Changing the protocol of adding surfactants with the aim of obtaining the same order of magnitude between results as in the foam index test should also be tested.

The results from the entrained flow reactor experiments suggest that lower AEA requirements of fly ash can be achieved by operating with more oxidizing conditions in the early stage of the combustion process. This can reduce the carbon content in the ash, lower the formation of soot and create carbon with a lower specific AEA adsorptivity. Applying more oxidizing conditions may be of interest for power producers, where the markability of the fly ash is an important operation parameter, but the improved fly ash quality has to be weighted toward the consequences of any increases in the NO_x formation. The influence from the type of burned coal should be tested at full-scale conditions. Some coal types may lead to a fly ash with very high AEA requirements and such coals should either be avoided or diluted by coal blending.

The specific AEA adsorptivity of the residual carbon in fly ash, produced at the most oxidizing conditions in the full-scale experiments, was significantly higher than in ashes investigated from other plants. This indicates that conditions leading to increased specific AEA adsorptivity, may still be present in the boiler, e.g. it could be highly fuel rich zones in the near burner area and a reduction of these could be attended in further work. A larger experimental matrix with the aim of testing the impact from different operating conditions on the plant performance, including the AEA requirements of the fly ash, is recommended. It could form the basis of a cost-benefit analysis that can be used to determine the optimal operation of the plant.

Exposing fly ash to ozone appears to be a potential alternative to lower the AEA requirements of the ash compared to changing the combustion conditions. The electricity costs of the ozone production can be substantially lower compared to having an unsaleable product. Further experimental work should attend the production of ozone from air and an investigation of the effect of increased temperature on the treatment process. In terms of the latter, the findings that pure oxygen can lower the AEA requirements of the fly ash at slightly increased treatment temperatures ($>$70 °C) is interesting and should be further investigated as well.